University of Stavanger

Faculty of Science and Technology

MASTER'S THESIS

Study program/ Specialization: Marine and Offshore Technology	Spring semester, 2020 Open/Restricted access
Writer: Wenxin Xu	Wenxin Xu (Writer's signatrue)

Faculty supervisor: Yihan Xing

External supervisor: Valentina Buratti

Title of thesis:

Failure Prediction of Carbon-Fibre Epoxy Composite Subsea Flowline Using Response Surface Methodology

Credits (ECTS): 30

Key words: Composite material Subsea flowline Correlation matrix Response surface Stochastic process Failure analysis	Pages: 84 Stavanger, June 10, 2020 Date / year

Abstract

Carbon Fibre Epoxy Composite is a relatively new material utilized in the subsea oil and gas industry. The fibre reinforced composite is competitive for its high strength-to-weight ratio and good corrosion resistance. This thesis addresses the stochastic process applied to the CFEC flowline using response surface methodology. The material properties, geometries, and loadings are considered as the input parameters of the finite element model of the CFEC flowline, while failure criteria are output parameters. To have a better understanding of which parameter will affect the results, studies of correlation matrices are performed. Input parameters with higher correlation coefficients are identified and chosen to generate the response surfaces. A stochastic process which requires the large size of "measured results" can be substituted by approximate "response values". The accuracy of the response surface is an essential issue that determines whether the approximate results are meaningful. Many factors that will affect the quality of the response surfaces, i.e. response surface type, number of selected parameters, size of the response surface, etc. Comparison studies about these possible factors are discussed in this thesis.

It is found that parameters that have correlation coefficients larger than a level should be selected for response surface generation. More parameters selected will increase both the time of generating response surface and the accuracy, while if extremely few parameters are selected, i.e. five, the accuracy will be significantly affected. Larger response surface size will slightly reduce the accuracy of response values, so the use of larger size becomes available, which can be utilized by more design cases. It is noted that the sample populations should avoid centralized at the boundary of response surfaces. With these approaches, the efficiency of using the response surface methodology in composite flowline design can be improved, where the percentage differences of predicted exceeding probabilities are usually below 10%. Based on these findings, a safety factor can be defined and used to describe these uncertainties.

Key words:
Composite material, flowline, failure analysis, response surface, Kriging, optimization.

Acknowledgement

I would like to thank Prof. Yihan Xing for his idea and suggestion of the project from the first day, which increased my interest in the topic. “Experience is the best teacher”, he always glad to share his experience with me whenever I meet problems. I appreciate him for his patience in the discussions in academic and common issues, which support me the most during the past year.

I would like to thank Co-supervisor Valentina Buratti for her effort during the project. Her constructive suggestion and opinions on my work, which helped me improve it in an efficient way. I would also appreciate her technical supports when I met problems with the software.

I also owe a debt of gratitude for all the faculty members and my friends, who support me spend an unforgettable study experience during these two years.

Table of Contents

List of Figures

List of Tables

Nomenclature

σ_h	Hoop stress	σ_l	Longitudinal stress
σ_1	Principle stress in x-direction	τ_{12}	Shear stress in xy-plane
σ_2	Principle stress in y-direction	τ_{23}	Shear stress in yz-plane
σ_3	Principle stress in z-direction	τ_{13}	Shear stress in xz-plane
σ_{uc1}	Compressive strength limit in x-direction	τ_{u12}	Shear strength limit in xy-plane
σ_{uc2}	Compressive strength limit in y-direction	τ_{u23}	Shear strength limit in yz-plane
σ_{uc3}	Compressive strength limit in z-direction	τ_{u13}	Shear strength limit in xz-plane
σ_{ut1}	Tensile strength limit in x-direction	D	Flowline Iinner Diameter
σ_{ut2}	Tensile strength limit in y-direction	OD	Flowline outer Diameter
σ_{ut3}	Tensile strength limit in z-direction	t	Ply thickness
$\rho_{rgX,rgY}$	Spearman correlation coefficient	t_{total}	Flowline wall thickness
$cov(r_{gX}, r_{gY})$	Covariance of the rank variable		
σ_{rg_X}	Standard deviation of the rank variable g_X		
σ_{rg_Y}	Standard deviation of the rank variable g_Y		
P	Internal pressure	A	Axial force
B	Bending moment	T	Torsion

1 Introduction and Background

1.1 Subsea Flowline

As an important component in the subsea oil and gas production system, subsea flowlines are pipelines that connect a wellhead to a manifold or processed equipment, which transport production/injection fluids between subsea wells and manifolds or processing facilities. With the constant development of the oil and gas industry, a higher number of deep-water oil and gas reservoirs are exploited. The average depth of oil wells drilled was 1108 m in 1949, increased to 1818 m in 2008.[1] With more reservoirs are drilled, the total length of the pipeline is increasing. Noted by Global data 2019,[2] the length of oil and gas pipeline is expected to increase from 1.9 million km to 2.2 million km in the next 4 years. However, the increasing depth and distance of pipeline would lead to the requirement of pipelines with better performance, which will unavoidably increase the cost. Mentioned by ICF International,[3] the average pipeline cost increased from $94000 per inch-mile in 2011 to $155000 per inch-mile in 2012. To reduce the associated costs, an attractive solution is to use composite materials instead of traditional steel material in the flowline manufacture. Several projects have utilized composite flowline in their production system, for example Åsgard and Alder fields.

1.2 Polymer Composite

Polymer composite has been well established in areas such as aerospace, automotive, architecture and infrastructure, where requiring structures with a higher

strength but lighter weight. Many applications have used composites for components, like aircraft fin and tailplane. The composite is valued for its high strength-to-weight ratio. Airbus 320, a narrow-body airliner designed and produced by Airbus, has used ranges of composite components, which reduces the weight of 800 kg compared to the aluminum alloy.[4] The good properties make the composite a cost-effective material in engineering design.

The composite material is not new in the subsea industry. Fiber-reinforced polymer composites (FRP) have been used in the subsea industry in the last 30 years for applications like modules, protections, pipes, pressure vessels, etc.[5] Their corrosion resistance properties additionally improving their competitiveness compared to metals in the offshore and subsea industry.

1.3 CFEC Flowline

Carbon Fibre Epoxy Composite is one of the attractive choices which have a high strength-to-weight ratio. As presented in Table 1, CFEC is nearly five times lighter than steel, but have more than two times of tensile strength.

Table 1: Comparison of Epoxy Carbon UD (230Gpa) and Steel AISI 4130

	Yield Strength (GPa)	**Ultimate Tensile Strength (GPa)**	**Density (g/cm3)**	**Strength to Weight Ratio**
Epoxy Carbon UD	3.53	2.231	1.49	1.497
Steel, AISI 4130	0.95	1.11	7.85	0.141

CFEC consists of epoxy matrix and carbon fibres. The epoxy matrix provides protection for the fibres from the external environment and transfers the loads between the fibres, while the fibres provide the strength and stiffness to the component, as shown

in Figure 1. This gives the CFEC ability to customize the material strength according to different applications by adjusting the laminate layout and fibre directions. However, in most situations, the subsea flowlines are subjected to a combination of loading such as internal pressure, external pressure, bending, axial forces. Thus, the anisotropic property of CFEC also demands a comprehensive and reliable stress analysis.

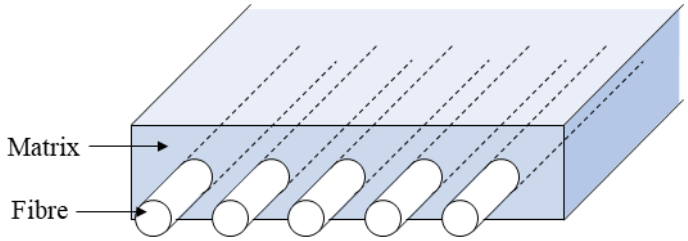

Figure 1: Structure of fibre reinforced polymer lamina

Numbers of studies were published related to the composite pipeline stress analysis. Yang analyzed the stresses at composite joints under tensile loading.[6] Jha et al analyzed the stresses of a fibre-reinforced flexible pipe for deepwater applications.[7] In addition, the complex subsea terrain, temperature, current and other factors make the CFEC flowline not only be affected by the loading. The joint action of random parameters like loading, environment, material properties and geometries require a stochastic model in engineering design. Several pieces of research have studied stochastic process in the pipeline designs. Bazan et al. studied the stochastic process of pipeline corrosion growth models.[8] Oliveira et al. carried on a probabilistic analysis of collapse pressure associated with corroded pipelines.[9] However, considering the requirements of a large size of samples, which means time consumed is increased, the stochastic process is not widely used in the engineering design.

1.4 Design Optimization.

To make the stochastic design available in engineering design, an optimized method of obtaining samples is required. Response surface methodology is an approach that can calculate approximate results by building a response surface model based on sample results, which can both obtained from several experiments or simulations. Compared to the traditional approach by which repeating the experiments or simulations, this method requires less time especially when the required sample size is large. Some studies were published associated with the response surface methodology in engineering problems. Jia et al. studied the Kriging-based response surface in the application of structure reliability analysis.[10] Simpson et al. carried a failure analysis comparison using the second-order response surface models and Kriging models for multidisciplinary design.[11] Gupta et al introduced an improved response surface method for the determination of failure probability.[12] These studies show that the response surface is a convenient tool in engineering design and optimization. However, the results obtained by the response surface are approximate values, which means the using of the response surface requires careful consideration. Many factors will affect the accuracy of the response values, including the interpolation method, the response surface type, the chosen of parameters, size of response surface, etc.

1.5 Thesis Outline

This dissertation suggests an optimized method to predict the failure rates associate with a CFEC flowline using the Kriging response methodology. The general flowchart is shown in Figure 2:

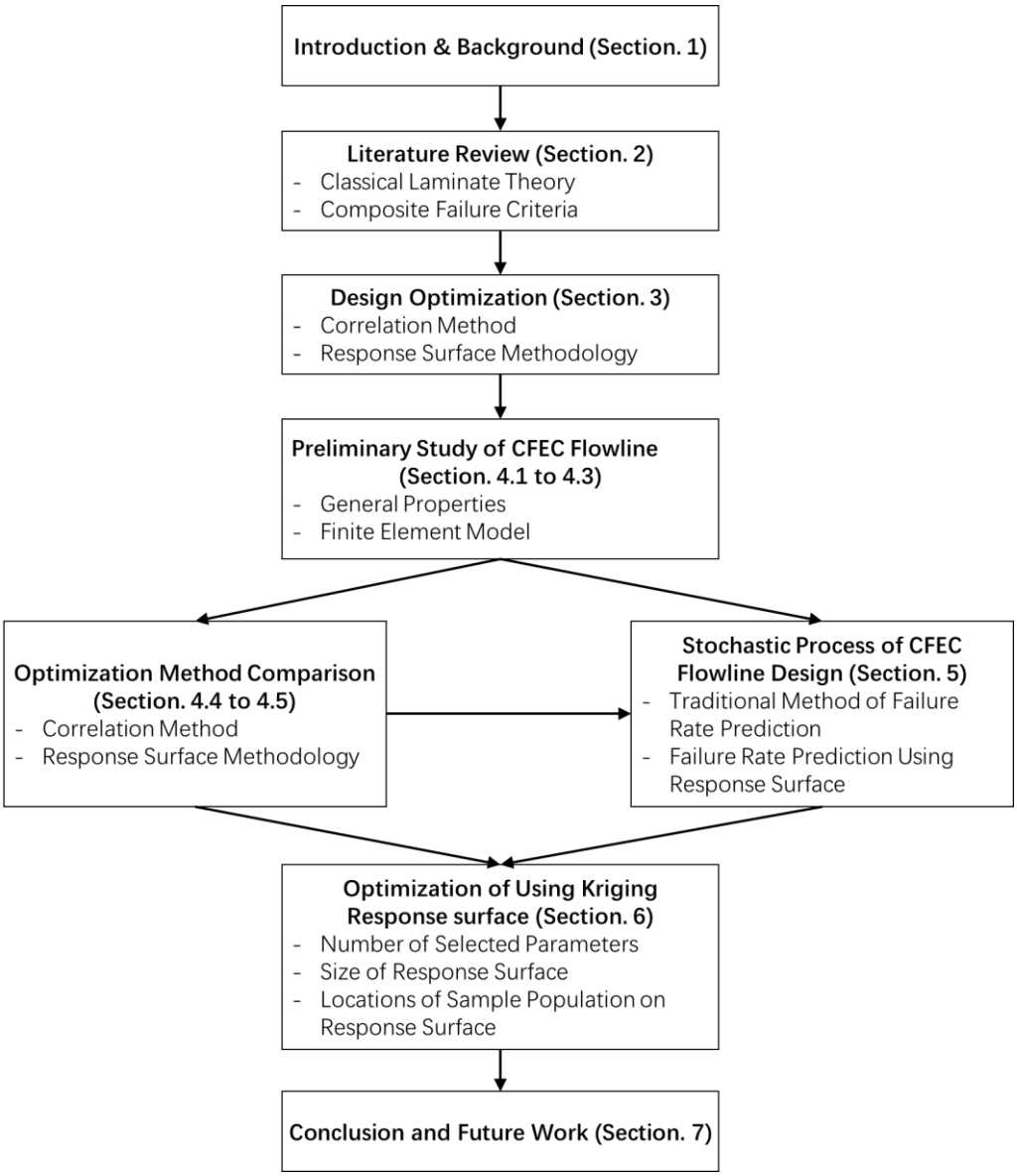

Figure 2: Flowchart of the thesis

In Section 1, the importance of flowline in the subsea oil and gas production system is discussed, Carbon Fibre Epoxy Composite used into the flowline design is introduced. An optimized method of CFEC flowline design using response surface methodology is put forward.

In Section 2, the importance of classical laminate theory in fibre-reinforced composite stress analysis is introduced and three commonly used failure criteria for the composite material are Maximum Stress, Tsai-Wu[13] and Hashin[14] criteria.

In Section 3, the principle of using response surface methodology is discussed. Two correlation methods are introduced: Spearman[15] and Pearson[16]. Four response surface types are introduced: Kriging[17], Non-Parameter Regression, Neural Network[18] and Genetic Aggregation.

In Section 4, a preliminary study of CFEC flowline under combined loads is presented. A finite element model of the CFEC flowline is built using ANSYS Composite Pre/Post, Mechanical and DesignXplorer. We will study how the different correlation methods will affect the correlation results between the input and parameter parameters. An approach of using correlation matrix to select parameters for the response surface generations is introduced. We will compare the difference between the three response surface methods.

In Section 5, a traditional stochastic process of failure rate prediction is investigated, which requires a large size of samples. The generation of sample population using Monte-Carlo simulation is introduced. Meanwhile, a new method using response surface to generate required samples is introduced. The results are compared with the traditional method.

In Section 6, we reveal the limits of using the response surface to predict the failure rates and promote some possible methods to improve the accuracy of the response surface.

In Section 7, conclusions are made based on the results and observation, and recommendations for future work are suggested.

2 Literature Review

2.1 Classical Laminate Theory

A laminate is a stack of composite plies which have unique directions and properties. The coupling effects between adjacent plies made the composite material have different stress and strain distribution with common isotropic materials. The classical lamination theory (CLT) is a widely accepted theory to analyze the stress within the composite laminates.

2.1.1 Assumptions

The classical lamination theory is an extension of classical plate theory (CPT) proposed by Kirchhoff[19] and Love[20], which have the following assumptions:

- Straight lines normal to the mid-plane remain normal and straight after deformation.
- The thickness of the plate does not change during any deformation.

As an extension of CPT, few more assumptions are made considering the difference between the stress-strain relationships of laminate:

- The adjacent laminas are well bounded (There is no slip between adjacent layers).
- The thickness of the plate is much smaller compared to other dimensions.
- Stress in thickness directions is negligible ($\gamma_{xz} = \gamma_{yz} = 0$).

The classical laminate theory provides a relation between the strain and stress within the laminate and loading applied on the composite, which made the stress and

deformation analysis within the laminate become possible by mathematical method.

2.1.2 Laminate Stacking

The composite consists of epoxy matrix reinforced by multiple carbon-fibre layers with different fibre direction. The direction of 0° usually defined in the same direction with primary loading (x-axis). The plies that do not have the same direction with 0° should be assigned an angle. One of the methods to define the other fibre direction is to rotate the ply from 0°, clockwise direction is defined as a positive angle, and counterclockwise is negative.[21] All the plies within the laminate should have an angle associate with 0°.

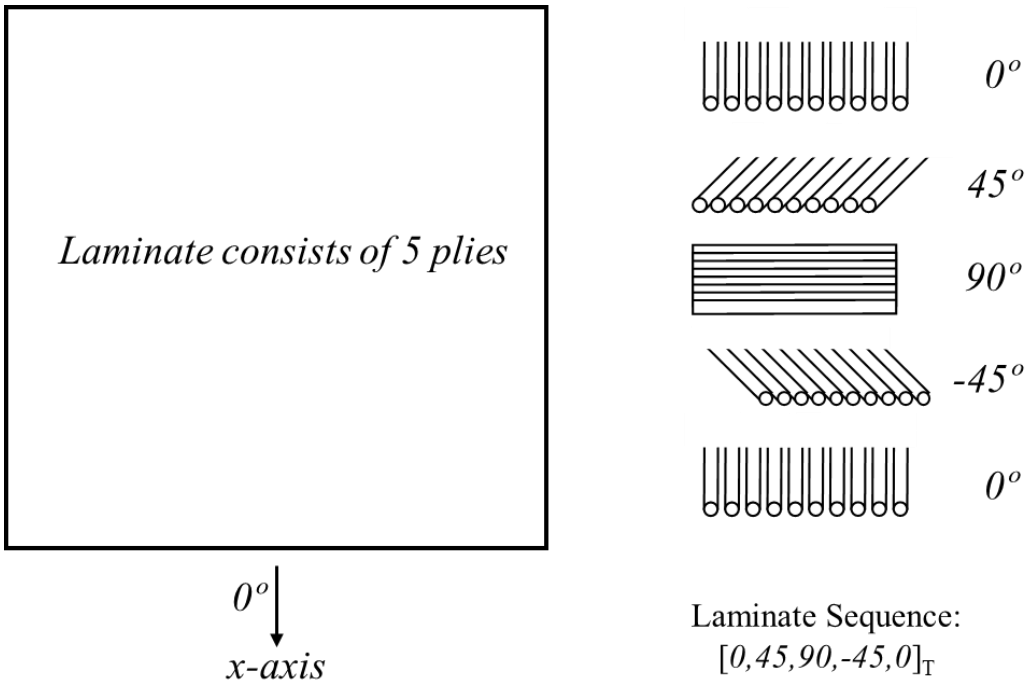

Figure 3: Explanation of laminate sequence.

The direction of each ply will be written to represent the stacking sequence of the laminate. For a non-symmetric laminate, the sequence starts from the outmost ply to the bottom and subscripted with “T” stand for total. For a symmetric laminate, the

sequence starts from the outermost ply to the middle ply, the bracket is subscripted with an “S” to represent symmetric. A bar put on the top of the angle of the middle plane represents the middle ply. Plies that have a same direction can be grouped together and mark the number of the groups at the corner. Some examples of layer sequences are shown below in Figure 4.

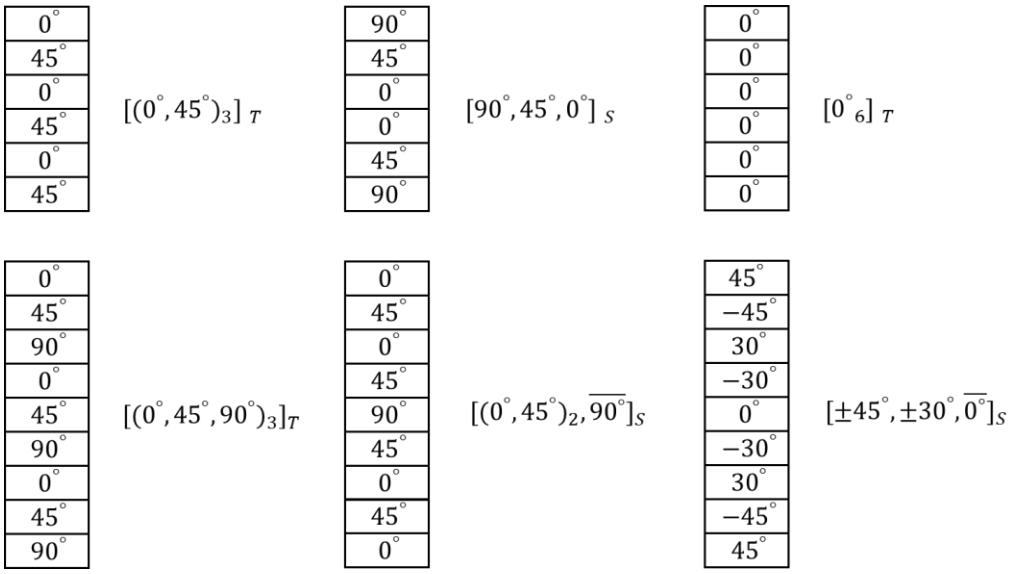

Figure 4: Laminate stacking sequences and their notation

2.2 Composite Failure Criterion

Failure criteria are frequently used in engineering to qualify the failure of the structure design. Generally, the failure criteria compare the stress that the structure experienced and the stress limit that the material can hold without reducing its stability. The failure criteria basically have a form:

$$\sigma_i \leq f \times \sigma_{ui} \tag{1}$$

Where σ_i is the actual stress, σ_{ui} is the ultimate strength of the material. When the ratio f is larger than 1, which means the stress within the structure is larger than

the strength limit of the material, the component will be considered “fail”. Failure criteria of composite materials can be divided into two categories: non-interactive failure criteria and interactive failure criteria.[22]

Non-Interactive failure criteria assume there is no interaction between stress or strain tensor components, which means the failure of the composite is determined by the stress or strain on one direction alone, and not related to other stress and strain in any directions. A typical non-interactive failure criterion of the composite is the Maximum Stress failure criterion.

On the contrary, the interactive failure criteria as its name suggested, assume that the failures are determined by joint effect of at least two stress or strain components, which means the failure value can be presented as a combination formula of the stress and strain tensor components. The Tsai-Wu failure criterion and Hashin failure criterion are two typical interactive failure criteria. We will go into details of the three failure criteria discussed above.

It is noted that as the classical laminate theory is used, the stress and strain in z direction is negligible. (i.e., $\sigma_3 = \tau_{23} = \tau_{13} = 0$)

2.2.1 Maximum Stress Failure Criterion

Maximum Stress failure criterion is a commonly used criterion for composite materials. It is a non-interactive failure criterion that assume the failure occurs when the stresses in any principle direction exceed the material strength in that direction. The failure value is calculated using Equation (2).

$$f = max\left(\left|\frac{\sigma_1}{X}\right|, \left|\frac{\sigma_2}{Y}\right|, \left|\frac{\sigma_3}{Z}\right|, \left|\frac{\tau_{12}}{S}\right|, \left|\frac{\tau_{13}}{R}\right|, \left|\frac{\tau_{23}}{Q}\right|\right) \quad (2)$$

Where:

$$X = \begin{cases} \sigma_{uc1}, \sigma_1 < 0 \\ \sigma_{ut1}, \sigma_1 \geq 0 \end{cases}, \qquad S = \tau_{u12}$$

$$Y = \begin{cases} \sigma_{uc2}, \sigma_2 < 0 \\ \sigma_{ut2}, \sigma_2 \geq 0 \end{cases}, \qquad R = \tau_{u13} \quad (3)$$

$$Z = \begin{cases} \sigma_{uc3}, \sigma_3 < 0 \\ \sigma_{ut3}, \sigma_3 \geq 0 \end{cases}, \qquad Q = \tau_{u23}$$

2.2.2 Tsai-Wu Failure Criterion

The Tsai-Wu failure criterion is a widely used failure criterion for anisotropic composite materials which have different strength for tension and compression. The Tsai-Wu failure criterion is based on the work of Gol'denblat and Koponov.[23] The criterion assumes the existence of a failure surface and distinguishes between the compressive and tensile strength in the ply failure prediction. The failure criterion uses the following quadratic formulation presented in Equation (4).

$$f = \frac{\sigma_1^2}{\sigma_{ut1}\sigma_{uc1}} + \frac{\sigma_2^2}{\sigma_{ut2}\sigma_{uc2}} + \frac{\tau_{12}^2}{\tau_{u12}{}^2} + \sigma_1\left(\frac{1}{\sigma_{ut1}} - \frac{1}{\sigma_{uc1}}\right) + \sigma_2\left(\frac{1}{\sigma_{ut2}} - \frac{1}{\sigma_{uc2}}\right) + 2F_{12}\sigma_1\sigma_2 \quad (4)$$

F_{12} is a parameter that only associated with principle stresses σ_1 and σ_2. This coefficient has a range from -1 to 1, which was related to the physical meaning of the material properties. F_{12} is also commonly obtained using bi-axial tests. Some examples can be found in Clouston et al.[24] and Li et al.[25] One commonly used form of F_{12} is presented in Equation (5):

$$F_{12} = -\frac{1}{2}\sqrt{\left(\frac{1}{\sigma_{ut1}} - \frac{1}{\sigma_{uc1}}\right)\left(\frac{1}{\sigma_{ut2}} - \frac{1}{\sigma_{uc2}}\right)} \quad (5)$$

2.2.3 Hashin Failure Criterion

Hashin failure criterion distinguishes three different types of failure modes: fibre failure, matrix failure and interlaminate failure. These failure modes are illustrated in Figure **5**.

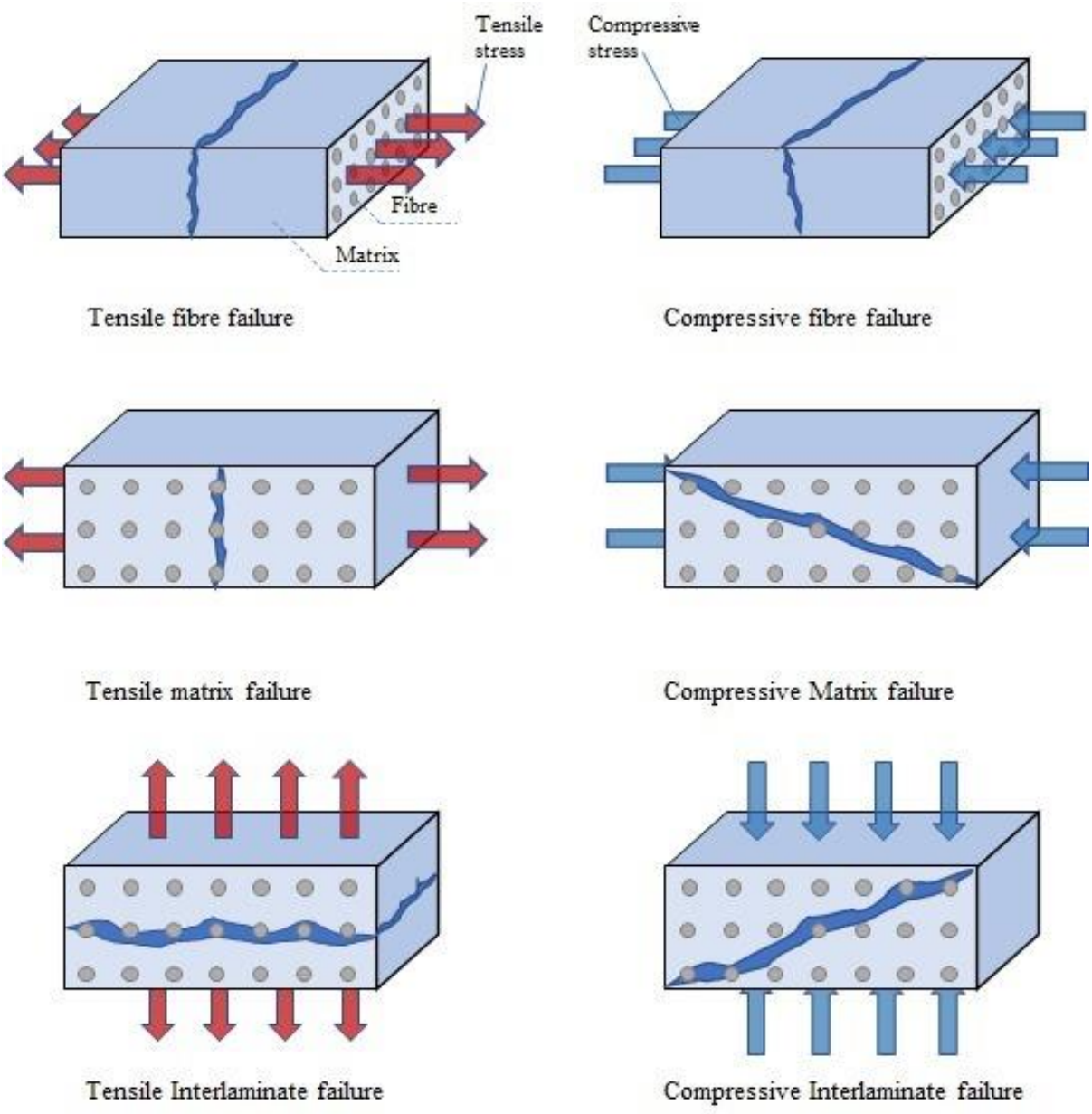

Figure 5: Illustration of the various failure modes in Hashin failure criterion

The tensile fibre failure considers the strength on the fibre direction, which have the following criterion:

$$f_f = \begin{cases} \left(\frac{\sigma_1}{\sigma_{ut1}}\right)^2 + \left(\frac{\tau_{12}}{\tau_{u12}}\right)^2 & ,\sigma_1 \geq 0 \\ -\frac{\sigma_1}{\sigma_{ut1}} & ,\sigma_1 < 0 \end{cases} \quad (6)$$

The matrix failure is caused by the tensile transverse stress perpendicular to the fibre direction, which have the criterion:

$$f_m = \begin{cases} \left(\frac{\sigma_2}{\sigma_{ut2}}\right)^2 + \left(\frac{\tau_{23}}{\tau_{u23}}\right)^2 + \left(\frac{\tau_{12}}{\tau_{u12}}\right)^2 + \left(\frac{\tau_{13}}{\tau_{u13}}\right)^2 & ,\sigma_2 \geq 0 \\ \left(\frac{\sigma_2}{2\tau_{u23}}\right)^2 + \left(\frac{\tau_{23}}{\tau_{u23}}\right)^2 + \left(\frac{\tau_{12}}{\tau_{u12}}\right)^2 + \left[\left(\frac{\sigma_{uc2}}{2\tau_{u23}}\right)^2 - 1\right]\frac{\sigma_2}{\sigma_{uc2}} & ,\sigma_2 < 0 \end{cases} \quad (7)$$

The criterion for tensile interlaminate failure is presented in Equation (8). This criterion evaluates the stress that normal to the laminate.

$$f_i = \begin{cases} \left(\frac{\sigma_3}{\sigma_{uc3}}\right)^2 + \left(\frac{\tau_{13}}{\tau_{u13}}\right)^2 + \left(\frac{\tau_{23}}{\tau_{u23}}\right)^2 , \sigma_3 < 0 \\ \left(\frac{\sigma_3}{\sigma_{ut3}}\right)^2 + \left(\frac{\tau_{13}}{\tau_{u13}}\right)^2 + \left(\frac{\tau_{23}}{\tau_{u23}}\right)^2 , \sigma_3 \geq 0 \end{cases} \quad (8)$$

The Hashin failure criterion value is decided by the maximum of failure values calculated above, as shown in Equation (9):

$$f = max(f_f, f_m, f_i) \quad (9)$$

2.2.4 Failure Criteria Calculation

The failure values are calculated using ANSYS Composite Pre/Post. The failure results and the corresponding failure modes are shown in the ACP solution. As introduced above, the failure criteria have different failure modes. The maximum stress failure criteria have failure modes associate with stress in different directions: σ_1, σ_2 and σ_3. The Tsai-Wu failure criteria using an integrated formula that do not differ any failure modes. The Hashin failure criteria distinguish the failure between fibre failure, matrix failure and interlaminate failure. An example of Tsai-Wu failure criterion

solution is shown in Figure 6. The solution is processed at the middle section of the flowline model, as shown in Figure 7.

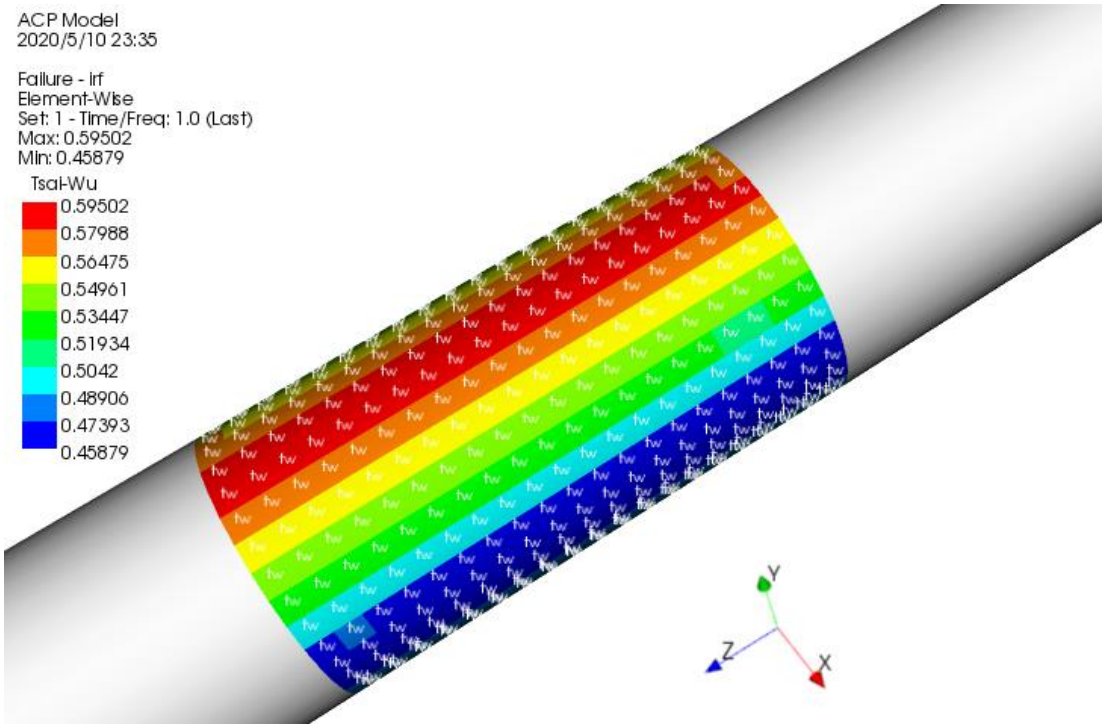

Figure 6: Example of Tsai-Wu failure criterion plot –failure criterion

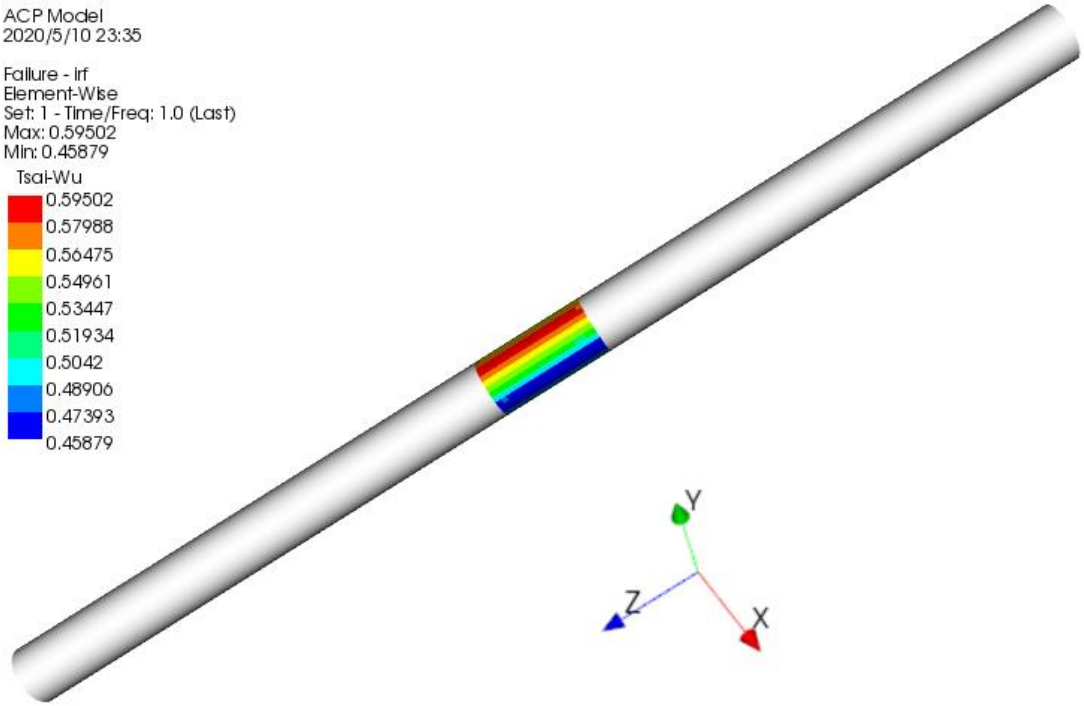

Figure 7: Example of Tsai-Wu failure values calculated at the middle of the flowline

2.3 Probabilistic Analysis

In engineering design, various design parameters will influence the performance of the structure, i.e. loading, environment, manufacture, etc. These parameters are always changing during the life cycle of the structure, which increases the uncertainty of the structures. Therefore, it is important to keep the structure performance above an acceptable level by performing the reliability analysis. The reliability analysis was first developed by Freudenthal in 1956,[26] and has been frequently introduced in many fields for decades, i.e. aerospace, manufacture, electronics, etc.

Reliability analysis is an estimation of failure probability, which should be considered in the conceptual design stage. The reliability can be defined as the probability of survival, as presented in Equation (10):

$$P_f = 1 - P_s \tag{10}$$

Where P_f is the failure probability, P_s is the survival probability. In this design of composite flowline, the "failure" is considered as the condition where failure criteria exceed 1. In contrast, "survival" means failure criteria below 1.

To calculate these probabilities, distributions of the failure criteria are required. The distributions are based on the sample population, to make these samples more continuous, the input parameters should be randomly distributed within a reasonable range. It is noted that a sample is usually measured by experiment or calculated from a simulation. A larger size of sample population we have, more accurate the distribution will be. The traditional approach to obtain sample populations is based on the repetitive

experiments or simulations, which we discuss in Section. When the distributions of output parameters are formed, the reliability analysis will become available, the design can be adjusted efficiently based on an acceptable failure probability.

3 Design Optimization Method

3.1 Parameter Correlation and Determination

In statistics, correlation shows the linear relationship between two random variables. The correlation study of engineering parameters is commonly used to reveal the relationship between different design parameters. The degree of correlation usually indicated by the correlation coefficient which range from -1 to 1. The correlation coefficient between two variables is 0 means there is no correlation between the selected parameters, and the coefficient closer to -1 or 1 means a stronger correlation. A positive coefficient indicates a positive correlation, which means one variable increase as the other variable increase, vice versa. In contrast, the negative coefficient means one variable increase as the other variable decrease. The values of the calculated coefficient can be interpreted as follows:

Table 2: Study of Sample Size and Correlation method

The absolute value of correlation coefficient ρ	**Degree of Relationship**
0.00~0.20	Slight correlated, the relationship is almost negligible.
0.20~0.40	Lowly correlated, but the relationship is definite.
0.40~0.60	Moderately correlated, the relationship is substantial.
0.60~0.80	Highly correlated, the relationship is marked
0.80~1.00	Very highly correlation, the relationship is very dependable

The correlation coefficient can be computed by different methods. Two correlation method are studied in the thesis: Pearson and Spearman.

3.1.1 Pearson Correlation

The Pearson correlation measuring the linear correlation between two variables X

and Y, which have the following equation:

$$\rho_{X,Y} = \frac{cov(X,Y)}{\sigma_X \sigma_Y} \tag{11}$$

Where $cov(X,Y)$ is the covariance, σ_X and σ_Y are the standard deviation.

As a most familiar measure of parameter correlation method, Pearson correlation method establishes a best-fitting line by datasets of two variables, and the coefficient evaluates how the actual values far away from the expected values.

3.1.2 Spearman Correlation

The spearman correlation is a rank-order[27] correlation method, which assesses the monotonic[28] relationship of two ranked variables. The Spearman correlation between two variables is equal to the Pearson coefficient between the rank values of the two variables. It has the following equation:

$$\rho_{rgX,rgY} = \frac{cov(rg_X, rg_Y)}{\sigma_{rg_X} \sigma_{rg_Y}} \tag{12}$$

Spearman's coefficient is useful for both continuous and discrete variables. In a monotonic relationship, the variables can change together but not necessarily with a same rate, the Spearman correlation coefficient will be high when the two variables have a similar rank.

The correlation coefficient is calculated between two variables, for an engineering model which have n design parameters, a correlation matrix is introduced. The correlation matrix collects the correlation coefficients between n design parameters, which can provide an overview of design parameter and identify the major design that will critically influence the result.

3.2 Response Surface Methodology

The response surface methodology was first introduced by Box and Wilson[29] in 1951. The purpose was to create a 'function' to approximate the relationship between several input parameters and several output variables, which means:

$$\text{Output1, Output 2, } \ldots = f\,(\text{Input1, Input2, } \ldots)$$

Where f is the response surface.

In engineering design, the real values are usually obtained from simulations or experiments, which is time-consuming and lack of efficiency. This is because the detailed function of input parameters and output variables is complex or unknown. However, the response surface methodology creates an 'approximate function' to calculate the approximate values, which is close to the real value we required. The efficient way to calculate the required value makes the analysis that needs a large sample size becomes available.

The response surface tool in Ansys uses the parameters with a stronger correlation to generate numbers of sample results, which is called 'Design of Experiment'. As we talked above, the response surface provides an 'approximate function' between input parameters and output parameters. However, errors exist between the approximate values (Response values) and the true values (Measured values). It is mentioned in the Ansys DesignXplorer User's Guide[30] that the accuracy of the response surface depends on the complexity of the variation of the solution, the size of samples (design of experiments) and response surface type. The existence of errors makes the refinement

of response surface become necessary, which means more design of experiments will be considered to improve the accuracy of the response model.

To study how the different factors will influence the accuracy of response results, four responses surface type are introduced in the thesis: Standard, Kriging, No-Parameter Regression, Neural Network and Genetic Aggregation.

3.2.1 Kriging

In statistic, Kriging is an interpolation method which gives the best linear unbiased prediction of the intermediate values. The Kriging method weighs the surrounding measured values to calculate a predicted result at an unknown location. The general formula for Kriging response surface method is presented in Equation 13.

$$\hat{Z}(s_0) = \sum_{i=1}^{n} \lambda_i \hat{Z}(s_i) \tag{13}$$

Where: $\hat{Z}(s_i)$ is the measured value at the ith location

λ_i is weight factor of the measured value at the ith location

s_0 is the predicted location

n is the number of measured values.

The Kriging response surface in ANSYS offers an auto refinement tool that iteratively updates the refinement points during the update of the response surface. A predicted relative error is evaluated at each iteration of refinement, which have the following equation:

$$Predicted\ relative\ error = \frac{Predicted\ error}{O_{max} - O_{min}} \times 100\% \tag{14}$$

Where: Predicted error = Measured value / (Predicted value - Measured value)

O_{max} is the maximum known value

O_{min} is the minimum known value

As observed in Equation (14), the predicted relative error is calculated considering the known maximum/minimum value, which provide an easy comparison across all the response results. 5% of the maximum predicted error is used in the Kriging response surface in this thesis. Figure 8 shows an example of Kriging response surface auto-refinement process, which will discuss in Section 4.5. As shown in the figure, three failure criteria: Tsai-Wu, Maximum Stress, Hashin reach a predicted relative error below 5% after two iterations.

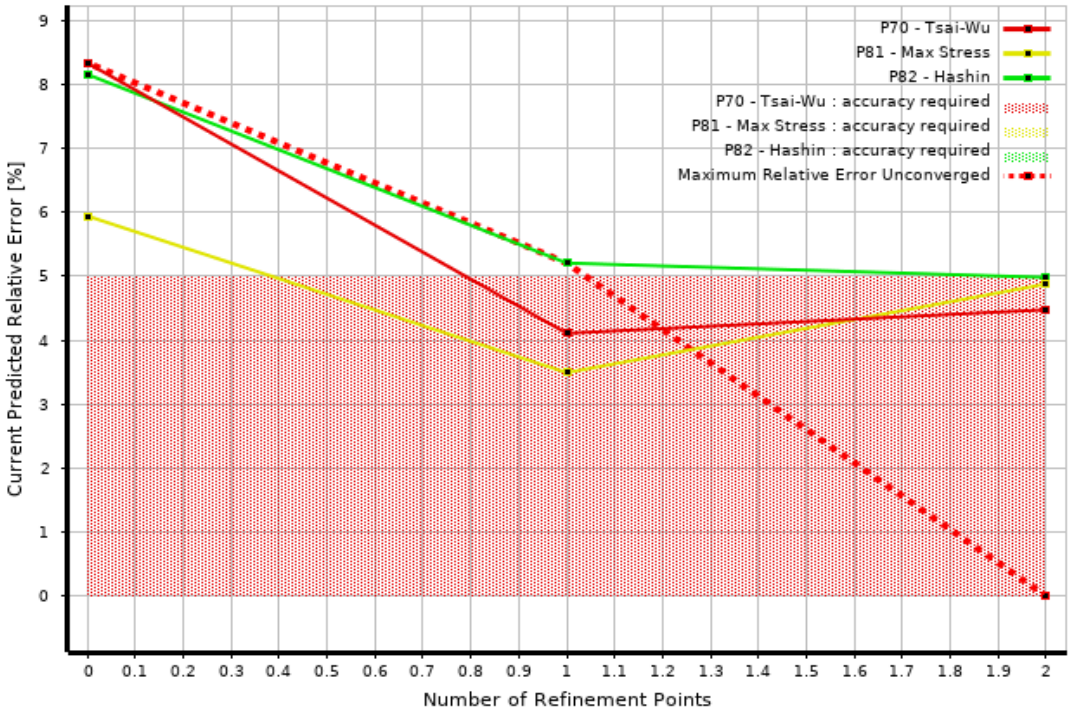

Figure 8: Refinement of Kriging response surface (Base Case)

3.2.2 Non-Parameter Regression

Non-parametric regression (NPR) is a kind of regression analysis where no pre-

determined model is used[31]. The result will be derived only based on the raw data. This leads to the requirement of a large sample size compared to other regression methods. The constants in NPR response surface are fixed and will not be optimized because the model strikes a compromise between the accuracy and the computational speed.

The NPR response surface can provide improved response surface accuracy for high nonlinear behavior of the response results compared to the input parameters. However, for the case where low order polynomials dominate, the result will have some oscillations.

3.2.3 Neural Network

This type of response surface is based on the neural network of human brain. To interpolate a function, three levels of Input, Hidden function and Output are built, see Figure 9.

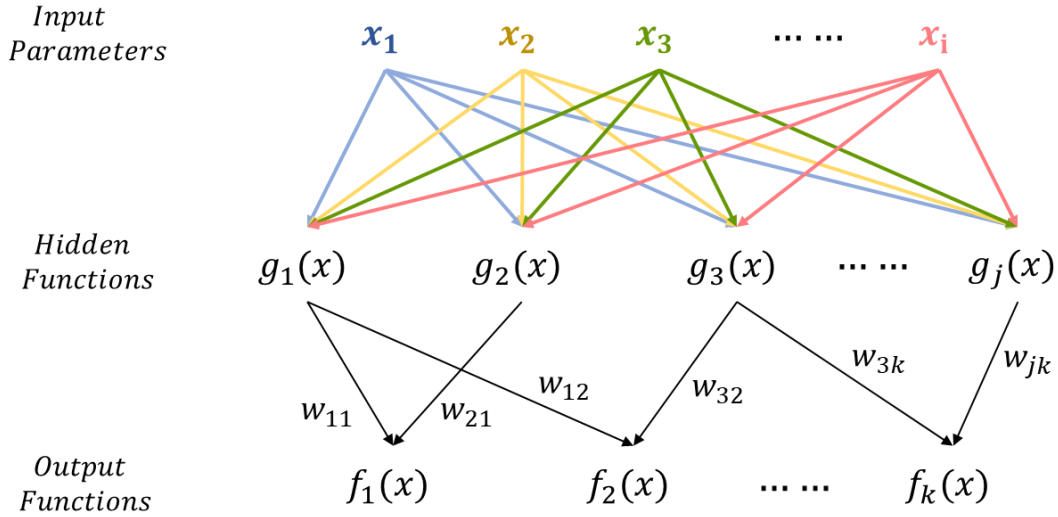

Figure 9: Neural network mechanism

The arrows between hidden functions and output functions can be considered as a 'weight'. The output functions have the following form:

$$f_k(x_i) = K(\sum w_{jk} g_j(x_i)) \quad (15)$$

Where: K is a predefined function (i.e. exponential based function),

x_i is the input parameter,

$g_j(x_i)$ is the hidden function,

w is the weight factor,

This method uses few numbers of design of experiment (DoE) to investigate the hidden function and will have better performance when the DoE are too much.

3.2.4 Genetic Aggregation

The Genetic Aggregation (GA) response surface is a combination of difference response surfaces. It automates a process of choosing and configuring the most suitable response surface type for each output parameter. The GA response surface can either be generated based on a single response surface, or a combination of different types of response surfaces. This makes the GA response surface take more time than the other response surfaces.

4 Preliminary study - Burst design correlation study of a subsea flowline

4.1 General Properties

The flowline studied in this paper has the general properties as listed in Table 2. The material properties of the ply are presented in Table 3. The stacking sequence is presented in Figure 5.

Table 3: General Properties of Subsea CFEC Flowline

Property	Symbol	Value	Unit
Outer Diameter	OD	125	mm
Wall Thickness	t_{total}	6	mm
Total Number of Ply	-	30	-
Ply Thickness	t	0.2	mm
Fibre Orientation	-	+/- 45	°

Table 4: Material Data – Ply (Prepreg Epoxy Carbon UD 230 GPa)

Material Property	Symbol	Value	Unit
Elastic Modulus	E_1, E_2, E_3	121 000, 8 600, 8600	MPa
Shear Modulus	G_{12}, G_{23}, G_{13}	4 700, 3 100, 4 700	MPa
Poisson's Ratio	ν_{12}, ν_{23}, ν_{13}	0.27, 0.4, 0.27	-
Tensile Strength	σ_{ut1}, σ_{ut2}, σ_{ut3}	2 231, 29, 29	MPa
Compressive Strength	σ_{uc1}, σ_{uc2}, σ_{uc3}	-1 082, -100, -100	MPa
Shear Strength	τ_{u12}, τ_{u23}, τ_{u13}	60, 32, 60	MPa
Tsai-Wu Constants	F_{12}, F_{23}, F_{13}	-1, -1, -1	-

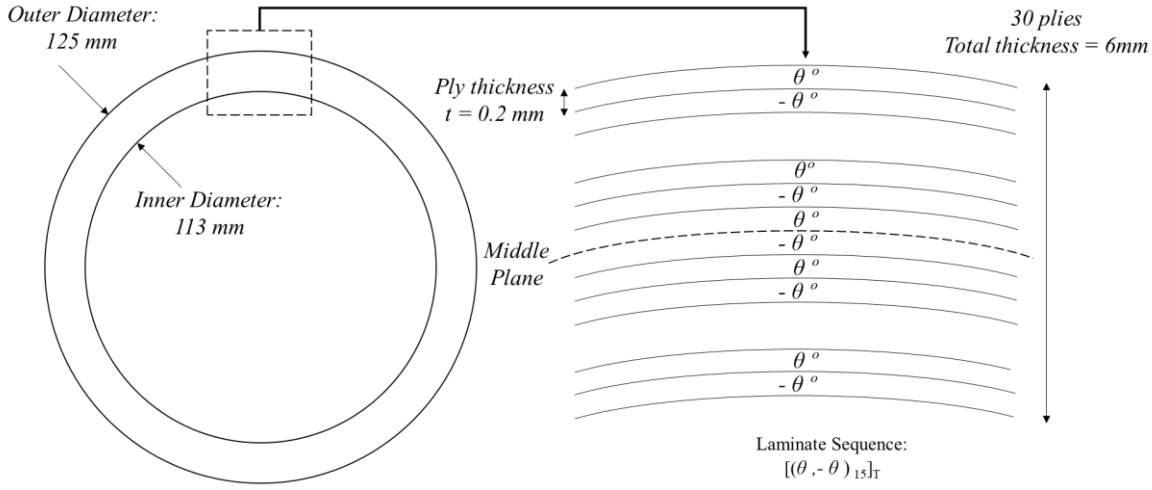

Figure 10: Stacking sequence of $[(\theta, -\theta)_{15}]_T$

4.2 Nominal Load Values

The nominal load values used in the correlation study are presented in Table 5.

Table 5: Nominal Load Values

Load	Value	Unit
Internal Pressure	6.9	MPa
Axial Force	20	kN
Torsion	2	kN·m
Bending	2	kN·m

The failure criteria values of the nominal loads applied are presented in Table 6.

The results are calculate using the finite element model introduced in Section 4.3

Table 6: Failure Values Corresponding to Nominal Loads

	Maximum Stress	Tsai-Wu	Hashin
Failure Criterion Value	0.508	0.595	0.592
Failure Mode	σ_2 exceeded	-	Matrix failure

4.3 Finite Element Model

A 2000 mm section of the CFEC flowline is modelled. This is sufficiently long by engineering judgement to avoid end effects of loads and boundary conditions in the finite element model. The solutions of failure criteria are calculated at the middle section of the flowline, as shown in Figure 7. Ansys 2019 R2 is used for the finite element modelling.

4.3.1 Loads and Boundary Conditions

Four loads are applied on the CFEC flowline. The loads and boundary condition are illustrated in Figure 11.

- Pressure (Load A) is applied in the interior of the flowline. The negative means the pressure direction from internal to external, while a positive pressure in the following study represents an external pressure.
- An end cap force (Load D) due to the internal pressure is applied on the left edge of the flowline. Which have the following equation:

$$F_{endcap} = \frac{\pi}{4}(OD - 2t_{total})^2 \times P \tag{16}$$

Where OD is the outer diameter, t_{total} is the total thickness of flowline wall, P is the internal pressure.

- Axial force (Load B), torsion (Load C) and bending (Load E) are also applied at the left edge.
- Fixed support (Load F) is applied on the right edge of the flowline.

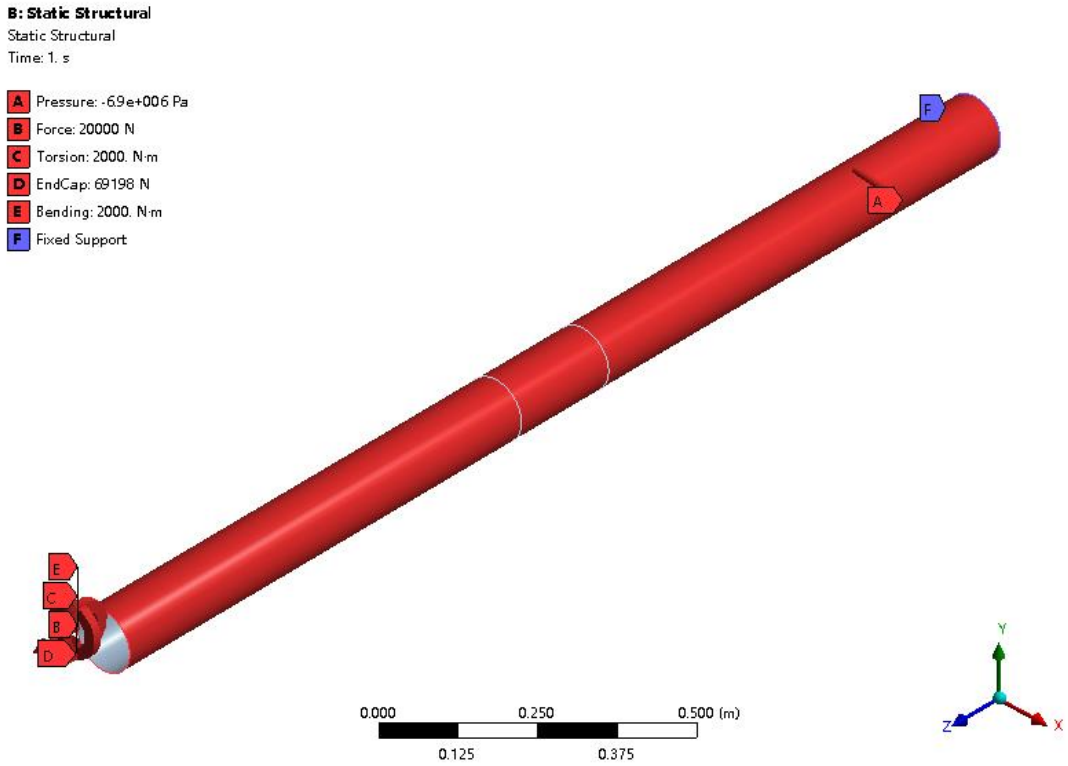

Figure 11: Loads and boundary conditions

4.3.2 Mesh Refinement Study

The mesh refinement study of the Base Case is illustrated in Table 7, The corresponded results obtained from different element sizes are presented in Figure 12.

Table 7: Cases Studied for Mesh Refinement Study

Element Size (mm)	No. of Elements	No. of Nodes
30	900	912
25	1040	1053
20	1536	1552
15	2803	2821
10	6430	6432
5	25344	25408

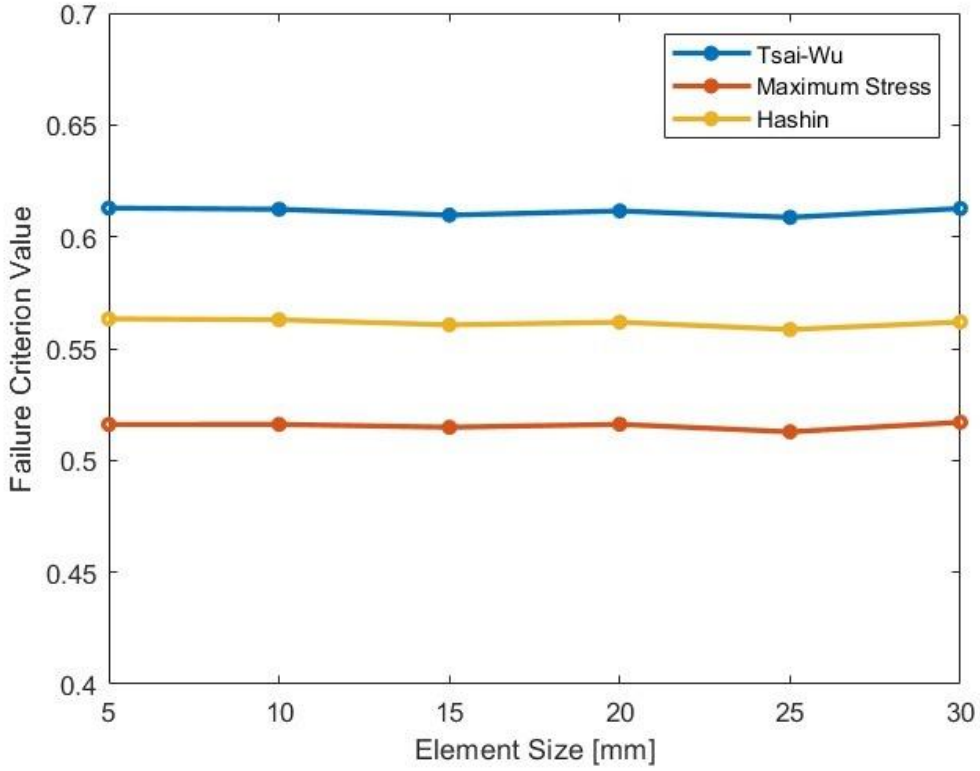

Figure 12: Results of mesh refinement study

The nominal load values as presented in Section 0 are used in the mesh refinement study. The element used is the 4-node SHELL181 element.[32] The results show that three failure criteria results have not completely converged until 10 mm element is used. 5 mm of element size is more accurate, but the element size is 4 times of the 10 mm element, which will increase the time required to calculate the results. To obtain both converged results and acceptable efficiency, an element size of 10 mm is used, as shown in Figure 13.

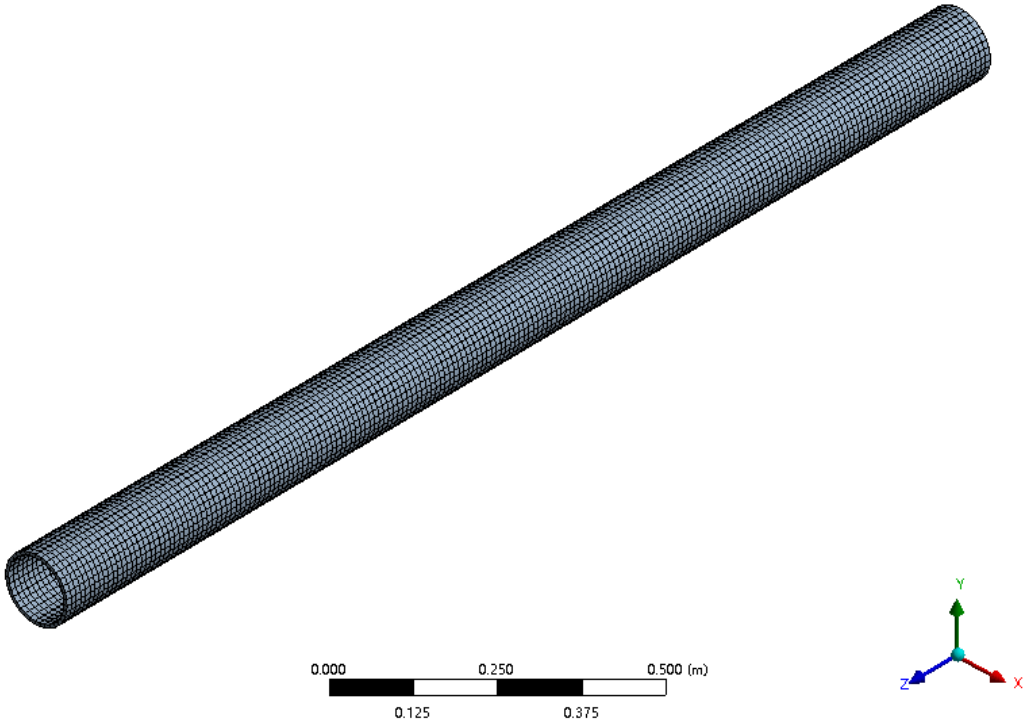

Figure 13: Mesh details, 10 mm element Size, 6430 SHELL181 elements with 6432 nodes

4.4 Parameter Correlation Study of the Base Case

A correlation matrix with sample size 200, Spearman correlation method, is calculated using ANSYS Composite Pre/Post, as shown in Figure 14. The correlation matrix reveals some meaningful information between different parameters. The following observations are made:

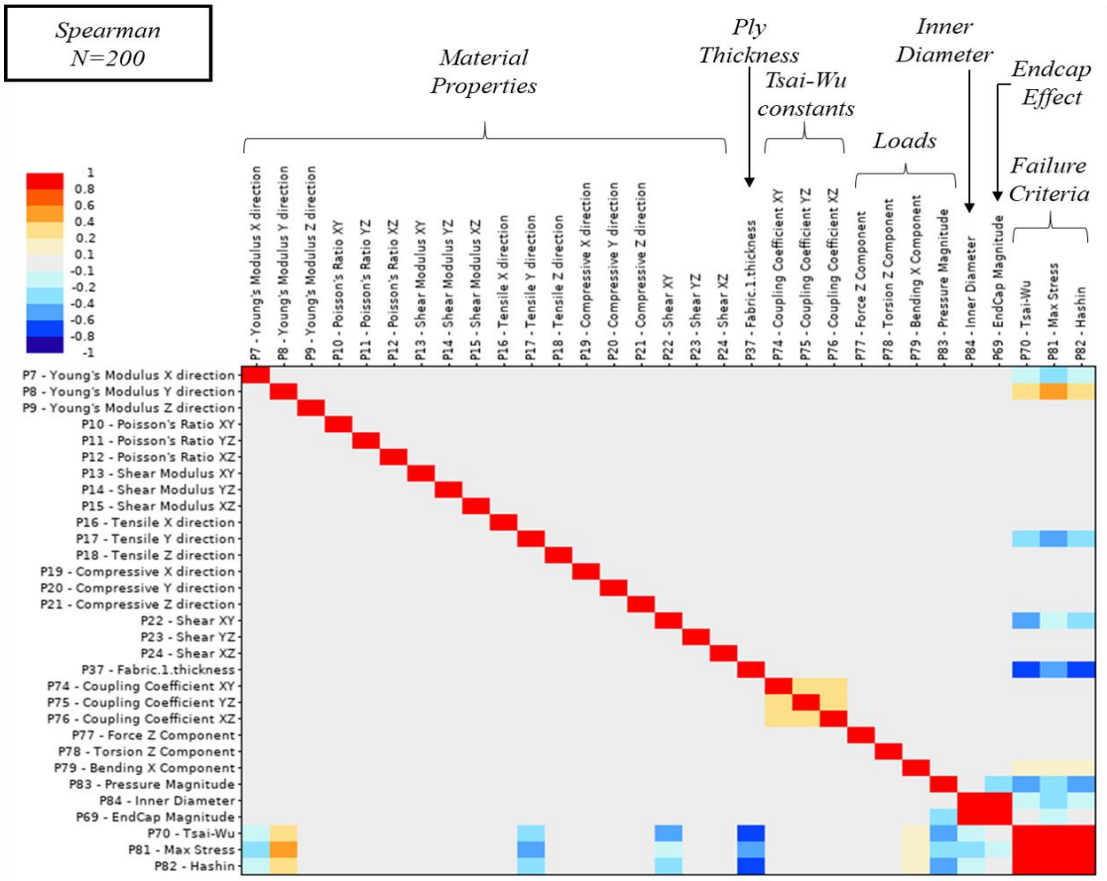

Figure 14: Correlation matrix of case studied, spearman, N=200

- **Failure results of Different failure criteria are strongly correlated.**

The failure criteria show very strong linear correlations between each other. The reason is that failure criteria are related to the stress within the laminate, a large stress which leads to a higher value of one failure criterion will logically contribute to the high values of others. The results of correlation coefficient between Tsai-Wu, Maximum stress and Hashin criteria are shown in Table 8.

Table 8: Correlation Coefficient of Failure Criteria, N=100, Spearman

	Tsai-Wu	Max Stress	Hashin
Tsai-Wu	1.000	0.837	0.970
Max Stress	0.837	1.000	0.894
Hashin	0.970	0.894	1.000

However, the Maximum Stress criterion has smaller coefficients with the other

two criteria. This is because the Maximum Stress criterion is a non-interactive failure criterion, which is different from the other criteria that consider stresses in at least two directions.

- **Internal pressure and ply thickness are moderately correlated to failure criteria**

The values of pressure and geometries correlated with the failure criteria are listed in Table 9:

Table 9: Correlation Coefficient of Internal Pressure and Ply Thickness

	Tsai-Wu	Max Stress	Hashin
Internal Pressure	-0.413	-0.291	-0.405
Ply Thickness	-0.628	-0.468	-0.608

As shown in Table 9, the internal pressure and ply thickness have generally moderate correlation with the failure criteria, which is logically reasonable. A close-up view of the scatter diagram of internal pressure and ply thickness verse Tsai-Wu failure criteria results are illustrated in Figure 15 and Figure 16. It is noted that the pressure magnitude is negative, the right side of the pressure axis represents a smaller pressure applied. As observed in the figures, the scatter is large for both pressure and ply thickness, which did not show a strong correlation as expected. The reason could be that these parameters are still important for the results of failure criteria, but the contribution is lighted by other parameters that not studied in this model, for example, the fibre direction and the stacking sequence of the laminate.

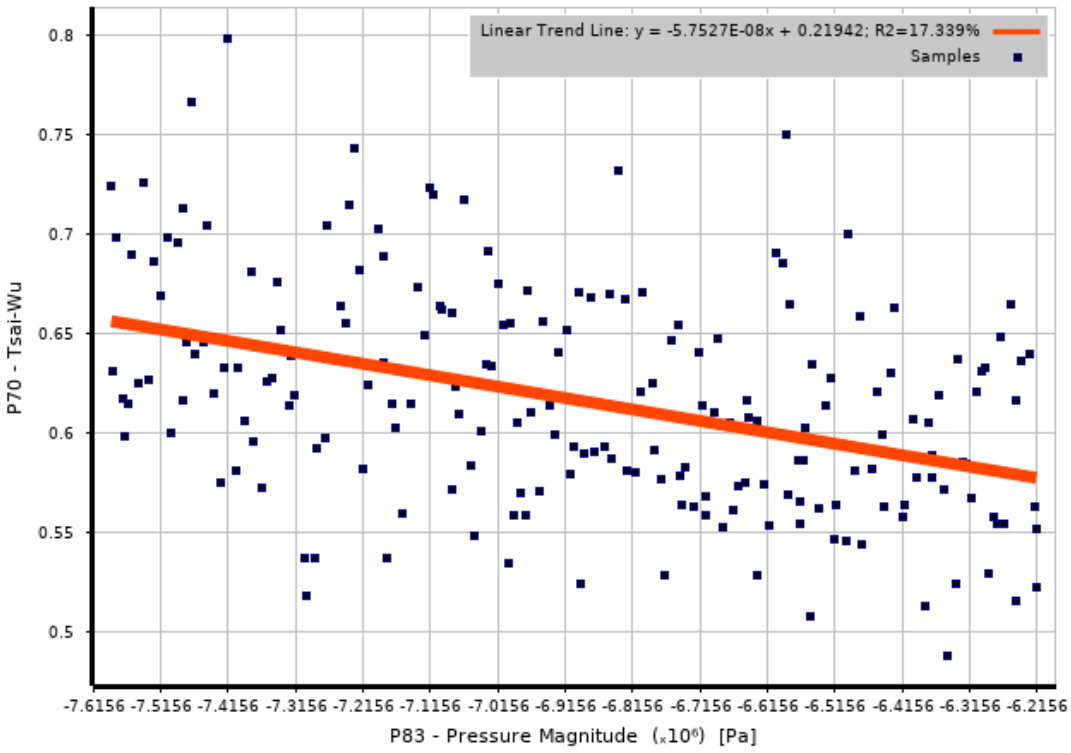

Figure 15: Correlation scatter diagram, Tsai-Wu vs. Internal pressure, Spearman, N=200

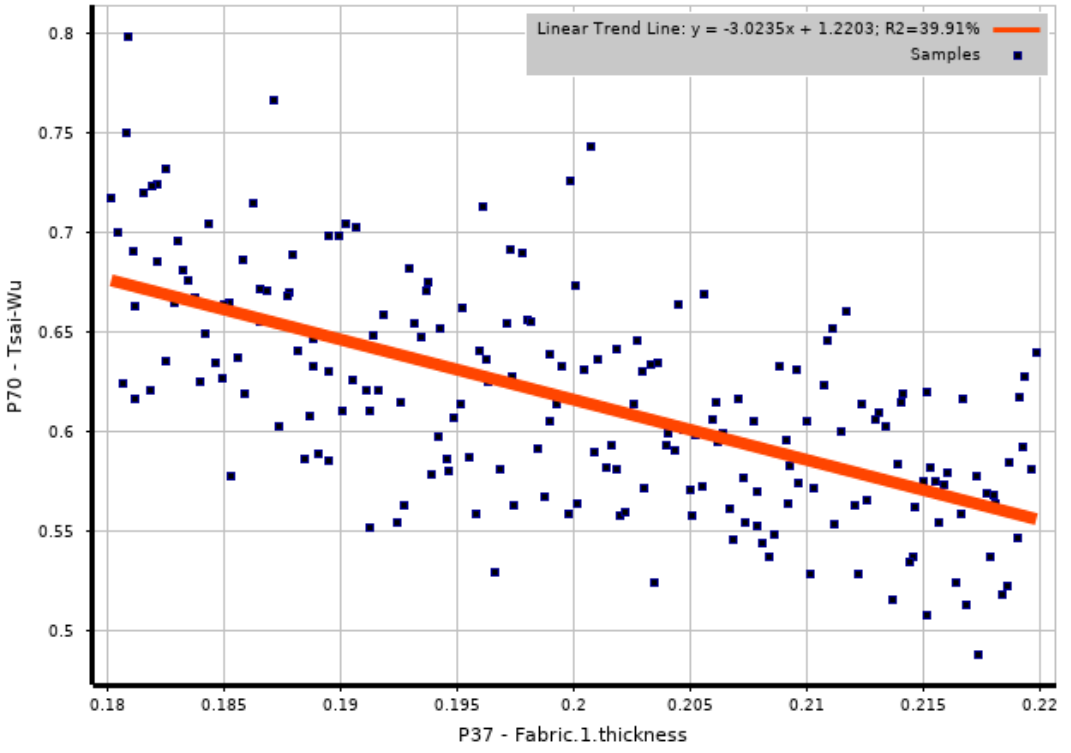

Figure 16: Correlation scatter diagram, Tsai-Wu vs. Ply thickness, Spearman, N=200

- **Parameters slightly or lowly correlated with failure criteria**

Also shown in Figure 14, parameters that have slight to low correlation with the failure criteria are Elastic modulus E_2, tensile stress σ_{u2}, shear stress τ_{u12} and inner diameter D. The correlation coefficients of these parameters are listed in Table 10:

Table 10: Correlation Coefficient of Slightly Correlated Parameters

	Tsai-Wu	Max Stress	Hashin
Elastic modulus E_2	0.252	0.447	0.320
Tensile Strength σ_{u2}	-0.273	-0.446	-0.334
Shear strength τ_{u12}	-0.429	-0.136	-0.339
Inner diameter D	-0.145	-0.262	-0.125

Except for the pressure, the bending moment is the second highest within the four loads. It is because that the flowline is easily influenced by the loads related to the z-directions. It is noted that E_2 and σ_{u1} have moderate correlation with the Maximum Stress criterion, and τ_{u12} has a moderate correlation with Tsai-Wu criterion.

- **Most Failure Parameters have almost No Correlation with Failure Criteria**

Except for the parameters related to the z-direction, some parameters show very small correlations with the failure criteria (the absolute value of failure criteria smaller than 0.1). They are Poisson's ratios ν12, shear modulus G12, tensile strength σut1, compressive strength σuc1, axial force, bending and torsion. The reason could be that these parameters are less affected by the pressure, which is the dominant load of the case studied. The three Tsai-Wu constants also have very small correlations with the Tsai-Wu criteria. It is expected that a higher correlation could be found for a more complex case, where the pressure is not the only dominate load

4.4.1 Influence of Sample Size on Correlation Matrix

The correlation matrices for Spearman and Pearson correlation method with different sample size are illustrated in Figure 17 and Figure 18:

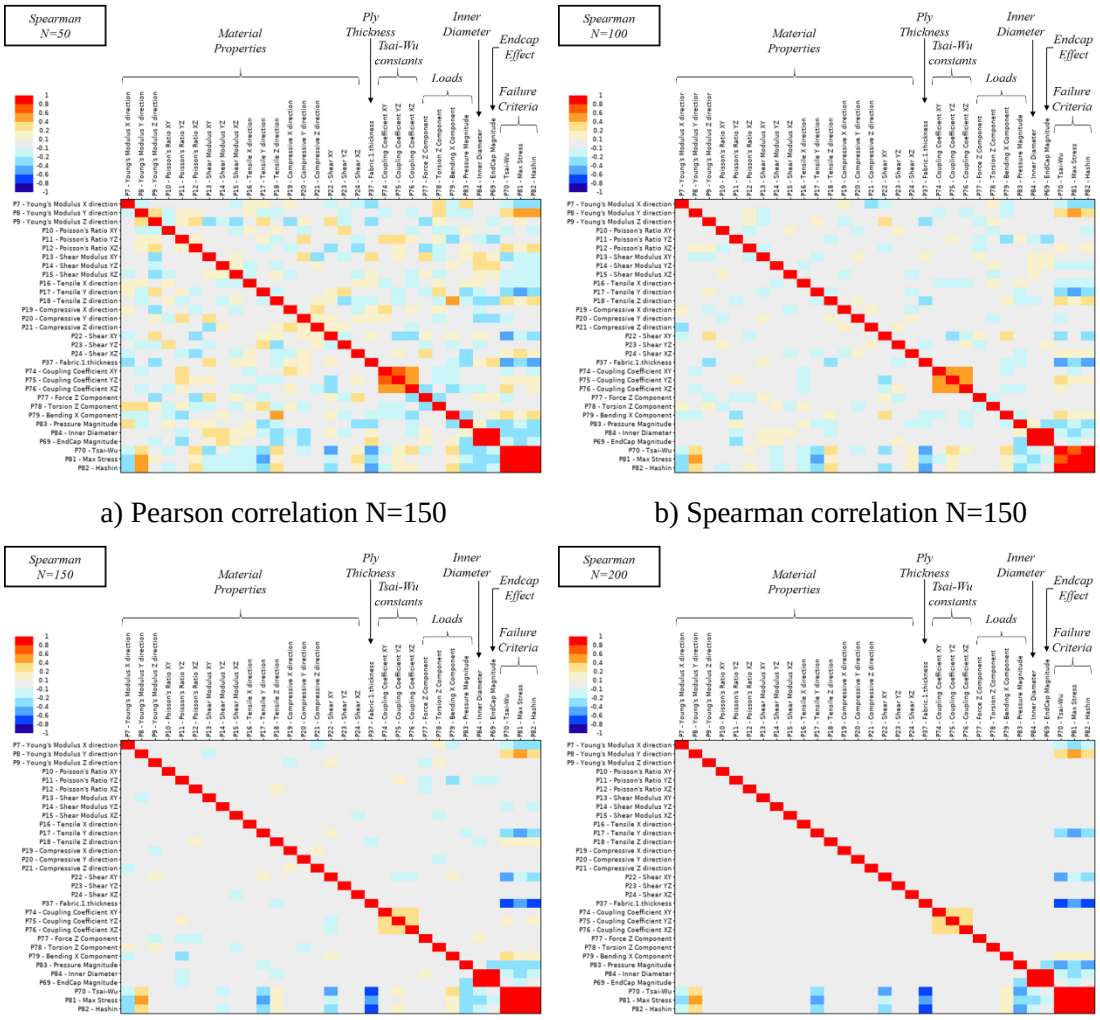

a) Pearson correlation N=150 b) Spearman correlation N=150

c) Pearson correlation N=200 d) Spearman correlation N=200

Figure 17: Linear correlation matrices with different sample size (Spearman)

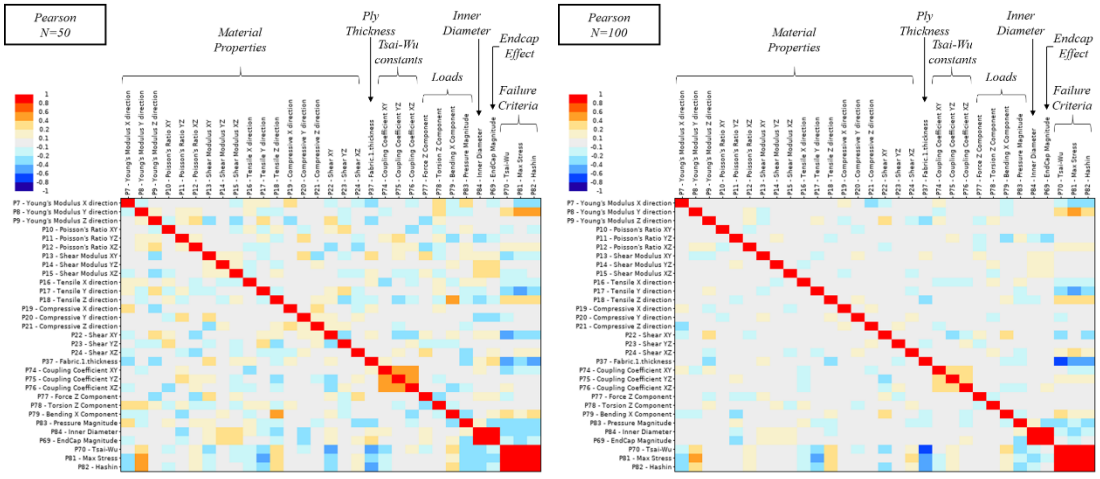

a) Pearson correlation N=50

b) Pearson correlation N=100

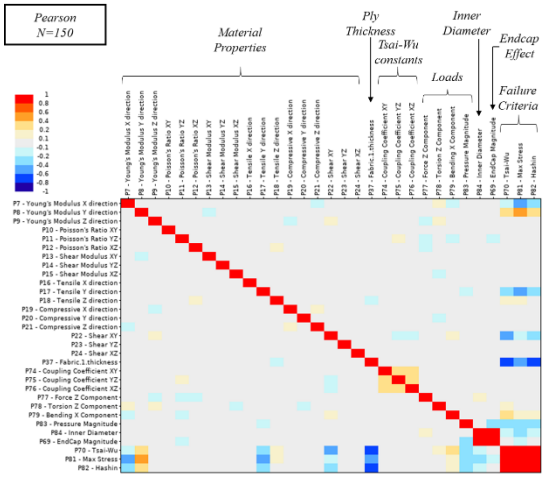

c) Pearson correlation N=150

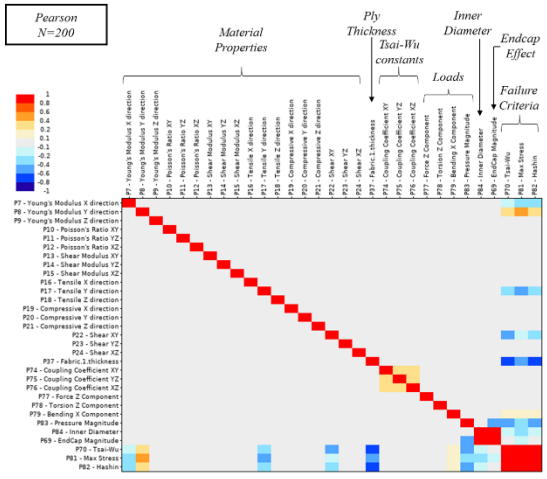

d) Pearson correlation N=200

Figure 18: Linear correlation matrices with different sample size (Pearson)

By observation of linear correlation matrices of Spearman and Pearson methods with a same sample size, we find that both two methods provide a similar result of correlation between parameters.

4.4.2 Influence of Correlation Method on Correlation Matrix

As shown in Figure 17 and Figure 18, for the Spearman correlation method and the Pearson correlation method, the number of samples used in the correlation matrix calculation significantly affects the correlation results. For the correlation coefficients between input parameters and the output parameters (failure criteria), the results show

a generally similar correlation. However, in the case of 50 samples used, the correlation matrices show a large scatter between input parameters. Besides the failure criteria, the parameters related to the material properties and loading are somehow correlated, which is unreasonable. With the number of samples increased, the correlation between these parameters become lighter. When 200 sample points are used, the correlations between these parameters are generally decayed, which means that the correlation matrix is finally 'converged'. The sample size of 200 is considered the most reasonable and accurate correlation matrix. For this reason, in the following study, the correlation matrix will go through with Spearman with sample size of 200.

4.5 Response Surface for Base Case

Table 11: Top 20 Most Influential Input Parameters

Parameters	Level of Correlation
Ply Thickness t Internal Pressure P	Moderate
Tensile Strength σ_{ut2} Elastic Modulus E_2	Low
Shear Strength τ_{u12} Inner Diameter D	Slight
Torsion T, Axial Force A Bending moment B Elastic Modulus E_1 Poisson's Ratio ν_{12}, ν_{23}, ν_{13} Shear Modulus G_{23}, G_{13} Tensile Strength σ_{ut1}, σ_{ut3} Shear Strength τ_{u23} Tsai-Wu constant F_{12}, F_{13}	Very slight

As mentioned in Section 4.4, Spearman method with sample size 200 is used to find the correlation coefficients between input parameters and failure criteria. The

generation of response surface needs to select 20 higher correlated parameters. According to Figure 14, the selected higher correlated parameters are listed in Table 11:

4.5.1 Range of Selected Parameters

The range of 20 selected input parameters used in the generation of the base case response surface is presented in Table 12. The range of these parameters will influence the accuracy of the response surface, which will be discussed in Section 6.

Table 12: Range of Input Parameters Used in Response Surface

Parameters	Symbol	Unit	Lower limit	Upper limit
Elastic Modulus	E_1	MPa	108900	133100
	E_2	MPa	7740	9460
Poisson's Ratio	ν_{12}, ν_{13}		0.243	0.297
	ν_{23}		0.36	0.44
Shear Modulus	G_{13}	MPa	4230	5170
	G_{23}	MPa	2790	3410
Tensile Strength	σ_{ut1}	MPa	2007.9	2454.1
	σ_{ut2}, σ_{ut3}		26.1	31.9
Shear Strength	τ_{u12}	MPa	54	66
	τ_{u23}	MPa	28.8	35.2
Tsai-Wu Constants	F_{12}, F_{13}		-1	1
Ply Thickness	t	mm	0.18	0.22
Inner Diameter	D	mm	88	138
Internal Pressure	P	MPa	6.21	7.59
Axial Force	A	N	18000	22000
Bending moment	B	Nm	1800	2200
Torsion	T	Nm	1800	2200

4.5.2 Response Value and Measured Value

The comparison of the response results calculated by different types of response surface are listed in Table 13.

Table 13: Response Value Comparison of Different Response Surface Types

Failure Criteria		Maximum Stress	Tsai-Wu	Hashin
Measured Values		0.508	0.595	0.592
Response Values	Kriging	0.506	0.593	0.591
	Non-Parameters	0.506	0.591	0.590
	Neural Network	0.506	0.593	0.590
	GA	0.507	0.594	0.591

As shown in Table 13, the different types of response surface generally show closed results for the three failure criteria compared to the measured values. The Genetic Aggregation gave the most accurate response results compared to others. However, the generation Genetic Aggregation requires much more time compared to the others, which reduce the efficiency of obtaining the response surface. By observing the response results except the Genetic Aggregation, the Kriging response surface provide a second-best response accuracy. Meanwhile, as introduced in Section 2.3, the Kriging response surface method provide an auto-refinement process, which is more convenient to refine the response surface. Therefore, the Kriging response surface is chosen as the response surface model in the following studies to predict the failure criteria and the failure rates.

5 Stochastic Process Using Response Surface

5.1 Generation of Measured Values

A set of measured values is generated to be used as the reference population, which is called “Base Case”. The mean and standard deviation of the input parameters used in Base Case are presented in Table 14. The input parameters are normally distributed.

Table 14: Mean and Standard Deviation of Input Parameters Used in Base Case

Parameter	Symbol	Unit	Mean	Standard Deviation
Elastic Modulus	E_1	MPa	121000	3630
	E_2, E_3	MPa	8600	258
Poisson’s Ratio	ν_{12}, ν_{13}	-	0.27	0.0081
	ν_{23}	-	0.4	0.012
Shear Modulus	G_{13}	MPa	4700	141
	G_{23}	MPa	3100	93
Tensile Strength	σ_{ut1}	MPa	2231	66.93
	σ_{ut2}, σ_{ut3}	MPa	29	0.87
Compressive Strength	σ_{uc1}	MPa	-1082	-32.46
	σ_{uc2}, σ_{uc3}	MPa	-100	-3
Shear Strength	τ_{u12}, τ_{u13}	MPa	60	1.8
	τ_{u23}	MPa	32	0.96
Internal pressure	P	MPa	-6.9	-0.207
Axial Force	A	N	20000	600
Bending	B	N • m	2000	60
Torsion	T	N • m	2000	60
Tsai-Wu Constants	F_{12}, F_{23}, F_{13}		0	0.3
Inner Diameter	D	mm	113	8.75
Thickness	t	mm	0.2	0.01

Using the values in Table 14, the random input parameters are generated using Monto Carlo simulation with normal distribution. Examples of cumulative probability distributions for the Elastic Modulus E_1, Inner Diameter D, Internal Pressure P are

plotted in Figure 19, Figure 20 and Figure 21. These random parameters are used to calculate the “Measured Values”, which are considered as the actual values obtained from the actual experiments.

It is obvious that larger population size will provide more continuous distribution, but meanwhile it will consume a longer time. Thus, it is necessary to determine a suitable population size. A convergence study of statistical moments is presented in Section 5.1.1 with a total population size of 500. The population size of 200 is chosen for the following study where the statistical moments are generally converged.

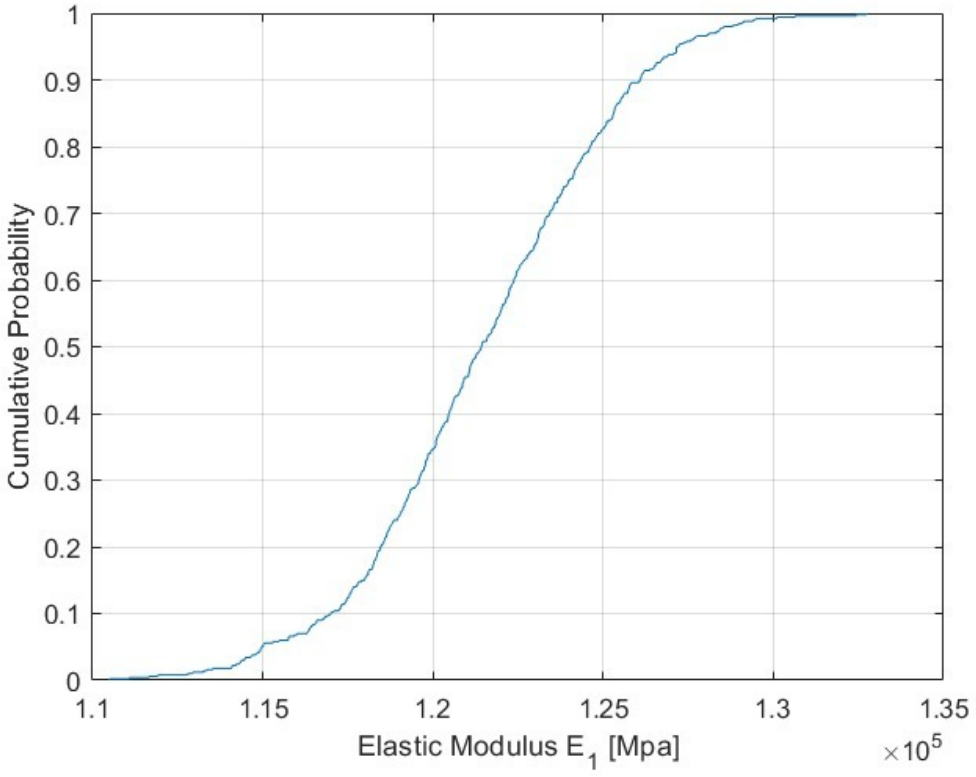

Figure 19: Cumulative probability distribution of elastic modulus E_1

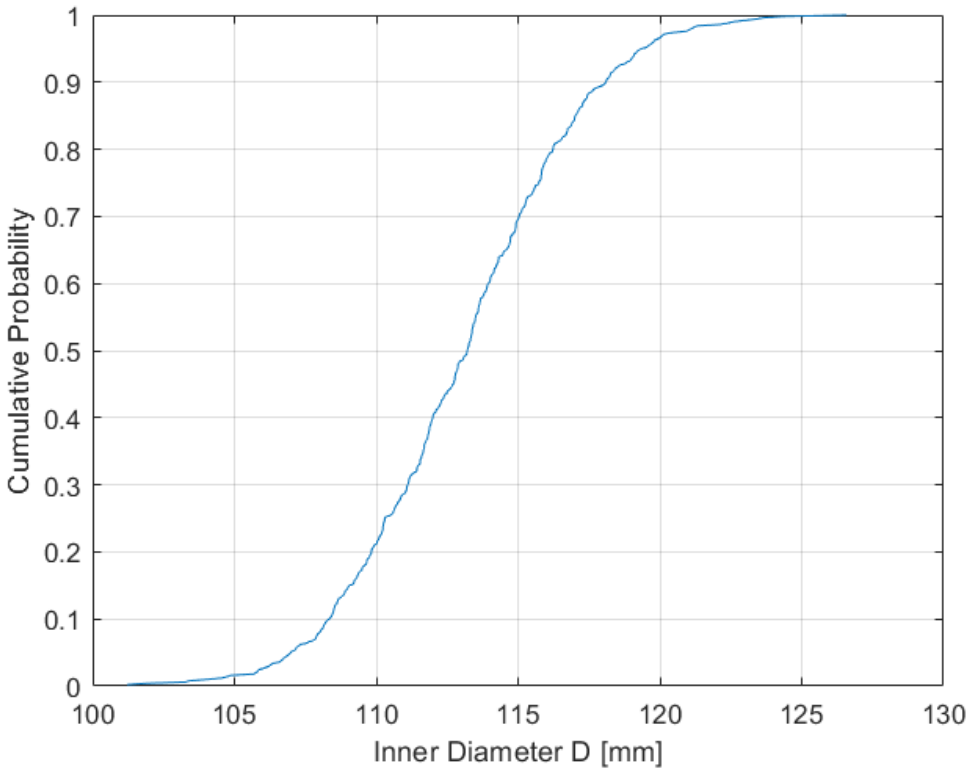

Figure 20: Cumulative probability distribution of inner diameter D

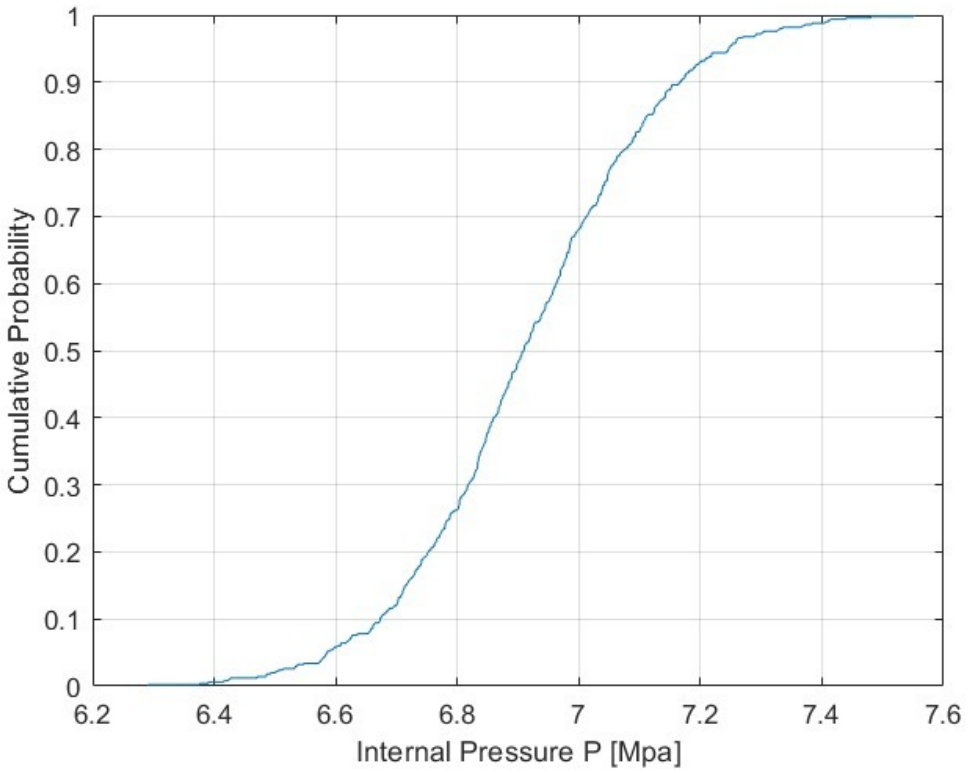

Figure 21: Cumulative probability distribution of internal pressure P

5.1.1 Convergence Study on Population Size

The convergence of statistical moments is studied to find an enough size of the population. Mean, standard deviation, skewness and kurtosis with different sample sizes are illustrated in Figure 22. The percentage difference for the same statistical moments shown in Figure 23 are compared with the values when the population size is 500. The percentage difference is calculated by the formula presented in Equation (17).

$$\% \text{ Difference} = \frac{Current\ value - Value\ @\ N = 500}{Value\ @\ N = 500} \times 100\% \qquad (17)$$

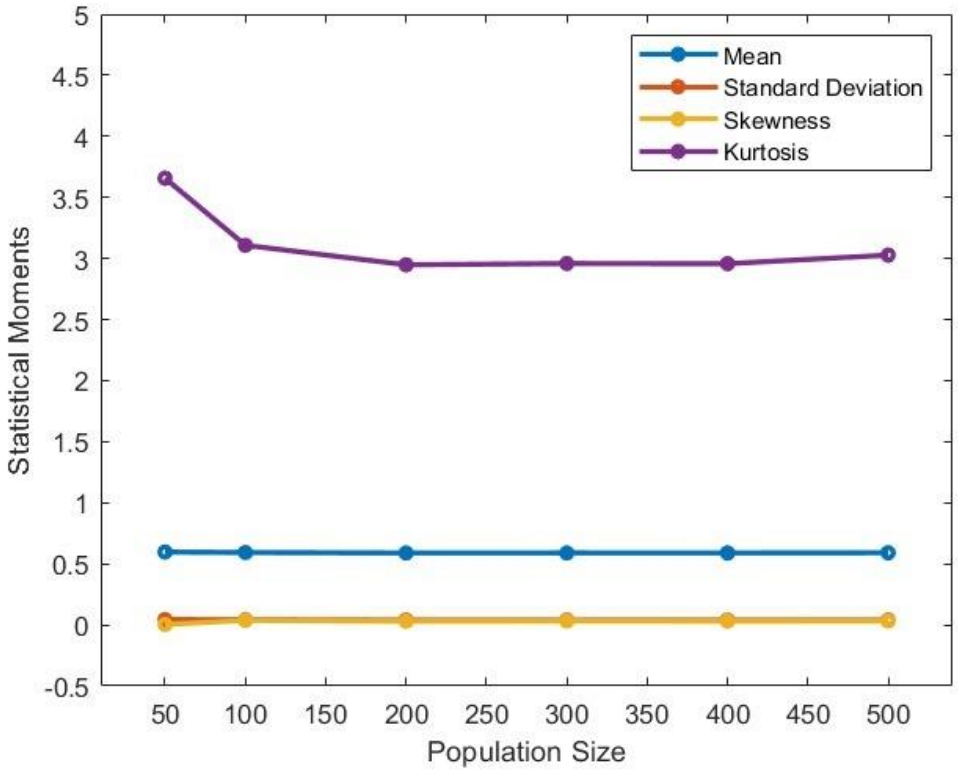

Figure 22: Values of Statistical moments vs Population Size

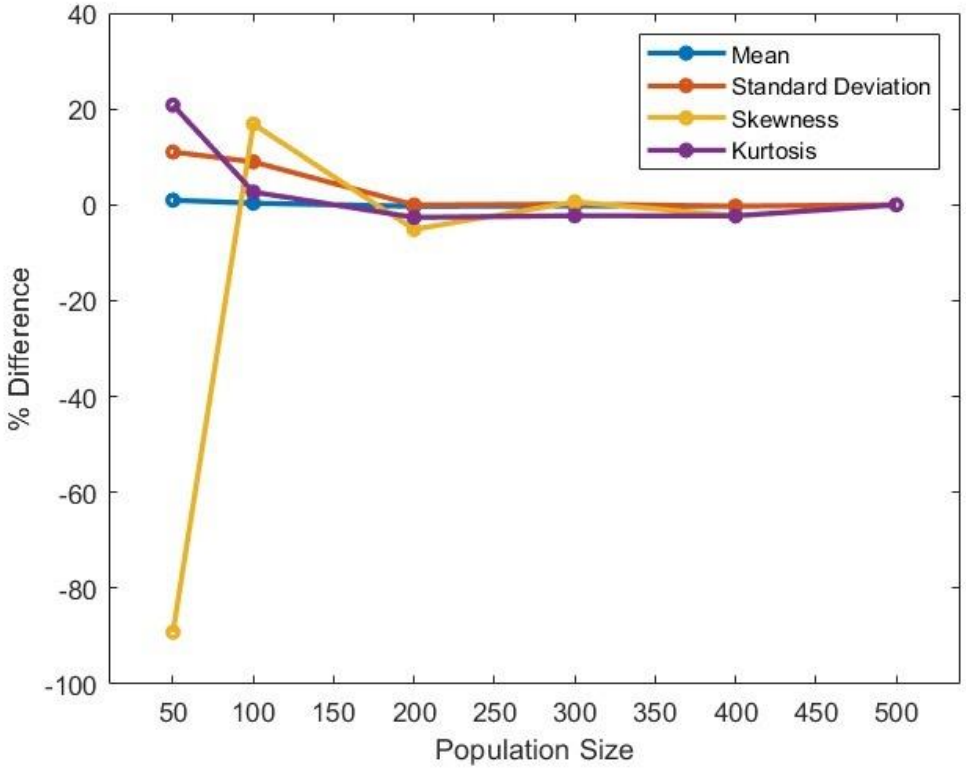

Figure 23: % difference of statistical moments values compared to population size (N=500)

The results presented in Figure 22 and Figure 23 show that converged statistical moments are obtained for a population size larger than 200. The sample size of 200 is considered more efficient and used in other cases. For the "Base Case", the sample size of 500 that have been calculated in the convergence study is more accurate.

5.1.2 Fitting Statistical Models to Measured Values

The exceedance probabilities (i.e., failure rates.) are considered the purpose of the stochastic process. In this section, fitting the measured values of 500 sample size to a suitable statistic model is studied. The Matlab distribution fitting tool is used. Four statistical distributions are used and compared the goodness of fitting, namely Exponential, Lognormal, Weibull and Normal. The fitting results are plotted in Figure 24 and Figure 25.

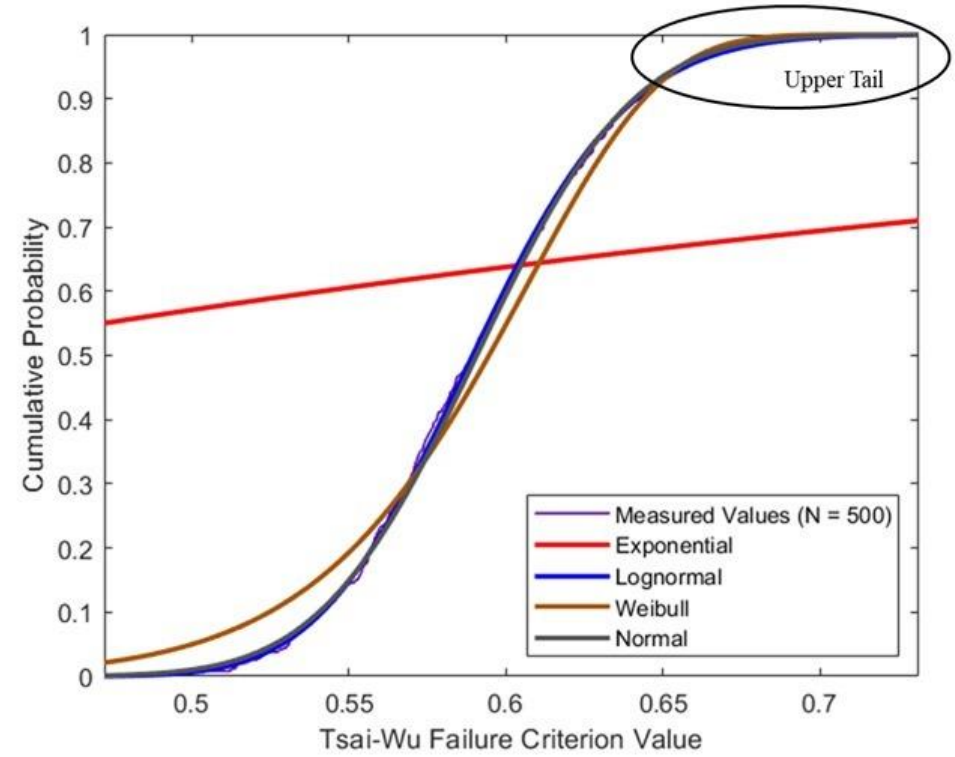

Figure 24: Statistical models fitted to measured values

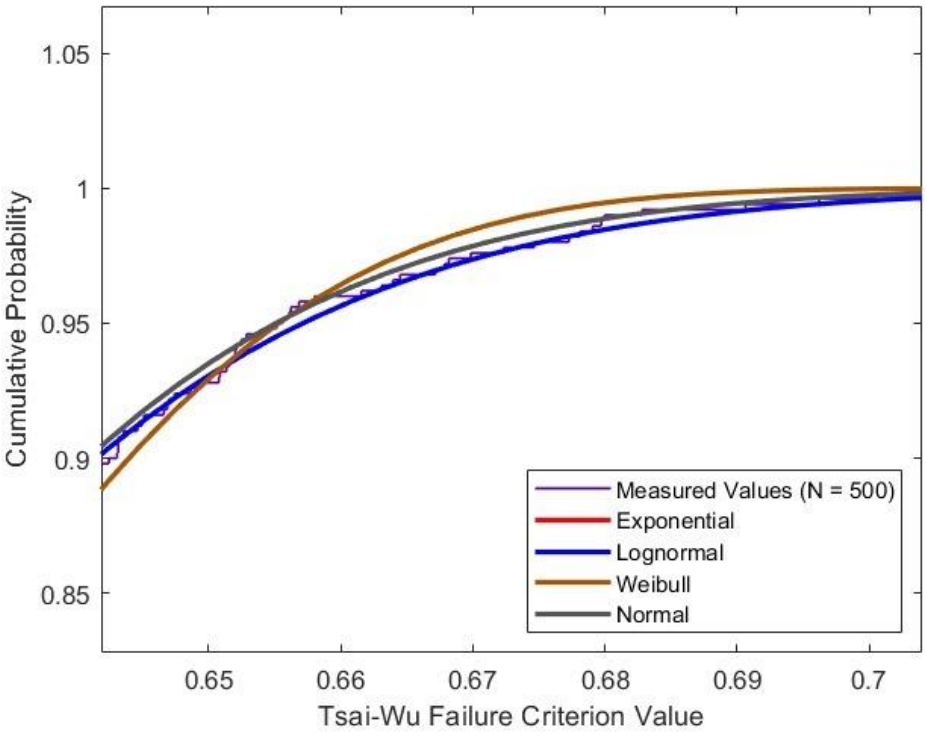

Figure 25: Statistical models fitted to measured values, zoom-In at upper tail region

As observed in Figure 24, the small differences exist between Lognormal, Weibull and Normal distribution, while the Exponential distribution has larger difference. With a closer inspection of the upper tail region (last 50 samples of the 500 samples population) as shown in Figure 25, small differences can be distinguished with the Weibull distribution, while the Lognormal and Normal distribution still difficult to differ. To evaluate the goodness of fitting, the corresponding R^2 values are calculated in Table 15. It is noted that the R^2 values closer to 1 represent better goodness of fitting.

Table 15: R^2 Value of Four Statistical Models

Statistical Model	Exponential	Lognormal	Normal	Weibull
R^2 Value	0.960	0.999	0.998	0.987

The R^2 values of the upper tail region suggest that the Lognormal distribution is a better statistical model fitted to the measured values compare to the Normal distribution. It is noted that the upper tail region is considered important for the prediction of the failure rates, which is the purpose of this study. Considering the better goodness of fitting at the upper tail region, the Lognormal distribution is chosen as the statistical distribution used to fit the measure values in the following studies.

5.1.3 Failure Rate Calculation

The lognormal distribution is adapted to fit the 500 measured values as mentioned above. The related exceedance rates are calculated based on the lognormal fitting distribution. The results are listed in Table 16.

Table 16: Failure Results at Different Failure Rates for Measured Values

Failure Criteria	Failure rate = 10^{-4}	Failure rate = 10^{-5}	Failure Rate = 10^{-6}
Maximum Stress	0.643	0.667	0.689
Tsai-Wu	0.754	0.782	0.808
Hashin	0.758	0.785	0.810

5.2 Using Response Surfaces for Prediction of Failure Rates

Kriging response surface is used to predict the failure results. In this section, using the kriging response surface to predict the failure rate is discussed. Compared to the failure rates calculated in Section 5.1.3, this method suggests an efficient way to calculate the required size of failure results, which provides time savings to calculate the failure rates.

The study of the failure rate prediction using the Kriging response surface is carried out. First, the statistical moments are compared between the samples generated from the measured values, response values, and their lognormal fitting distributions, respectively. Then, the probability density and cumulative distribution are plotted and compared. In the end, the failure rates will be calculated for the response value fitted to lognormal distribution and compared with the measured value fitted to the lognormal distribution. A workflow is presented in Figure 26.

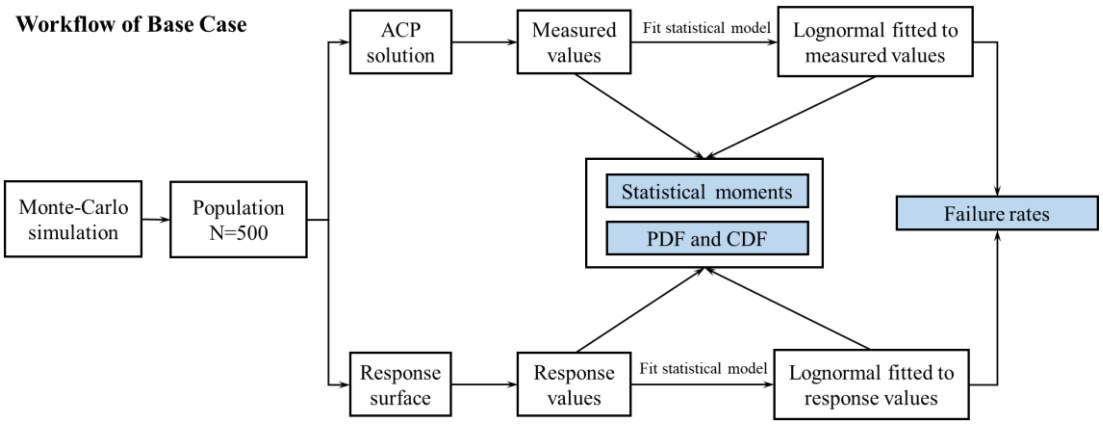

Figure 26: Workflow used to compare the response accuracy

5.2.1 Comparison of Statistical Moments

As shown in Figure 26, four groups of results will be compared with statistical moments, PDF and CDF, they are Measured values, Lognormal distribution fitted to measured values, Response values and Lognormal distribution fitted to response values. The source of these four results are explained as follow:

- Measured values: These are 500 sample points calculated directly from the finite element model using ACP solution. These 500 samples are considered as accurate as the samples measured from experiments.
- Lognormal distribution fitted to measured values: This is a Lognormal distribution fitted to “Measured values”.
- Response values: These are 500 sample points calculated from the kriging response surface.
- Lognormal distribution fitted to response values: This is a Lognormal distribution fitted to “Response values”.

The statistical moments of the four groups of results are listed in

Table **17**, the percentage differences in the brackets are calculated with respect to "Measured values" using Equation (18):

$$\% \text{ Difference} = \frac{Current\ value - value\ of\ Measured\ values}{value\ of\ Measured\ values} \times 100\% \quad (18)$$

Table 17: Comparison of Statistical Moments

Source	Mean	Standard Deviation	Skewness	Kurtosis
Measured values, 500 samples	0.591	0.039	0.232	3.027
Lognormal distribution fitted to measured values	0.591 (0.0%)	0.039 (0.1%)	0.199 (-14.1%)	3.071 (1.4%)
Response surface, 500 samples	0.592 (0.3%)	0.036 (-8.5%)	0.209 (-9.8%)	2.980 (-1.6%)
Lognormal distribution fitted to response values	0.592 (0.3%)	0.036 (-8.6%)	0.182 (-21.7%)	3.059 (1.0%)

The following observations are made from the results presented in Table 17:

- The difference between the mean of the four groups of results are negligible.
- The standard deviation of the response values is about 8.5% smaller than the measured values. The lognormal fitted to response values showed a similar result (-8.6%). This difference may lead to the difference on the failure rate prediction, we will discuss later.
- Large differences exist in the skewness values of the four groups. The response values gave a 10% smaller skewness compared to the measured values, and both fitting distributions gave an extra 12% ~ 14% smaller skewness value.
- The difference between the four Kurtosis values are small, all beyond 2%.

5.2.2 Comparison of Probability and Cumulative Distribution Plots

The comparisons of the probability density and cumulative distribution for the four groups of results are presented in Figure 27 and Figure 28. The following observations are made:

- There are small differences between the lognormal fitting distributions to the raw data, i.e., Measured values and Response values, the fitted distribution curves overlap the Measured values' and Response values' curves.
- The Response values have a higher probability density at the most probable value, see area A in Figure 27.
- As observed in Figure 28, there are some differences in the tail regions of the cumulative probability distribution curves. However, the difference is not significant, which leads to the differences between calculated failure rates become negligible, which will discuss in Section 5.2.3.

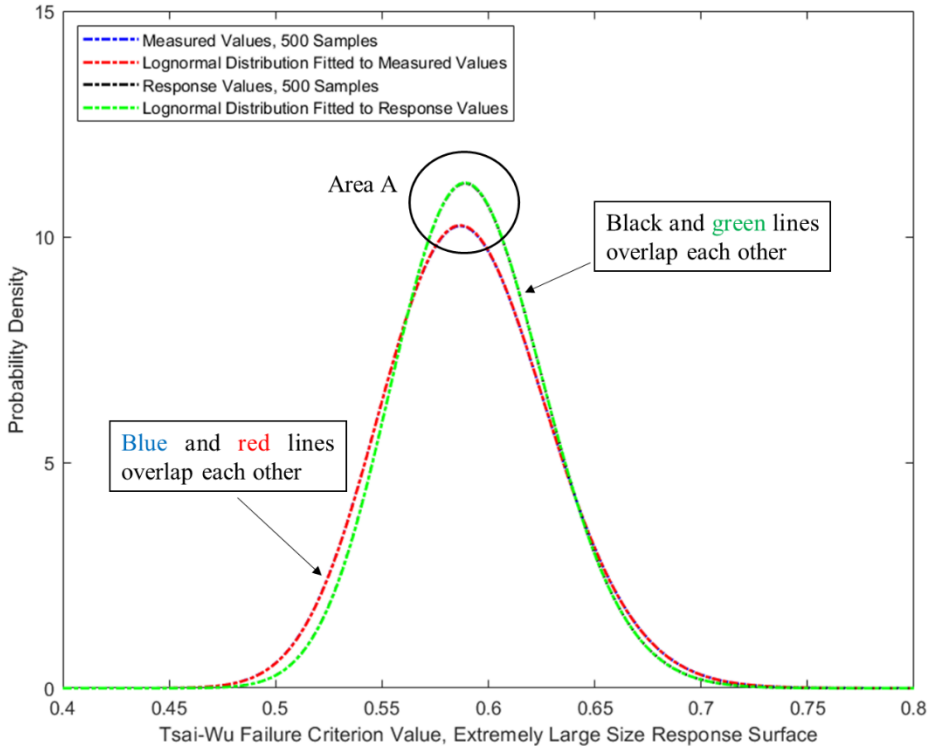

Figure 27: Comparison of probability density functions

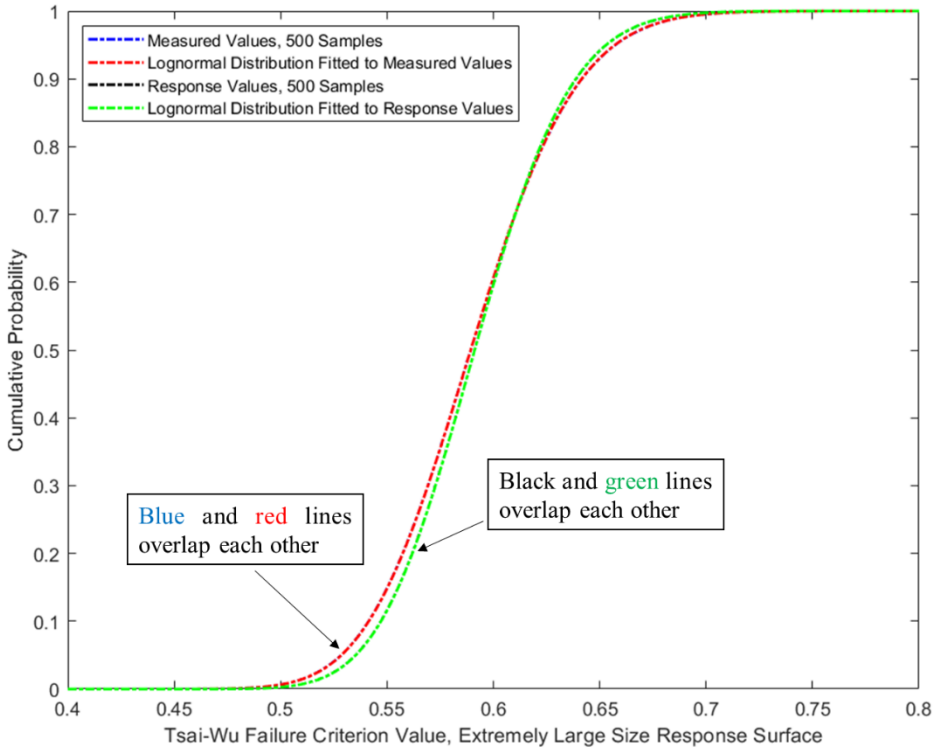

Figure 28: Comparison of cumulative probability distribution functions

5.2.3 Comparison of Failure Values

The above studies suggest that the lognormal distribution fitted to measured values can predict accurate failure rates. In this section, the accuracy of the failure rates predicted by response surface are compared, the comparisons are shown in Table 18.

Table 18: Comparison of Failure Values

Source	Failure Criterion	Failure rate = 10^{-4}	Failure rate = 10^{-5}	Failure Rate = 10^{-6}
Lognormal distribution fitted to measured values	Maximum Stress	0.64	0.67	0.69
	Tsai-Wu	0.75	0.78	0.81
	Hashin	0.76	0.79	0.81
Lognormal distribution fitted to response values	Maximum Stress	0.64 (0.0%)	0.66 (-1.5%)	0.68 (-1.4%)
	Tsai-Wu	0.74 (-1.3%)	0.77 (-1.3%)	0.79 (-2.5%)
	Hashin	0.75 (-1.3%)	0.78 (-1.3%)	0.80 (-1.2%)

The difference of predicted failure rates can be calculated using Equation (19):

$$\%\ \text{Difference} = \frac{\text{Current value} - \text{value predicted by measured values (Lognormal fitted)}}{\text{value predicted by to measured values (Lognormal fitted)}} \times 100\% \quad (19)$$

The comparisons reveal that the failure rates predicted by the response surface are very close to the failure rates predicted by the measured values, which is considered the results of actual failure rates. Therefore, the Kriging response surface can be used as a reliable tool for failure prediction of the CFEC flowline subjected to combined loads.

6 Optimising Response Surface Generation

6.1 Number of Input Parameters

The number of selected input parameters determined the number of sample points used to generate the response surface. In the previous study in Section 4.5 and 5, 20 parameters were used to generate the response surface, where more than 500 samples are created in the design of experiments. In this section, the reduced accuracy caused by fewer selected input parameters are studied. Using a smaller number of input parameters requires a smaller size of samples in the design of experiments, as listed in Table 19.

Table 19: Size of Design of Experiment for Different Number of Input Parameters

Number of Input Parameters	**20**	**15**	**10**	**5**
Size of Design of Experiment, Number of Samples	551	287	149	27
Minimum Parametric Correlation Value	0.046	0.079	0.131	0.271

As observed in Table 19, the required size of the design of experiments reduced with the decrease of the selected parameters significantly, i.e., choosing 10 parameters will reduce 70% required size of samples compared to 20 parameters. The effect on the statistical moments, probability distributions and predicted failure value are presented in subsection 6.1.1, 6.1.2 and 6.1.3.

6.1.1 Number of Parameters - Effect on Statistical Moments

Four response surfaces are generated with different number of selected parameters mentioned in Table 19. The calculated statistical moments of Tsai-Wu response values

are presented in

Figure **29** together with the ‘Measured Values’ and ‘Lognormal fitted to Measured Values’.

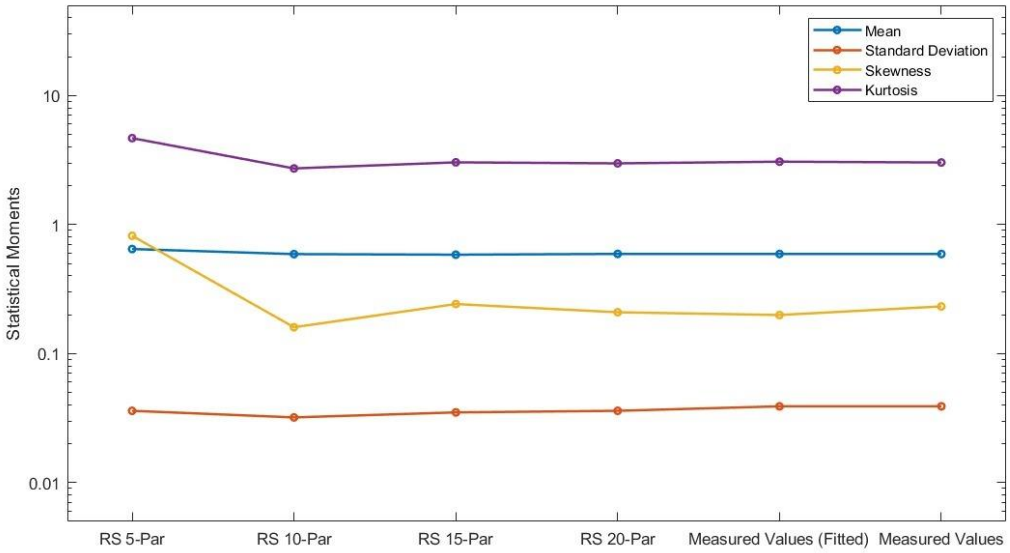

Figure 29: Number of parameters – Effect on statistical moments

The corresponding percentage differences compared with the measured values are presented in

Figure **30**. The calculation of percentage difference is using Equation (18), which introduced in Section 5.2.1.

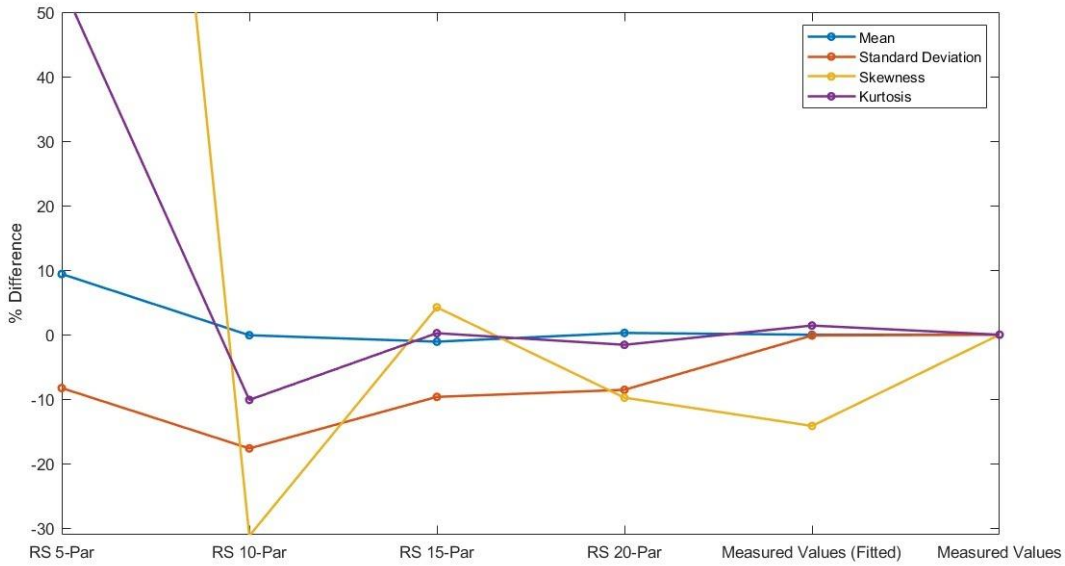

Figure 30: Number of parameters – Effect on statistical moments (% difference)

The statistical moments values and calculated percentage difference are listed in Table 20.

Table 20: Statistical Moments of Different Parameter Number and Measured Values

Source		**Mean**	**Standard Deviation**	**Skewness**	**Kurtosis**
Measured Values		0.591	0.039	0.232	3.027
Lognormal Distribution Fitted to Measured Values		0.591 (0.0%)	0.039 (0.1%)	0.199 (-14.1%)	3.071 (1.4%)
Response Value	20-Parameters Response Surface (Base Case)	0.592 (0.3%)	0.036 (-8.5%)	0.209 (-9.8%)	2.980 (-1.6%)
	15-Parameters Response Surface	0.584 (-1.1%)	0.035 (-9.6%)	0.242 (4.2%)	3.035 (0.2%)
	10-Parameters Response Surface	0.590 (-0.1%)	0.032 (-17.6%)	0.160 (-31.2%)	2.722 (-10.1%)
	5-Parameters Response Surface	0.646 (9.4%)	0.036 (-8.3%)	0.818 (253.0%)	4.673 (54.4%)

The following observations are made:

- The mean values are not significantly affected by the number of select parameters, especially for the cases that more than 10 parameters are selected, where the differences are within 1%.
- The standard deviations are moderately affected by the number of selected input parameters. The largest difference appears where 10 parameters are used, which doubles the difference calculated from the case where 20 parameters are used (from -8.5% to -17.6%).
- The skewness values are significantly affected by the number of selected parameters. The skewness calculated from the 20 parameters response surface (Base Case) is 10% and increased to 250% when 5 parameters are used. These effects of statistical moments on the failure rates.
- The kurtosis values are fairly affected by the number of selected parameters, where the 15 parameters case has the smallest difference (0.2%), and 5 parameters case shows the largest difference (54.4%).

6.1.2 Number of Parameters – Effect on Fitted Probability Distributions

The probability density function and cumulative distribution of lognormal fitted distribution of response value with different numbers of selected input parameters are plotted in Figure 31, Figure 32, Figure 33 together with the Measured Values.

The following observations are made:

- An extremely large difference appeared when only 5 parameters are used. As shown in Figure 31 and Figure 32, both the distributions have a large bias.

- The probability density functions fitted from the response surface generally do not fit well with the measured values, as presented in Figure 31.
- For the cumulative distribution, the differences become small for most cases with larger size of selected parameters. By taking a close-up observation at the tail region of the cumulative distribution, as shown in Figure 33, the distances increase when fewer parameters are selected. However, these do not lead to large differences in the predicted failure values, which we will discuss in Section 6.1.3.

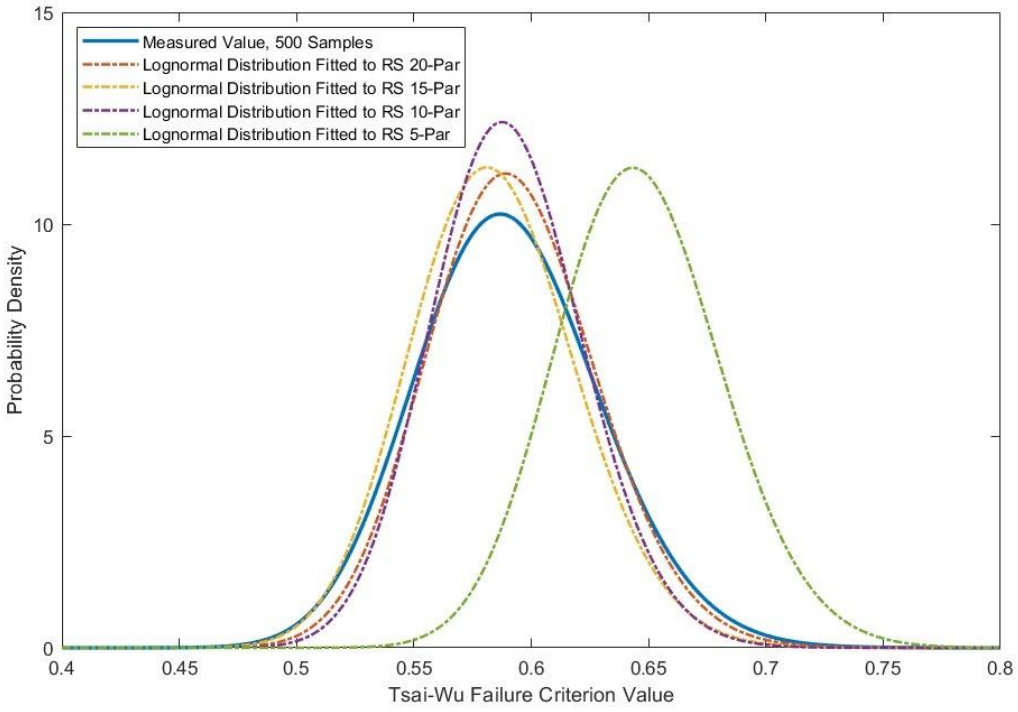

Figure 31: Number of parameters – Effect on probability density functions

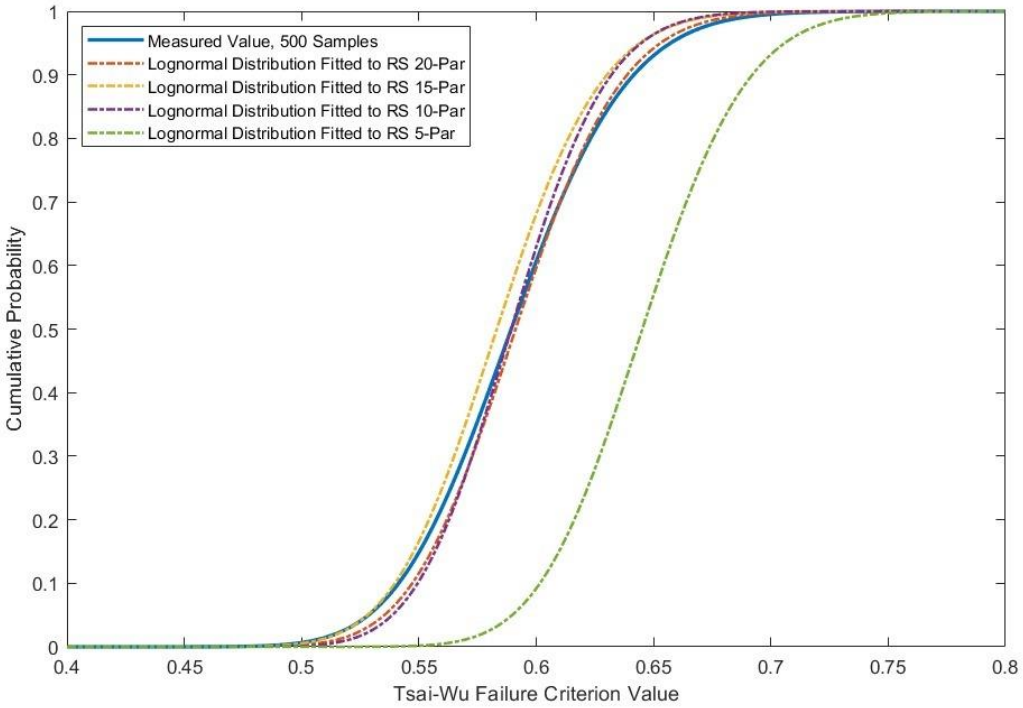

Figure 32: Number of parameters – Effect on cumulative probability functions

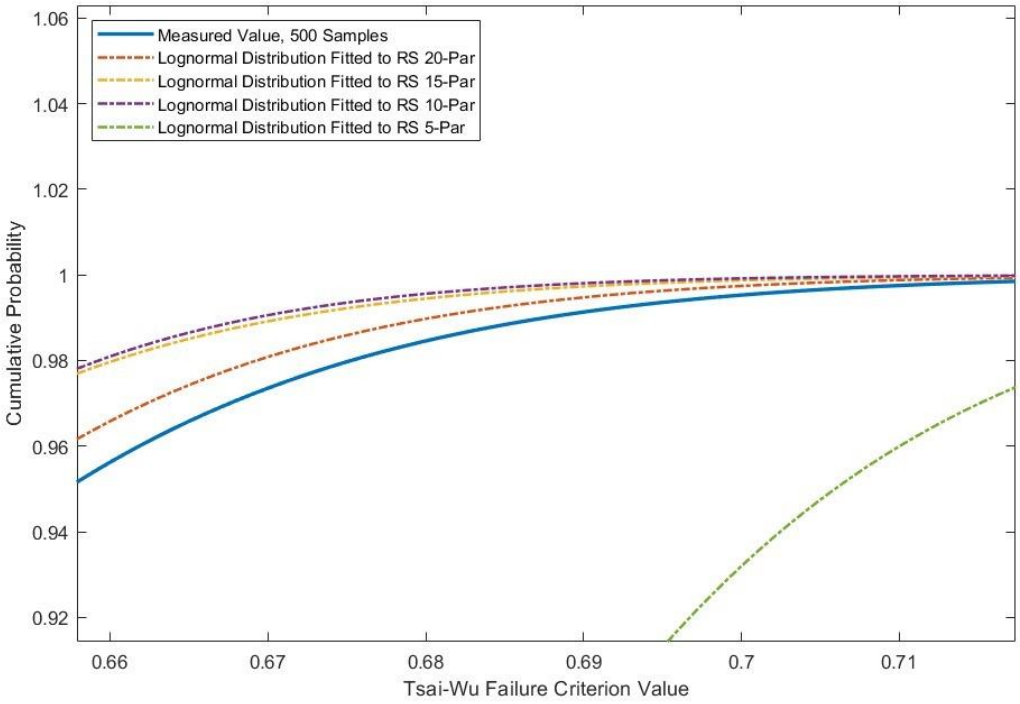

Figure 33: Number of parameters – Effect on cumulative probability functions

(Zoom-In at Upper Tail Region)

6.1.3 Number of Parameters – Effect on Predicted Failure Values

Table 21 compared the predicted failure rates and percentage differences calculated from the Lognormal distribution fitted to the response values, which produced by response surfaces generated by different numbers of selected parameters. The percentage differences are calculated by Equation (19) presented in Section 5.2.3. As observed from Table 21, with selected parameters reduced to 10, the results do not show a poor accuracy, where the largest difference is Tsai-Wu failure value calculated at failure rate of 10^{-6}. The differences caused by the reduced selected are small. It is acceptable that the failure rates of lognormal distribution fitted to Measured values can be considered as the actual failure rates, which is enough accurate. The results are coincident with the previous discussion, that the number of parameters will not significantly affect the results unless the number of selected parameters is much smaller than the total parameters, i.e. 5 parameters are used. It is noted that the results of 10 selected parameters are still acceptable, where the minimum correlation coefficient is 0.131, as listed in Table 19. This suggests that the parameters which have correlation coefficients larger than 0.13 are better selected to ensure an acceptable accuracy.

Table 21: Number of Parameters – Effect on Predicted Failure Values

Source	Failure Criterion	Failure Rate = 1 in 10^4	Failure Rate = 1 in 10^5	Failure Rate = 1 in 10^6
Lognormal distribution fitted to measured values	Maximum Stress	0.64	0.67	0.69
	Tsai-Wu	0.75	0.78	0.81
	Hashin	0.76	0.79	0.81
Lognormal distribution fitted to response values (20 input parameters)	Maximum Stress	0.64 (0.0%)	0.66 (-1.5%)	0.68 (-1.4%)
	Tsai-Wu	0.74 (-1.3%)	0.77 (-1.3%)	0.79 (-2.5%)
	Hashin	0.75 (-1.3%)	0.78 (-1.3%)	0.80 (-1.2%)
Lognormal distribution fitted to response values (15 input parameters)	Maximum Stress	0.64 (-1.6%)	0.67 (-3.0%)	0.69 (-1.4%)
	Tsai-Wu	0.75 (-2.7%)	0.78 (-2.6%)	0.81 (-3.7%)
	Hashin	0.76 (-2.6%)	0.79 (-2.5%)	0.81 (-2.5%)
Lognormal distribution fitted to response values (10 input parameters)	Maximum Stress	0.64 (0.0%)	0.66 (-1.5%)	0.68 (-1.4%)
	Tsai-Wu	0.74 (-4.0%)	0.77 (**-5.1**%)	0.79 (**-6.2**%)
	Hashin	0.75 (-1.3%)	0.78 (-1.3%)	0.8 (-1.2%)
Lognormal distribution fitted to response values (5 input parameters)	Maximum Stress	0.63 (**15.6**%)	0.65 (**14.9**%)	0.68 (**15.9**%)
	Tsai-Wu	0.73 (**5.3**%)	0.76 (**5.1**%)	0.78 (3.7%)
	Hashin	0.74 (2.6%)	0.77 (2.5%)	0.79 (2.5%)

6.2 Size of Response Surface

To improve the efficiency of the response surface, another approach is to increase the available range of the input parameters to enlarge the size of the response surface, which allows the response surface can be applied to more design cases. In this section, the effects of the response surface size are studied. The inner diameter and the ply thickness are selected to enlarge the response surface size. Two larger response surfaces are generated using the same approach with the "Base Case", namely "Larger Size" and "Extremely Large Size". The illustration of response surface size is presented in Figure 34, the corresponding range of parameters are listed in Table 22.

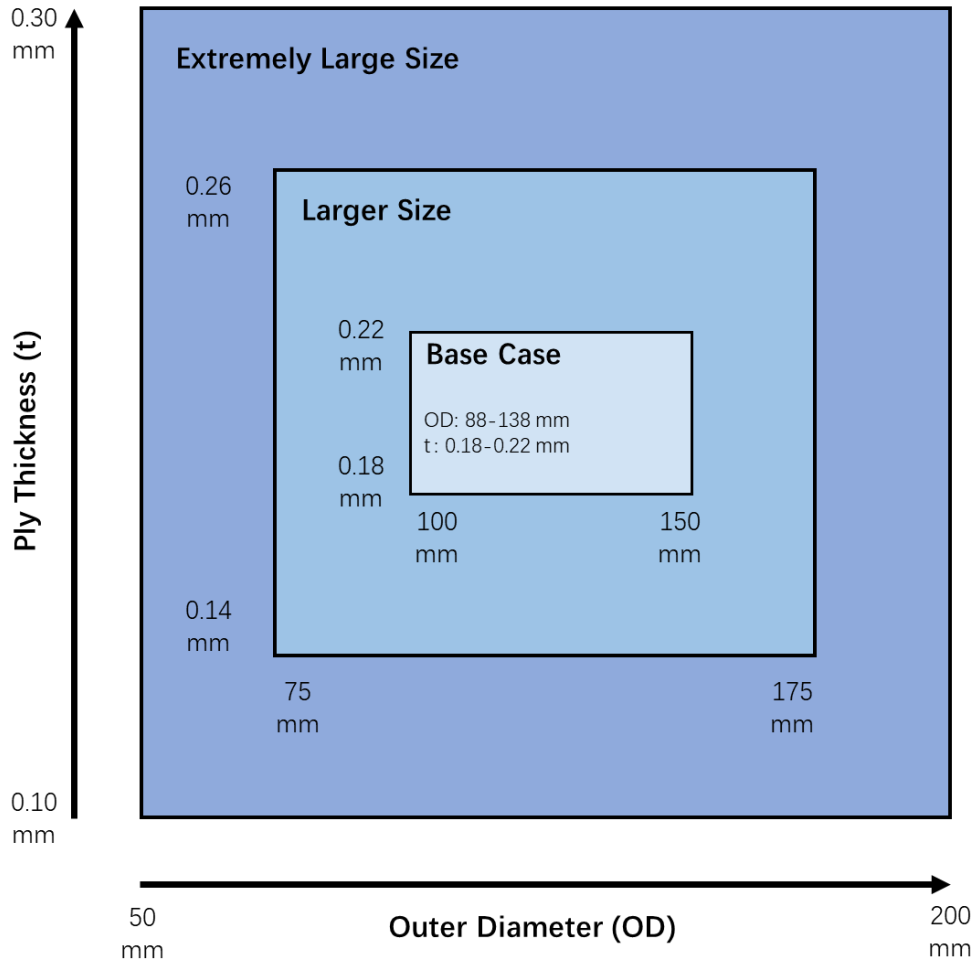

Figure 34: Different sizes of response surfaces

Table 22: Range of Diameter and Ply Thickness Studied

	Ply Thickness [mm]	**Diameter [mm] (Inner diameter)**
Base Case	0.18-0.22	100-150 (88-138)
Larger Size	0.14-0.26	75-175 (63-163)
Extremely Larger Size	0.10-0.30	50-200 （38-188）

The effects of response surface size on statistical moments, probability distributions and predicted failure values are presented and discussed in subsection 6.2.1, 6.2.2 and 6.2.3.

6.2.1 Size of Response Surface - Effect on Statistical Moments

The statistical moments of the response value calculated from “Larger size” and “Extremely Large size” response surfaces are calculated and compared with the “Base Case”, together with “Measured Values” and “Lognormal distribution fitted to Measured Values”, as shown in Figure 35.

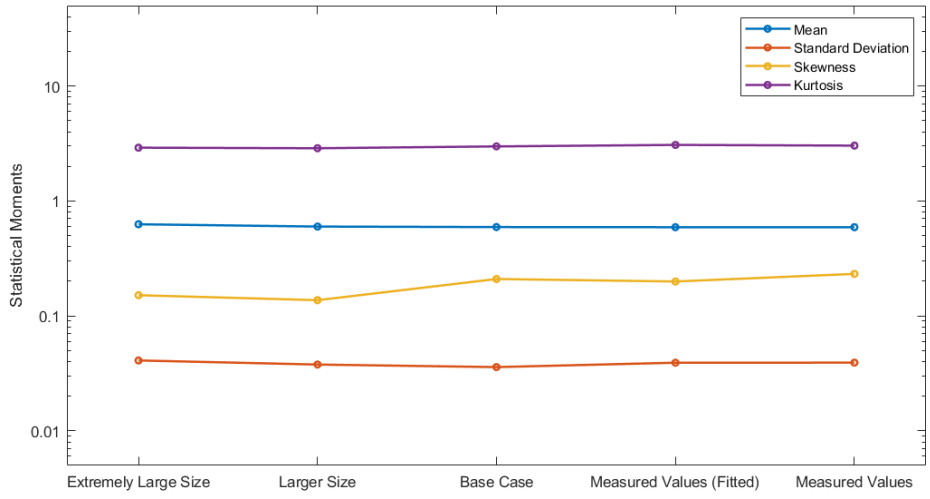

Figure 35: Size of response surface – Effect on statistical moments

The percentage differences compared with the measured values are calculated and illustrated in Figure 36.

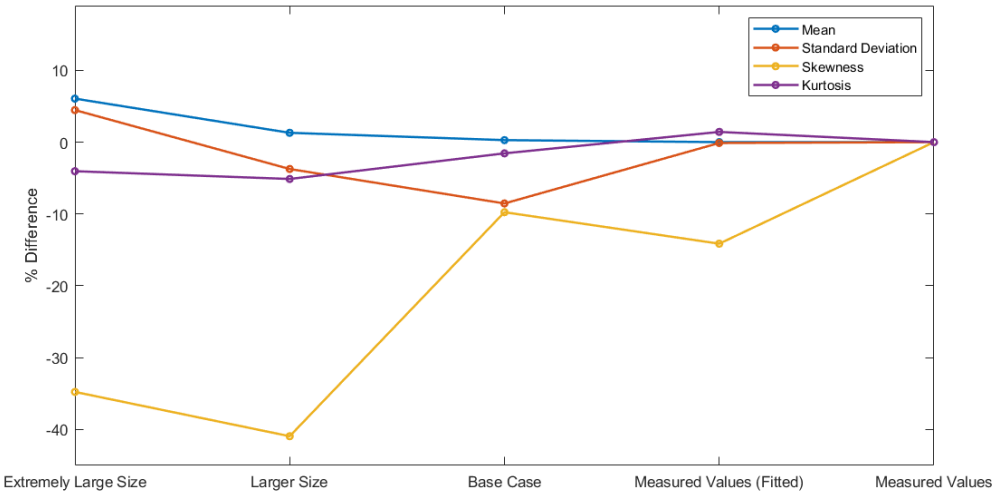

Figure 36: Size of response surface – Effect on statistical moments (% difference)

The values of statistical moments and corresponded percentage difference are listed in Table 23.

Table 23: Comparison of Statistical Moments of Different Response Surface Size

Source		**Mean**	**Standard Deviation**	**Skewness**	**Kurtosis**
Measured Values		0.591	0.039	0.232	3.027
Lognormal Distribution Fitted to Measured Values		0.591 (0.0%)	0.039 (0.1%)	0.199 (-14.1%)	3.071 (1.4%)
Response Value	Base Case	0.592 (0.3%)	0.036 (-8.5%)	0.209 (-9.8%)	2.980 (-1.6%)
	Larger Size	0.598 (1.3%)	0.038 (-3.7%)	0.137 (-40.9%)	2.872 (-5.1%)
	Extremely Large Size	0.626 (6.1%)	0.041 (4.5%)	0.151 (-34.8%)	2.905 (-4.0%)

The following observations are made:

- Generally, the differences in statistical moments increase with the increased size of the response surface used.
- The mean values increase with the size of the response surface, but still within 10% for “Extremely Large Size”.
- The standard deviation has no obvious difference with the changing of response surface size. The differences are within 10% for the three compared response surfaces.
- The skewness is significantly affected by the response surface size. The differences are around 40% for ‘Larger Size’ and ‘Extremely Large Size’, while for the “Base Case” is only 10%.
- The kurtosis values do not have big differences when response surfaces with different size are used, the largest difference is within 10% for “Extremely Large Size”.

6.2.2 Size of Response Surface – Effect on Fitted Probability Distributions

The probability density function and cumulative distribution of lognormal fitted distribution of response value with different size response surfaces are plotted in Figure 37, Figure 38 and Figure 39, together with the Measured Values.

The following observations are made:

- In general, using ‘Extremely Large Size’ leads to large differences in the probability distribution.
- The probability density functions fitted from the response surface generally do not fit well with the measured values, as presented in Figure 37, the ‘Extremely Large Size’ is far away from the others.
- As shown in Figure 38, the cumulative distributions of ‘Base Case’ and ‘Larger Size’ are very close to ‘Measured Values’. Furthermore, as presented in Figure 39, these differences are reduced at the tail region.

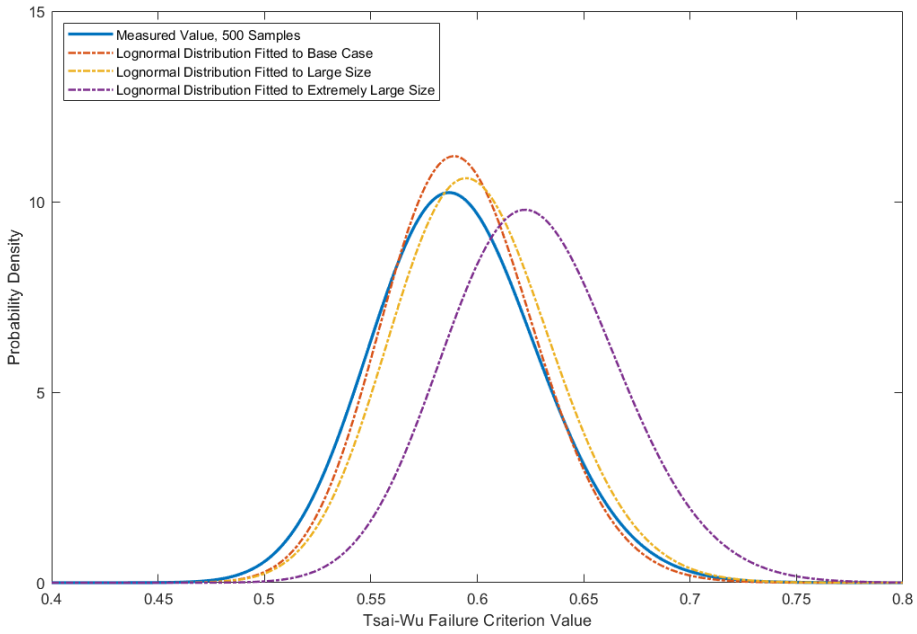

Figure 37: Size of response surface – Effect on probability density functions

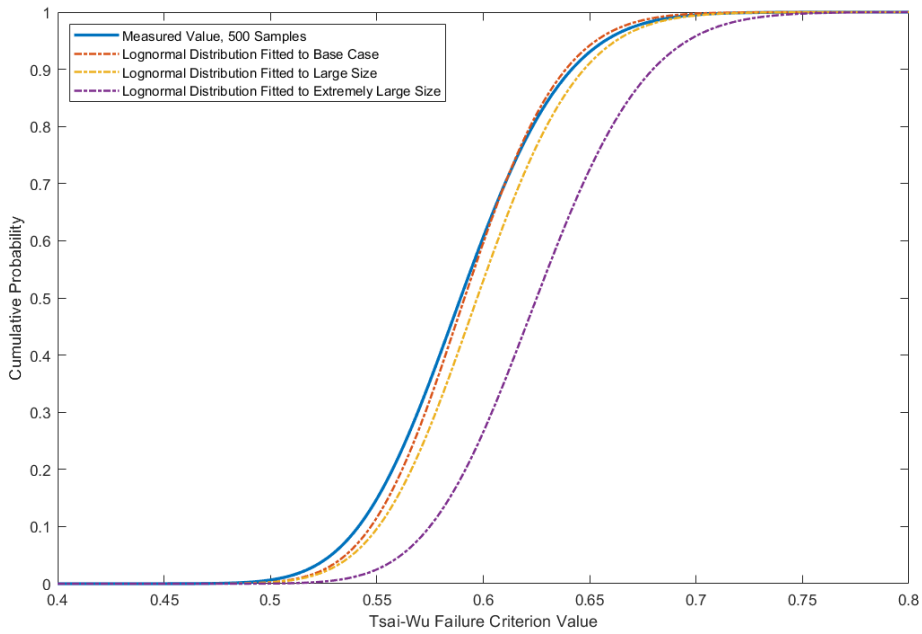

Figure 38: Size of response surface – Effect on cumulative probability functions

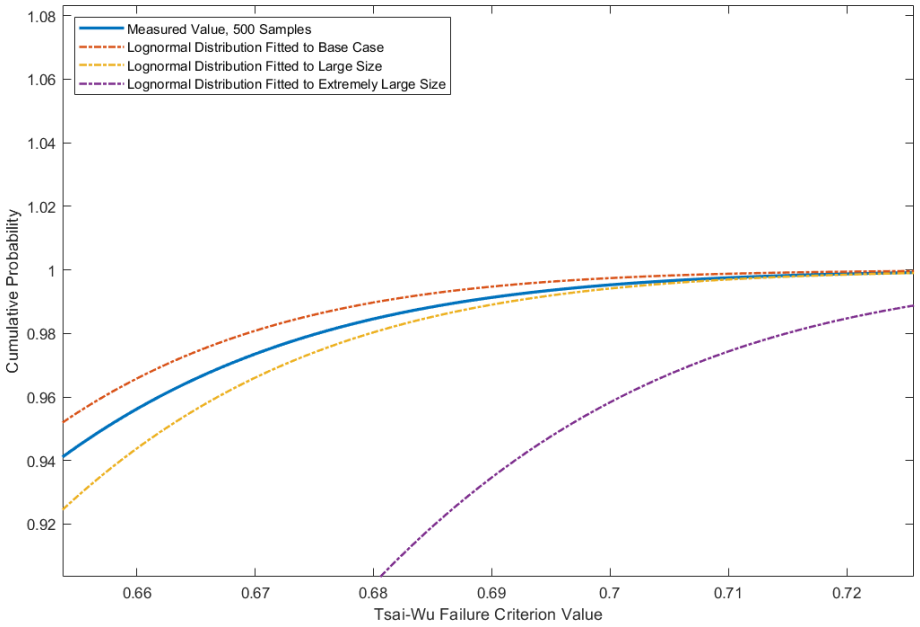

Figure 39: Size of response surface – Effect on cumulative probability functions (Zoom-In at upper tail region)

6.2.3 Size of Response Surface – Effect on Predicted Failure Values

Table 24 compared the predicted failure rates and percentage differences calculated from the Lognormal distribution fitted to the response values calculated by

response surfaces with different sizes. As observed in Table 24, the size of response surfaces does not significantly affect the predicted failure values. The predicted failure values generally have a small increase when a larger size of response surface is used, but the difference is almost acceptable. Except for the Tsai-Wu failure values predicted by 'Extremely Large Size', most of the predicted failure values have differences within 5%.

Table 24: Size of Response Surface – Effect on Predicted Failure Values

Source	Failure Criterion	Failure Rate = 1 in 10^4	Failure Rate = 1 in 10^5	Failure Rate = 1 in 10^6
Lognormal distribution fitted to measured values	Maximum Stress	0.64	0.67	0.69
	Tsai-Wu	0.75	0.78	0.81
	Hashin	0.76	0.79	0.81
Lognormal distribution fitted to response values (Base Case)	Maximum Stress	0.64 (0.0%)	0.66 (-1.5%)	0.68 (-1.4%)
	Tsai-Wu	0.74 (-1.3%)	0.77 (-1.3%)	0.79 (-2.5%)
	Hashin	0.75 (-1.3%)	0.78 (-1.3%)	0.80 (-1.2%)
Lognormal distribution fitted to response values (Larger Size)	Maximum Stress	0.63 (-1.8%)	0.65 (-1.9%)	0.67 (-2.1%)
	Tsai-Wu	0.75 (-0.1%)	0.78 (-0.1%)	0.81 (-0.3%)
	Hashin	0.75 (-1.2%)	0.77 (-1.4%)	0.80 (-1.5%)
Lognormal distribution fitted to response values (Extremely Large Size)	Maximum Stress	0.63 (-1.4%)	0.66 (-1.8	0.67 (-2.1%)
	Tsai-Wu	0.80 (**5.7**%)	0.83 (**5.6**%)	0.85 (**5.6**%)
	Hashin	0.76 (0.6%)	0.79 (0.4%)	0.81 (0.2%)

6.3 Location of Sample Population

In Section 6.2, we talked about the availability of enlarging the size of the response surface and discovered the small differences of using the “Extremely Large Size”. It is noted that the comparisons were based on the centre-located sample population, as shown in Figure 34, the sample population is located at the centre of the response surface. In this section, the different locations of sample population on the “Extremely Large Size” are studied. Four extra locations are studied: Boundary Case 1, Boundary Case 2, Intermediate Case 1, Intermediate Case 2. The ranges of inner diameter and ply thickness are listed in Table, the illustration of the sample populations is shown in Figure 40. The other parameters are same as the “Base Case”. A sample size of 200 is used as discussed in Section 5.1.1 for each population group.

Table 25: Mean and Standard Deviation of Inner Diameter and Thickness for New Population Cases

Population Groups		Unit	Mean	Std	Lower	Upper
Boundary Case 1	D	mm	168	6	148	188
	t	mm	0.27	0.01	0.24	0.3
Boundary Case 2	D	mm	168	6	160	200
	t	mm	0.13	0.01	0.10	0.16
Intermediate Case 1	D	mm	73	4	70	100
	t	mm	0.15	0.01	0.12	0.18
Intermediate Case 2	D	mm	153	4	150	180
	t	mm	0.15	0.01	0.12	0.18

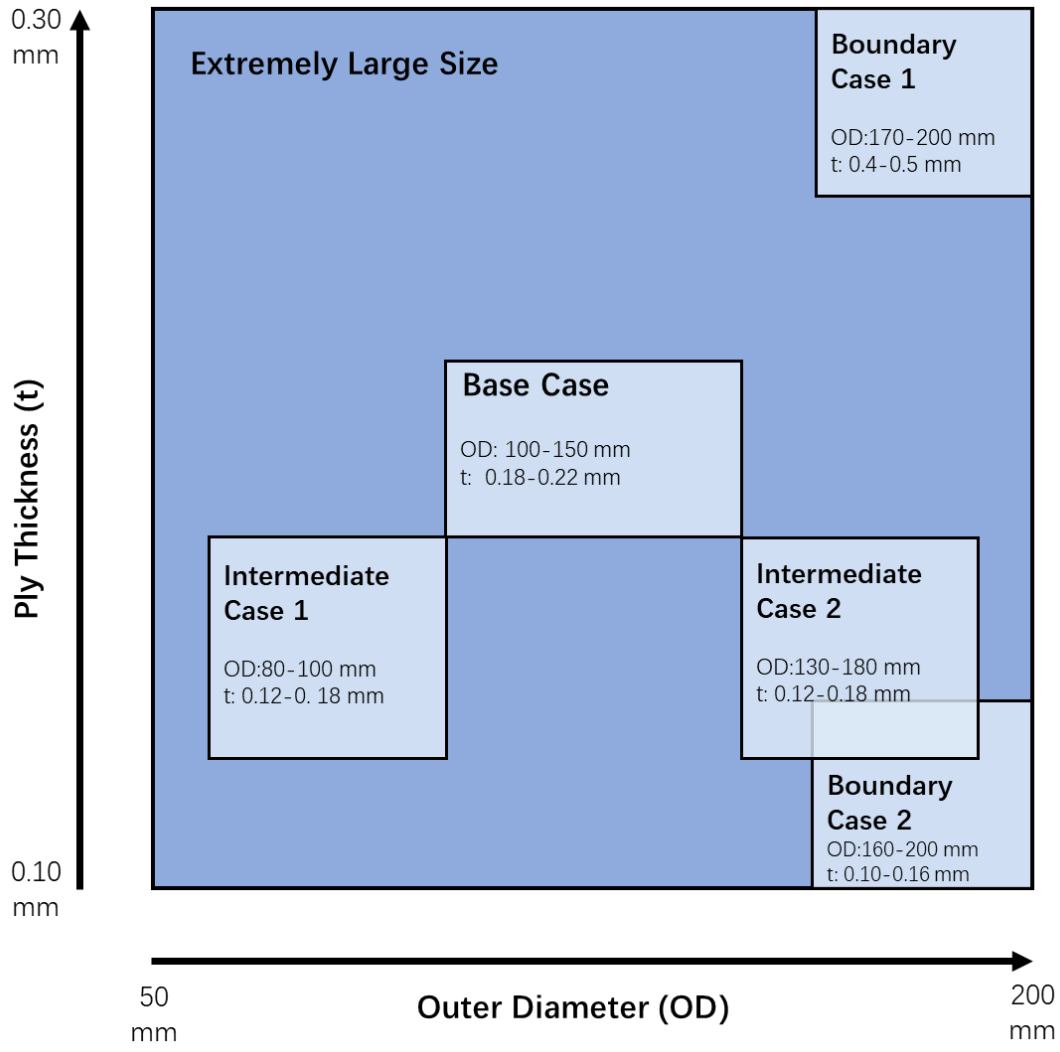

Figure 40: Locations of study cases on the response model.

The new population groups are input into the "Extremely Large Size" response surface and ACP Solution, respectively. The response values and measured values are fitted to the lognormal distributions. The percentage difference of failure rate predicted by lognormal fitted distributions of response values compared to measured values are listed in Table 26. The following observations are made:

- The accuracy of predicted failure rates is different at different locations of the response surface.

- Generally, the populations on the boundary show larger percentage differences compared to the populations inside, i.e. the percentage difference of Tsai-Wu exceeding 10^{-4} is 7.0% for "Intermediate Case 1" and 8.1% for "Boundary Case 2".
- Except the "Boundary Case 1", the maximum percentage difference is 9.0% for Tsai-Wu criterion at 10^{-6} in "Boundary Case 2", which is still acceptable.
- Using the sample populations located at the boundary of the response surface should be avoided.

Table 26: % difference of Failure Rate at Different Locaiton on Extremly Large Size

Population Group	Failure Criterion	Failure Rate = 1 in 10^4	Failure Rate = 1 in 10^5	Failure Rate = 1 in 10^6
Base Case (Section 6.2.3)	Maximum Stress	-1.4%	-1.8%	-2.1%
	Tsai-Wu	5.7%	5.6%	5.6%
	Hashin	0.6%	0.4%	0.2%
Boundary Case 1	Maximum Stress	7.3%	16.0%	24.2%
	Tsai-Wu	15.3%	22.4%	29.0%
	Hashin	5.5%	9.3%	12.8%
Boundary Case 2	Maximum Stress	-1.8%	-5.0%	-7.7%
	Tsai-Wu	8.1%	8.5%	9.0%
	Hashin	0.6%	-1.9%	-4.1%
Intermediate Case 1	Maximum Stress	3.4%	4.5%	5.4%
	Tsai-Wu	7.0%	7.2%	7.3%
	Hashin	3.4%	3.6%	3.8%
Intermediate Case 2	Maximum Stress	4.2%	4.1%	4.1%
	Tsai-Wu	6.4%	6.8%	7.2%
	Hashin	3.9%	4.4%	4.7%

7 Conclusion and Future Work

7.1 Conclusion

This dissertation introduced an efficient method of applying stochastic process on a CFEC flowline using response surface methodology. We studied the different factors that will affect the accuracy of using the Kriging response surface to predict the failure values of different exceeding probabilities for a CFEC flowline, which subjected to combined loading. A flow chart of failure values prediction using response surface is illustrated in Figure 41:

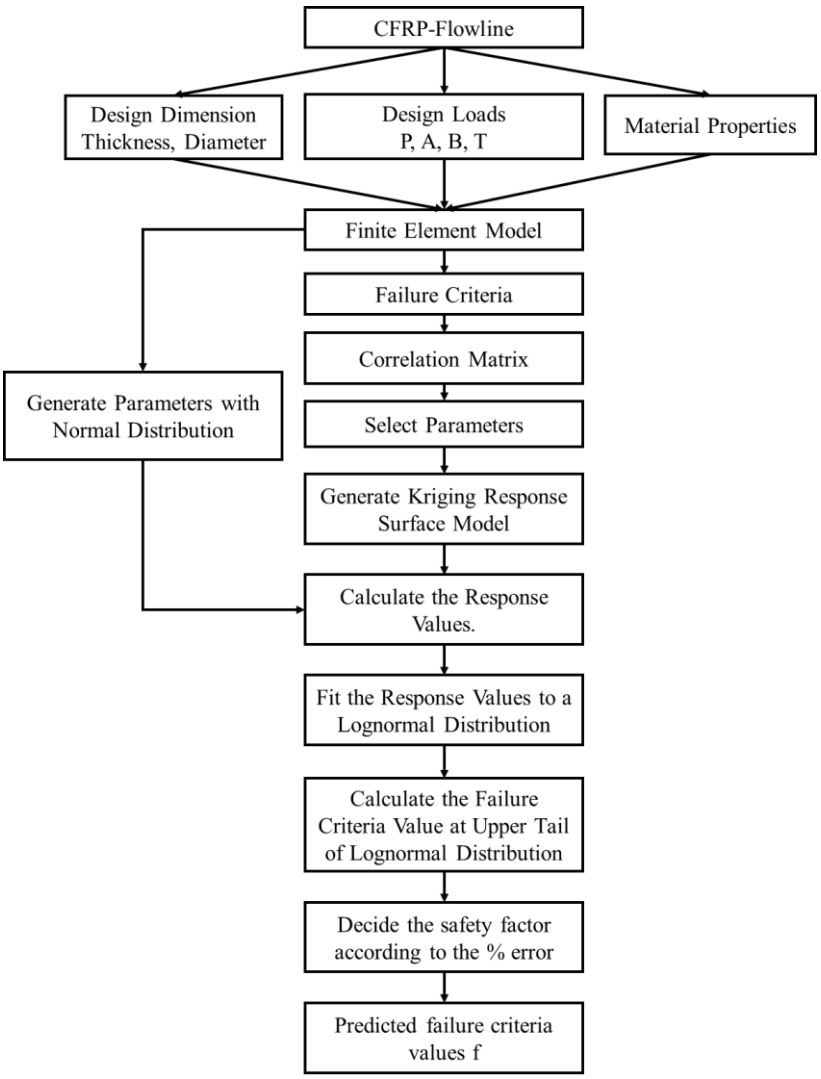

Figure 41: Flow chart of exceeding failure value prediction using response surface.

First, parameters of the flowline such as the dimension, material properties, laminate stacking of the flowline should be decided. Based on these input parameters, a finite element model of the CFEC flowline can be built in ACP, the solution of failure criteria can be calculated. It is recommended to adjust these parameters to let the failure criteria have the basic value around 0.8~0.9, which is easier for the final distribution of failure criteria to cover 1, which is the boundary to judge whether the flowline fail or not.

Then, a correlation matrix is calculated. It is suggested to use more than 200 samples to calculate the correlation matrix. The Spearman and Pearson generally have no differences. With the correlation matrix, parameters that have stronger correlation with the failure criteria values should be selected to build the Kriging response surface. By the studies in Section 6.1, it is suggested that the parameters have correlation coefficients higher than 0.13 be chosen for the response surface modelling.

With selected parameters, the Kriging response surface can be modelled. It is suggested to have an auto-refinement process to reduce the predicted relative error below 5%. The range of the response surface could be extended to an appropriate size, where the response failure values of exceeding probabilities would keep an acceptable difference compared to “Measured Values”. In the studies in Section 6.2, we extended the range of inner diameter from 50 mm to 150 mm, and ply thickness from 0.04 mm to 0.20 mm, which kept the percentage difference of predicted failure values within 10% compared to “Measured Values”.

Meanwhile, a sample population with a size larger than 200 can be generated and

input into the response surface, by which we can get converged statistical moments as studied in Section 5.1.1, and the "Response Values" of these sample populations are obtained. As studied in Section 6.3, the sample populations should avoid being centralized at the boundary of the response surface, which will increase the inaccuracy.

Finally, fit the response values with a lognormal distribution, which can be used to calculate the exceeding probabilities, i.e. failure rate. The calculated failure values at the upper tail region usually have within 10% difference compared to the "Measured Values", so a safety factor of 1.1 can be applied to calculate the modified failure value of exceeding probability $f_{modifed}$, as shown in Equation(20):

$$f_{modifed} \leq 1.1 \times f_{predicted} \tag{20}$$

Where $f_{predicted}$ is the failure values for the exceeding probability predicted by the response surface.

7.2 Recommendation for Future Work

Response surface methodology is especially helpful for the failure prediction of flowline where need large size of samples. Considering the simplification of the model studied in this thesis, the recommendation for the future work are listed as follow:

- The effect of the stacking sequence could be taken into consideration. As we mentioned above, the fibre direction and stacking will influence the loads transformation, which will directly change the strength within the laminate. This means the strengths in some direction are not fully utilized. Detailed studies of the stacking sequence and fibre direction can be carried out.

- Dynamic loading could be studied. In this thesis, the load combination is simplified as constants, while the loads applied on the flowline in actual applications will be more complicated and varied with time. A time interval can be set to find the maximum failure criteria that happened during the changing of the loads as a substitution of the failure criteria sample calculated by the static loading, which made the results more realistic.
- Safety factor used to adjust the failure criteria predicted by the response surface, as mentioned in Equation (20), can be determined more specifically. In the studies above, the safety factor is determined by the general error between the response fitting value and the measured value, which did not distinguish between different failure rates and different failure criteria. Safety factors related to failure rate and failure criteria can be determined separately

References

1. U.S. Energy Information Administration. U.S. average depth of crude oil and natural gas wells, https://www.eia.gov/dnav/ng/hist/e_ertw0_xwd0_nus_fwa.htm (2020, assessed 12 April 2020).

2. GlobalData, H1 2019 global length and capital expenditure outlook for oil and gas pipelines – natural gas Pipelines take lead in new-build projects, 2019

3. ICF International for The INGAA Foundation. North America midstream infrastructure through 2035: capitalizing on our energy abundance, https://www.ingaa.org/File.aspx?id=21527&v=6be6e34a (2020, accessed 12 April 2020).

4. Composite UK. Use of composite materials in aerospace, https://compositesuk.co.uk/composite-materials/applications/aerospace (2020, assessed 8 May 2020)

5. Composite UK. Use of composite materials in the oil and gas industry, https://compositesuk.co.uk/composite-materials/applications/aerospace (2020, assessed 8 May 2020)

6. Yang C. Design and analysis of composite pipe joints under tensile loading. *J Compos Mater* 2000; 34: 332-349.

7. Jha V, Dodds N, Finch D, et al. Flexible fiber-reinforced pipe for 10,000-foot water depths: performance assessments and future challenges. In: *Offshore technology conference*, Texas, USA, 5 May-8 May 2014, OTC-25393-MS.

8. Bazán F and Beck A. Stochastic process corrosion growth models for pipeline reliability. *J Corros Sci* 2013; 74: 50.

9. Oliveira N, Bisaggio H and Netto T. Probabilistic analysis of the collapse pressure of corroded pipelines. In: *ASME 2016 35th international conference on ocean, offshore and arctic engineering*, Busan, South Korea, 19 June-24 June 2016, OMAE2016-54299.

10. Jia B, Yu X and Yan Q. A new sampling strategy for Kriging-based response surface method and its application in structural reliability. *Adv Struct Eng* 2016; 20(4): 564-581.

11. Simpson T, Mauery T, Korte J, et al. Comparison of response surface and Kriging models for multidisciplinary design optimization. In: *7th AIAA/NASA/USAF/ISSMO symposium on multidisciplinary analysis and optimization*, 2 September-4 September 1998, AIAA-98, p4755.

12. Gupta S and Manohar C. An improved response surface method for the determination of

failure probability and importance measures. *Struct Saf* 2004; 26: 123-139.

13. Tsai SW, Wu EM. A general theory of strength for anisotropic materials. *J Compos Mater* 1971; 5(1): 58-80.
14. Hashin Z. Failure criteria for unidirectional fiber composites. *J Appl Mech* 1980; 47(2): 329.
15. Spearman C. Correlation calculated from faculty data. *Br J Psychol* 1904-1920 1910; 3(3): 271-295.
16. Pearson K. Notes on the history of correlation. *Biometrika*. 1920; 13(1): 25-45
17. Krige DG. *A statistical approach to some mine valuations and allied problems at the Witwatersrand.* Master Thesis, University of Witwatersrand, South Africa, 1951.
18. Rosenblatt F. The perceptron: a probabilistic model for information storage and organization in the brain. *Psychological review*. 1958; 65(6): 386.
19. Kirchhoff G. Über das gleichgewicht und die bewegung einer elastischen scheibe. *J. Reine Angew. Math*. 1850; 40: 51-88.
20. Love AEH. *A treatise on the mathematical theory of elasticity.* Cambridge; 1906.
21. Jones RM. Mechanics of composite material: Hemisphere; 1975.
22. Daniel IM. Failure of composite materials. *Strain*. 2007; 43(1): 4-12.
23. Gol'denblat II and Kopnov VA. Strength of glass-reinforced plastics in the complex stress state. *Polymer Mechanics* 1965; 1(2): 54-59.
24. Clouston P, Lam F and Barrett D. Interaction term of Tsai-Wu theory for laminated veneer. *J Mater Civ Eng* 1998; 10(2): 112-116.
25. Li S, Sitnikova E, Liang Y, et al. The Tsai-Wu failure criterion rationalised in the context of UD composites. *Composites Part A 2017*; 102: 207-217.
26. Freudenthal AM. Safety and the probability of structural failure. American Society of Civil Engineers Transactions. 1956.
27. Labovitz, S. The assignment of numbers to rank order categories. American sociological review 1970, pp.515-524.
28. McDermott D, Doyle J. Non-monotonic logic I. *Artif. Intell*. 1980; 13(1-2): 41-72.
29. Box GEP and Wilson KB. On the experimental attainment of optimum conditions (with discussion). *J R Stat Soc Series B* 1951; 13(1): 1-45.
30. Ansys®. DesignXplorer. release 2019 R3, help system, DesignXplorer User's Guide,

Using Response Surfaces, ANSYS Inc.

31. Altman NS. An introduction to kernel and nearest-neighbor nonparametric regression. The American Statistician. 1992 Aug 1; 46(3): 175-85.

32. Ansys®. Mechanical APDL. Release 2019 R2, help system, element reference, chapter 7: Element Library, SHELL181, ANSYS Inc.

Appendix I

Paper 1: The Correlation and Determination Matrices Associated with the Burst Design of a Subsea Carbon-Fibre-Epoxy Composite Flow-Line[1]

Appendix I contains the paper which has been accepted by IOP Conference Series: Materials Science and Engineering.

[1] Xing YH, Xu WX and Buratti V. The correlation and determination matrices associated with the burst design of a subsea carbon-fibre-epoxy composite flow-line. In: *IOP conference series: materials science and engineering*, Stavanger, Norway, 27 November-29 November 2019, Vol 700, p012021.

The correlation and determination matrices associated with the burst design of a subsea carbon-fibre-epoxy composite flow-line

Y Xing[1], W Xu[1], V Buratti[2]

[1]Department of Mechanical and Structural Engineering and Material Science, University of Stavanger, Kjell Arholmsgate 41, 4036 Stavanger, Norway
[2]Aibel AS, Vestre Svanholmen 14, 4313 Sandnes, Norway

Corresponding author: yihan.xing@uis.no

Abstract. This paper examines the correlation and determination matrices of the burst design in a subsea carbon-fibre-epoxy composite flow-line. A case study of a 4" flow-line is investigated. The correlation and determination matrices are calculated and compared using Pearson and Spearman correlation methods. A comprehensive suite of failure modes that comprises of Maximum Stress, Tsai-Wu, Hashin and Puck failure criteria is used to quantify the burst design. The results reveal that the failure criteria are strongly correlated to each other. The applied pressure and ply thickness are moderately correlated to the failure criteria. It is observed that due to the nature of burst loads, most material failure parameters with the exception of the Tsai-Wu constant, F_{12} do not exhibit correlations with the failure criteria. Second, both Pearson and Spearman correlation methods identified the same set of major design parameters. Third, it was found that the identification of the major design parameters is not affected by the sample size. This paper provides an analysis framework to aid in the identification of the major design parameters which is the initial and crucial step of a design optimisation exercise.

1. Introduction and background

Carbon-fibre-epoxy composite (CFEC) materials consist of an epoxy matrix reinforced by carbon fibres. The principal advantage of using CFEC materials is the high strength to weight ratio; carbon fibres are characterized by a strength-to-weight ratio 50 times higher than steel. Hence, structures made from CFEC materials are typically 20 % lighter than steel and 30% to 50% stronger. However, unlike isotropic materials, CFEC materials have directional strength properties. The orthotropic property is both an advantage and a disadvantage. CFEC materials can be aligned in the strong direction optimally to achieve higher strength-to-weight ratios in the structure. However, it requires careful design to ensure that the loads transverse to the fibre directions are not overly large; this is the weak direction. Another advantage of CFEC materials is their high fatigue strength. The fatigue limit of CFEC materials is as much as 70 % of the ultimate strength compared to only 30 % in the case of steel materials. A third advantage of using CFEC materials is their corrosion resistant properties. The above-mentioned properties make CFEC flow-lines attractive in high demanding applications.

The stress analysis and strength evaluation of CEFC flowlines have been well-studied. Some studies are briefly described here. Azar et al. [1] calculated the optimum angle of filament-wound pipelines used for natural gas transmission using approximation methods. Theotokoglou [2] used finite element analyses to quantity the effect of delamination on the loss in load carrying capacity. Xia et al. [3] analysed multi-layered filament-wound composite pipes under internal pressure using a simplified elastic solution. Chouchaoui et al. [4] studied the stresses and displacements of a laminated cylindrical tube using analytical models. Guz et al. [5] analysed the stress distributions through the pipe thickness for various lay-ups when the pipe is subjected to different outer pressure loads. These papers presented some form of parametric studies. However, there has not been any published studies applying the parametric correlation method to composite flowlines to identify the major design parameters.

This paper examines the correlation and determination matrices associated with the burst design of a 4" CFEC flow-line. Four failure criteria based on different failure theories are investigated. These are the Maximum Stress, Tsai-Wu [6], Hashin [7] and Puck [8-10] failure criteria. Furthermore, two correlation methods, namely Pearson [11, 12] and Spearman [13-15] correlation are studied. The purpose is to investigate the identification of the major design parameters associated with each individual failure criterion. The identification of the major design parameters is the initial and crucial step in a design optimization exercise [16].

1.1. Nomenclature

$\rho_{P_1P_2}$	*Pearson linear correlation coefficient*
$cov(P_1, P_2)$	*Covariance*
σ_{P_1}	*Standard deviation of variable P_1*
σ_{P_2}	*Standard deviation of variable P_2*
$\rho_{P_1{}^2,P_2{}^2}$	*Pearson quadratic correlation coefficient*
$\rho_{rg_{P_1},rg_{P_2}}$	*Spearman linear correlation coefficient*
$cov(rg_{P_1}, rg_{P_2})$	*Covariance of the rank variable*
$\sigma_{rg_{P_1}}$	*Standard deviation of the rank variable P_1*
$\sigma_{rg_{P_2}}$	*Standard deviation of the rank variable P_2*
$\rho_{rg_{P_1}{}^2,rg_{P_2}{}^2}$	*Spearman quadratic correlation coefficient*
σ_A	*Axial stress*
σ_H	*Hoop stress*
σ_1	*Stress in the x-direction*
σ_2	*Stress in the y-direction*
σ_3	*Stress in the z-direction*
τ_{12}	*Shear stress in the xy-plane*

τ_{23}	*Shear stress in the yz-plane*
τ_{13}	*Shear stress in the xz-plane*
σ_{ut1}	*Ultimate tensile strength in the x-direction*
σ_{uc1}	*Ultimate compressive strength in the x-direction*
σ_{ut2}	*Ultimate tensile strength in the y-direction*
σ_{uc2}	*Ultimate compressive strength in the y-direction*
σ_{ut3}	*Ultimate tensile strength in the z-direction*
σ_{uc3}	*Ultimate compressive strength in the z-direction*
τ_{u12}	*Ultimate shear strength the in the xy-plane*
τ_{u13}	*Ultimate shear strength the in the xz-plane*
τ_{u23}	*Ultimate shear strength the in the yz-plane*

2. Correlation and determination matrix

The correlation matrix measures the linear correlation between the identified design input parameters and the output variables using correlation coefficients. The correlative coefficient is a number between -1 and 1. A positive value indicates that P_2 increases with P_1, while a negative value indicates that P_2 decreases with P_1. The closer the value of correlation is to +1 or -1, the stronger the correlation between the input and the output variables. The objective of using a correlation matrix is to identify the major design parameters. The following correlation methods are used in this paper:

- Pearson correlation (Ref. Section 2.1.)
- Spearman correlation (Ref. Section 2.2.)

The determination matrix measures the quadratic correlations between P_1 and P_2. It indicates how close the points are to a quadratic curve. The determination matrix provide a measure of how well future outcomes are likely to be predicted. The correlation and determination matrices can be used to reduce the number of input parameters to a selection of major parameters in the design of experiments, or to reduce the number of output variables considered in a design optimization study.

2.1. Pearson correlation

The Pearson correlation [11, 12] is a measure of the linear correlation between two variable P_1 and P_2. The Pearson correlation coefficient is defined as:

$$\rho_{P_1 P_2} = \frac{cov(P_1, P_2)}{\sigma_{P_1}\sigma_{P_2}} \tag{1}$$

Equation (1) is used in the correlation matrix. For the determination matrix, i.e., quadratic correlation, the Pearson correlation coefficient is defined as:

$$\rho_{P_1{}^2, P_2{}^2} = \frac{cov\left(P_1{}^2, P_2{}^2\right)}{\sigma_{P_1{}^2}\sigma_{P_2{}^2}} \tag{2}$$

2.2. Spearman correlation

The Spearman correlation [13-15] is defined as the Pearson correlation between the rank variables. It is given as:

$$\rho_{rg_{P_1},rg_{P_2}} = \frac{cov\left(rg_{P_1}, rg_{P_2}\right)}{\sigma_{rg_{P_1}}\sigma_{rg_{P_2}}} \tag{3}$$

Similar to the Pearson correlation, Equation (3) is used in the correlation matrix. For the determination matrix, the Spearman correlation coefficient is defined as:

$$\rho_{rg_{P_1{}^2},rg_{P_2{}^2}} = \frac{cov\left(rg_{P_1{}^2}, rg_{P_2{}^2}\right)}{\sigma_{rg_{P_1{}^2}}\sigma_{rg_{P_2{}^2}}} \tag{4}$$

Note that the symbol σ in Equation (1) to (4) is used to represent standard deviations. The symbol σ is used to represent stresses in the rest of the paper.

3. Burst design of a subsea carbon-fibre-epoxy composite flow-line

3.1. Thin wall cylinder

The flow-line is a long thin wall cylinder subjected to internal pressure. Under this load condition, an element in the cylinder wall will experience two distinct stresses, axial (σ_A) and hoop stresses (σ_H) as illustrated in Figure 1.

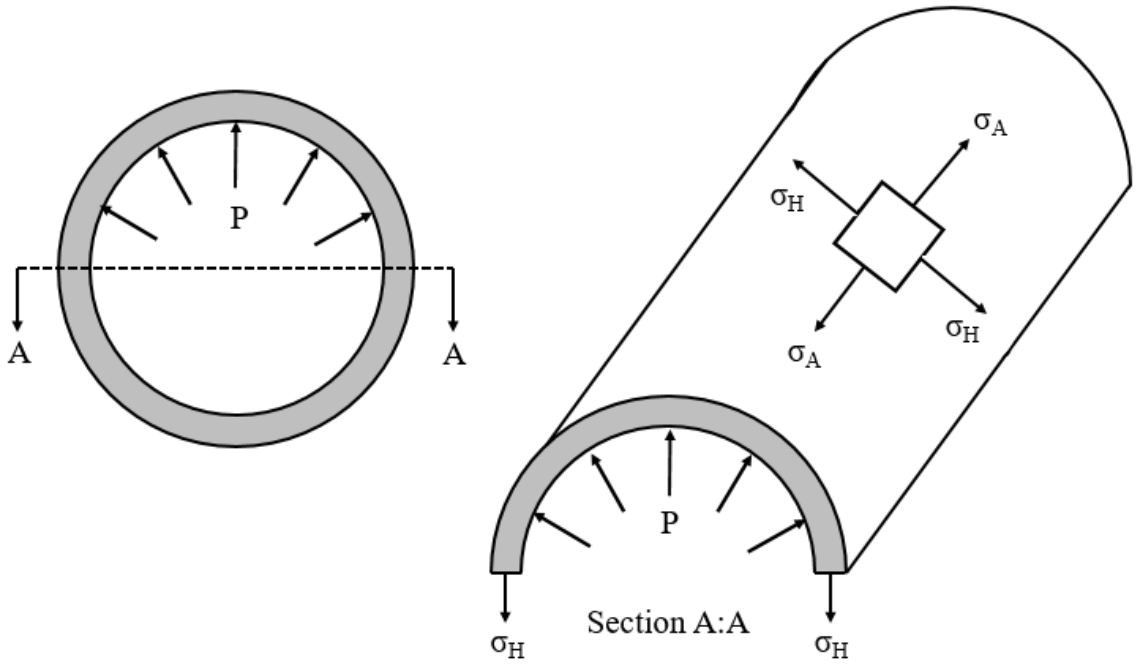

Figure 1. Stresses in a thin wall cylinder

3.2. Classical laminate theory

The classical laminate theory (CLT) [17-19] is used in this paper. This theory extends the classical plate theory for isotropic and homogeneous materials proposed by Kirchhoff [20, 21]. The CLT assumes the following:

- There is no slip between the adjacent layers. This means that the laminate is perfectly bonded.
- Each lamina is a homogenous layer with its effective properties known and uniform throughout the lamina.
- Each lamina is in a state of plane stress
- Each lamina can be isotropic, orthotropic or inversely isotropic.
- The laminate deforms in accordance with Kirchhoff's theory. This means the normal to the mid-plane remain straight and normal to the mid-plane after deformation. In addition, the normal to the mid-plane does not change lengths.

3.3. Failure criteria

The four failure criteria listed in Table 1 are investigated in this paper. The corresponding failure theories and their failure functions are described in some details in the following sub-sections. It is mentioned that failure is defined to occur when the failure function returns a value equal or greater than 1.0.

Note that since CLT is used, the inter-laminar normal and shear stresses are zero and not computed, i.e., $\sigma_3 = \tau_{23} = \tau_{13} = 0$. However, for completeness, the generalized 3D failure criteria are presented in Section 3.3.1. to 3.3.4.

Table 1. Failure criteria studied

Failure Criterion	Physical Basis	Usage Convenience	Ref. Section
Maximum Stress	Tensile behaviour of brittle material	Requires only few parameters by testing	3.3.1.
Tsai-Wu	Interactive tensor polynomial fitted to the failure behaviour of the material	Requires numerous parameters by a comprehensive testing program	3.3.2.
Hashin	Interactive criterion considering failure in fibre, transverse and delamination separately.	Requires only few parameters by testing	3.3.3.
Puck	Complex interactive criterion considering fibre and inter-fibre failures separately.	Requires numerous parameters by a comprehensive testing program	3.3.4.

3.3.1. Maximum stress failure criterion. This failure criterion compares the ratios of the actual stresses to the failure stresses in the ply principal coordinate system. The generalized failure function is defined as:

$$f = max\left(\left|\frac{\sigma_1}{X}\right|, \left|\frac{\sigma_2}{Y}\right|, \left|\frac{\sigma_3}{Z}\right|, \left|\frac{\tau_{12}}{S}\right|, \left|\frac{\tau_{13}}{R}\right|, \left|\frac{\tau_{23}}{Q}\right|\right) \quad (5)$$

where:

$$X = \begin{cases} \sigma_{uc1}, \sigma_1 < 0 \\ \sigma_{ut1}, \sigma_1 \geq 0 \end{cases}, \qquad Y = \begin{cases} \sigma_{uc2}, \sigma_2 < 0 \\ \sigma_{ut2}, \sigma_2 \geq 0 \end{cases}, \qquad Z = \begin{cases} \sigma_{uc3}, \sigma_3 < 0 \\ \sigma_{ut3}, \sigma_3 \geq 0 \end{cases}$$

$$S = \tau_{u12}, \quad R = \tau_{u13}, \quad Q = \tau_{u23}$$

3.3.2. Tsai-Wu failure criterion. The Tsai-Wu failure criterion [6] uses a quadratic failure function and is a simplification of Gol'denblat and Kapnov's generalised failure theory for anisotropic materials [22]. It is expressed as:

$$f = f_i\sigma_i + f_{ij}\sigma_i\sigma_j \tag{6}$$

where *i, j* = 1, 2, 3, 4, 5, 6.

In the plane stress condition, Equation (6) reduces to:

$$f = F_{11}\sigma_1^2 + F_{22}\sigma_2^2 + F_{66}\tau_{12}^2 + 2F_{12}\sigma_1\sigma_2 + F_1\sigma_1 + F_2\sigma_2 \tag{7}$$

where:

$$F_{11} = \frac{1}{\sigma_{ut1}\sigma_{uc1}},\ F_{22} = \frac{1}{\sigma_{ut2}\sigma_{uc2}},\ F_{66} = \frac{1}{S^2},\ F_1 = \frac{1}{\sigma_{ut1}} - \frac{1}{\sigma_{uc1}},\ F_2 = \frac{1}{\sigma_{ut2}} - \frac{1}{\sigma_{uc2}}$$

and the nominal value of F_{12} is defined in Table 3.

3.3.3. Hashin failure criterion. This Hashin failure criterion [7] distinguishes the various different failure modes and model each of the modes separately. This is in contrast to the Tsai-Wu failure criterion (Ref. Section 3.3.2.) which uses a quadratic failure function that 'mixes' all the failures modes together. The Hashin failure function is defined as:

$$f = max(f_f, f_m, f_d) \tag{8}$$

where ff, fm and fd are the failure functions for failures in the fibre direction, transverse direction and delamination, respectively.

For failure in the fibre direction, f_f is defined as:

$$f_f = \begin{cases} \left(\frac{\sigma_1}{\sigma_{ut1}}\right)^2 + \left(\frac{\tau_{12}}{\tau_{u12}}\right)^2 + \left(\frac{\tau_{13}}{\tau_{u13}}\right)^2, \sigma_1 \geq 0 \\ -\frac{\sigma_1}{\sigma_{uc1}}, \sigma_1 < 0 \end{cases} \tag{9}$$

For failure in the transverse direction, f_m is defined as:

$$f_m = \begin{cases} \left(\frac{\sigma_2}{\sigma_{ut2}}\right)^2 + \left(\frac{\tau_{23}}{\tau_{u23}}\right)^2 + \left(\frac{\tau_{12}}{\tau_{u12}}\right)^2 + \left(\frac{\tau_{13}}{\tau_{u13}}\right)^2, \sigma_2 \geq 0 \\ \left(\frac{\sigma_2}{2\tau_{u23}}\right)^2 + \left(\frac{\tau_{23}}{\tau_{u23}}\right)^2 + \left(\frac{\tau_{12}}{\tau_{u12}}\right)^2 + \left[\left(\frac{Y_c}{2\tau_{u23}}\right)^2 - 1\right]\frac{\sigma_2}{\sigma_{uc2}}, \sigma_2 < 0 \end{cases} \tag{10}$$

For delamination failure, f_d is defined as:

$$f_d = \begin{cases} \left(\frac{\sigma_3}{\sigma_{uc3}}\right)^2 + \left(\frac{\tau_{13}}{\tau_{u13}}\right)^2 + \left(\frac{\tau_{23}}{\tau_{u23}}\right)^2, \sigma_3 < 0 \\ \left(\frac{\sigma_3}{\sigma_{ut3}}\right)^2 + \left(\frac{\tau_{13}}{\tau_{u13}}\right)^2 + \left(\frac{\tau_{23}}{\tau_{u23}}\right)^2, \sigma_3 \geq 0 \end{cases} \tag{11}$$

3.3.4. Puck failure criteria. The Puck's action plane strength criterion is used in this paper. The criterion considers two separate failures, namely fibre failure (FF) and inter-fibre failure (IFF). For FF, the Maximum Stress criterion as defined below is used [8-10]:

$$f_{FF} = \begin{cases} \frac{\sigma_1}{\sigma_{uc1}}, \sigma_1 < 0 \\ \frac{\sigma_1}{\sigma_{ut1}}, \sigma_1 \geq 0 \end{cases} \quad (12)$$

The failure function for IFF is complex and will not be presented here. Briefly, the IFF failure function considers a 3D stress state using the definition of fracture resistances, R and slope parameters of the fracture curves, p. The Puck IFF failure function also takes into account that some fibres might already break under uniaxial loads much lower than loads which cause ultimate factors using degradation factors. Details of the IFF failure function can be found in Puck et al. [8, 9]

4. Case study

The flow-line studied is a 4" pipe with an applied pressure of 2500 psi.

4.1. Base case

The general base case properties are presented in Table 2.

Table 2. General properties of flow-line, Base case

Property	Symbol	Value	Unit
Outer Diameter	OD	114.3	mm
Wall Thickness	WT	6	mm
Total Number of Ply	-	30	
Ply Thickness	t_{ply}	0.2	mm
Fibre orientation	-	+/- 45	°
Applied Pressure	$P_{applied}$	17.25	MPa

Table 3. Material data - ply (prepreg epoxy carbon UD)

Material Property	Symbol	Value	Unit
Elastic Modulus	E_1, E_2, E_3	121000, 8600, 8600	MPa
Shear Modulus	G_{12}, G_{23}, G_{13}	4700, 3100, 4700	MPa
Poisson's Ratio	ν_{12}, ν_{23}, ν_{13}	0.27, 0.4, 0.27	-
Tensile Strength	σ_{ut1}, σ_{ut2}, σ_{ut3}	2231, 29, 29	MPa
Compressive Strength	σ_{uc1}, σ_{uc2}, σ_{uc3}	-1082, -100, -100	MPa
Shear Strength	τ_{u12}, τ_{u23}, τ_{u13}	60, 32, 60	MPa
Tsai-Wu Constants	F_{12}, F_{23}, F_{13}	-1, -1, -1	-
Puck Constants	p_{21+}, p_{22+}, p_{21-}, p_{22-}	0.35, 0.25, 0.3, 0.25	-
Additional Puck Constants	s, M, F_{IW}	0.5, 0.5, 0.8	-

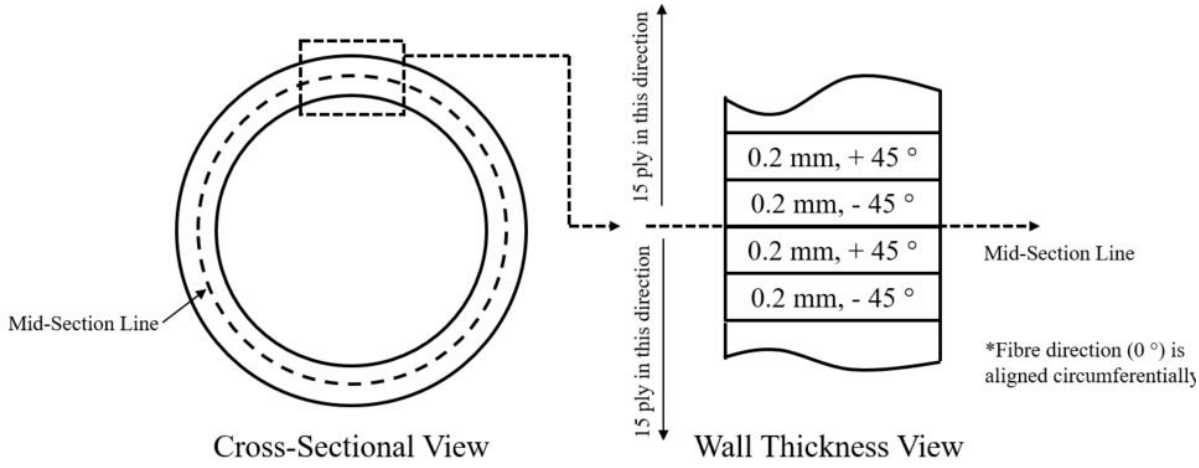

Figure 2. Stacking sequence

The base case failure criteria values, corresponding to the base case design talked into this sub-section, are presented in Table 4. These are calculated using the finite element model presented in Section 4.2. The results are calculated using the mesh size of 10 mm as discussed in Section 4.2.2. The failure modes are mainly caused by the matrix, i.e., the material fails in shear. The Tsai-Wu failure criterion does not distinguish failure modes. One can also notice the large difference in failure values calculated using Maximum Stress failure criterion vs. the rest of the criteria. This is because Maximum Stress failure criterion does not consider the strength contribution from the fibre when evaluating matrix failure. In this particular case, the strength contribution from the fibres would be significant as they are aligned 45° to the direction of hoop stress and therefore help to share some of the load away from the matrix.

Table 4. Base case failure criteria values

	Maximum Stress	Tsai-Wu	Hashin	Puck
Failure Criterion Value	0.642	0.905	0.899	0.934
Failure Mode	τ_{u12} exceeded	-	Matrix failure	Matrix tension failure

4.2. Finite element model

A 2 000 mm section of the flow-line is modeled. This is considered to be sufficiently long by engineering judgement in order to avoid end effects due to loads and boundary conditions in the finite element model. The results are obtained at the middle part of the section, i.e., at the 1 000 mm point. ANSYS R17.0 is used for the finite element modelling.

4.2.1. Loads and boundary conditions. The loads and boundary conditions applied on the model are illustrated in Figure 3. Pressure (Load A) is applied in the interior of the flow-line. Fixed support (Load B) is applied on the right edge of the flow-line. An end cap force (Load C) due to the internal pressure is applied on the left edge of the flow-line.

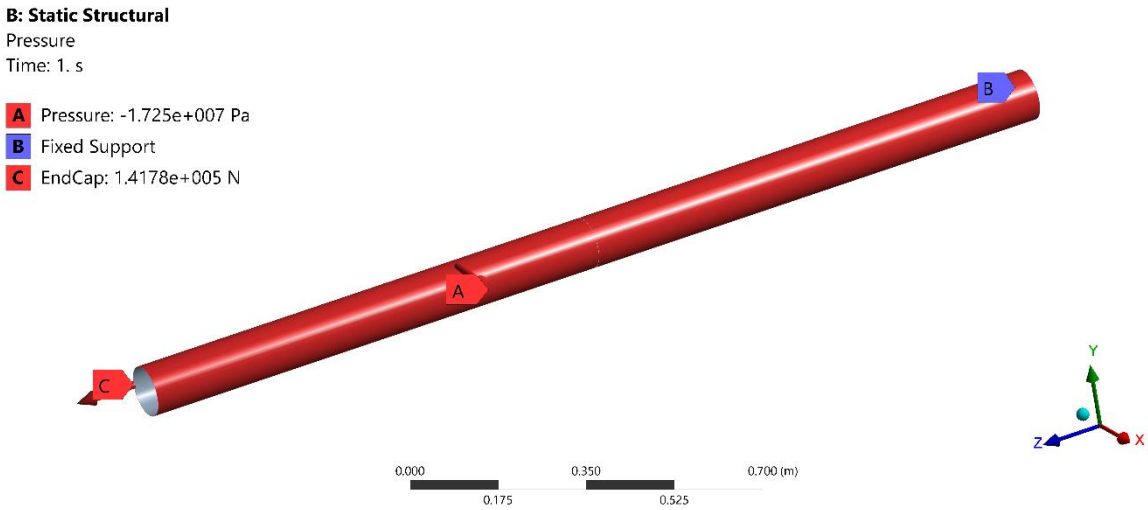

Figure 3. Loads and boundary conditions

4.2.2. Mesh refinement study. The cases studied and the corresponding results obtained for the mesh refinement study are presented in Table 5 and Figure 4 respectively. The element used is the 4-node SHELL181 element [23]. The results show that a 10 mm element size is sufficient to produce converged solutions for the four failure criteria investigated in this paper. The mesh details used in this paper are presented in Figure 5.

Table 5. Cases studied for mesh refinement study

Element Size (mm)	No. of Elements	No. of Nodes
30	888	900
20	900	1 552
15	2 904	2 926
10	6 386	6 400
5	24 896	24 960

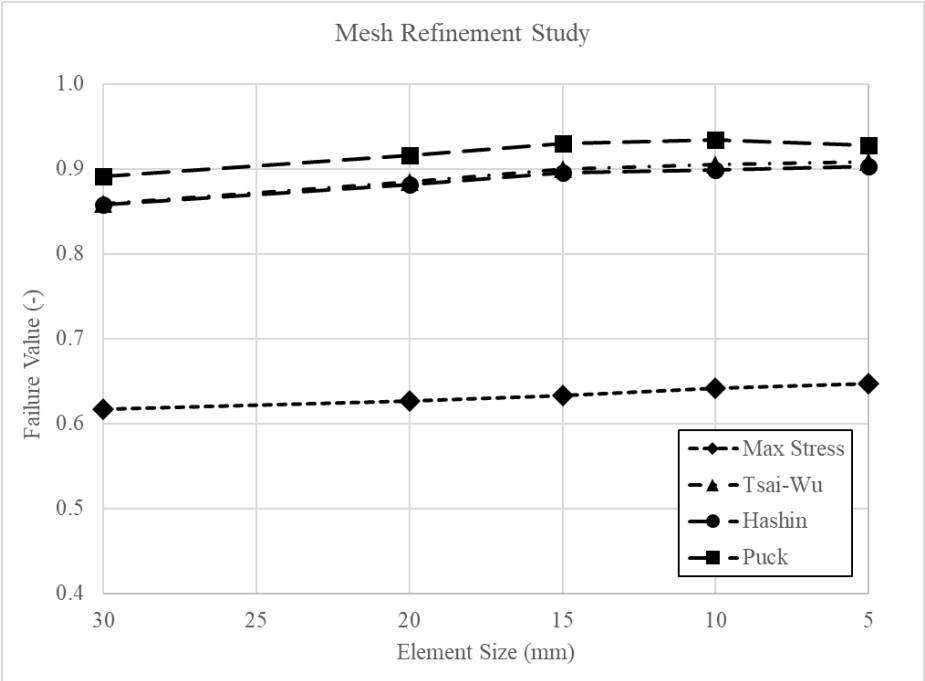

Figure 4. Results of mesh refinement study

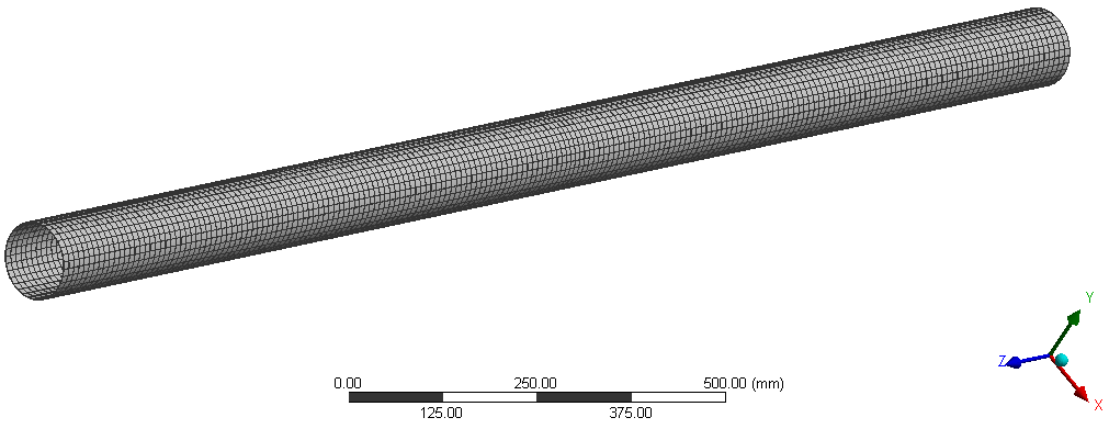

Figure 5. Mesh details, 10 mm element size, 6 386 SHELL181 elements with 6 400 nodes

4.2.3. Example result plots. An example plot of the maximum stress failure is presented in Figure 6. The maximum value generated by the failure function in the middle of the 2 000 mm flow-line is extracted and used in this paper.

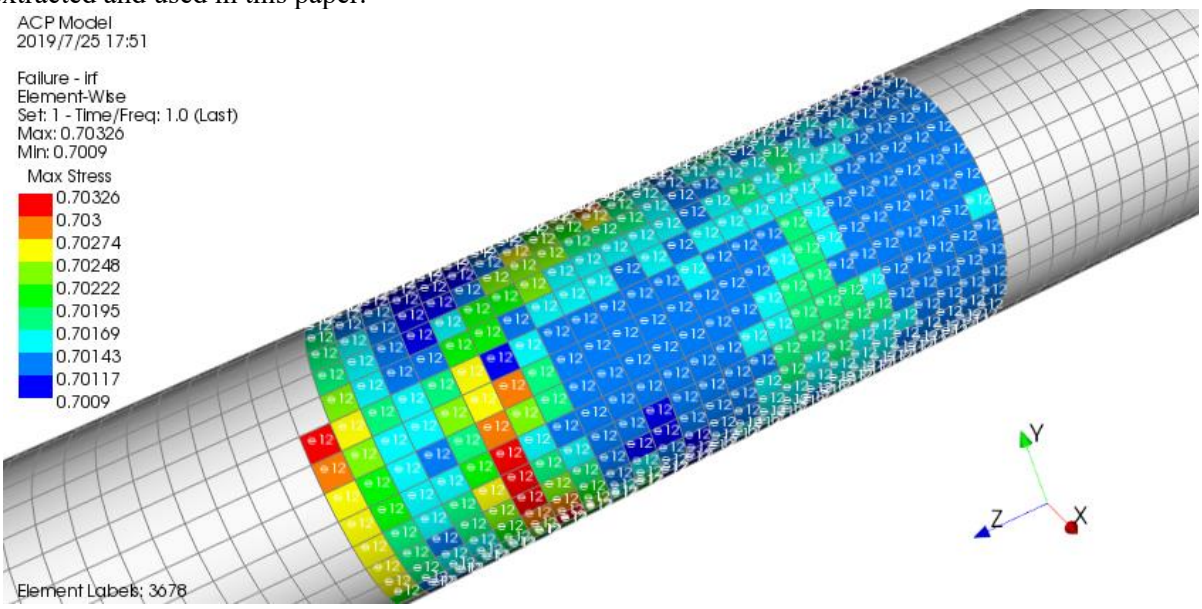

Figure 6. Example plot of maximum stress failure

5. Results and discussions

5.1. Correlation and determination matrices

The correlation and determination matrices are presented in Figure 7 and Figure 8, respectively. The matrices are calculated using Spearman correlation method and a sample size of 200. Notice that the correlation matrix is symmetrical. However, the determination matrix is not symmetrical. This is because $Cov(P_1^2,P_2^2) \neq Cov(P_2^2,P_1^2)$ The matrix calculated using the Pearson correlation identified the same set of major design parameters and therefore not presented here. The comparison of Pearson and Spearman correlation methods is presented in Section 5.2. The observations made are presented in the following sub-sections.

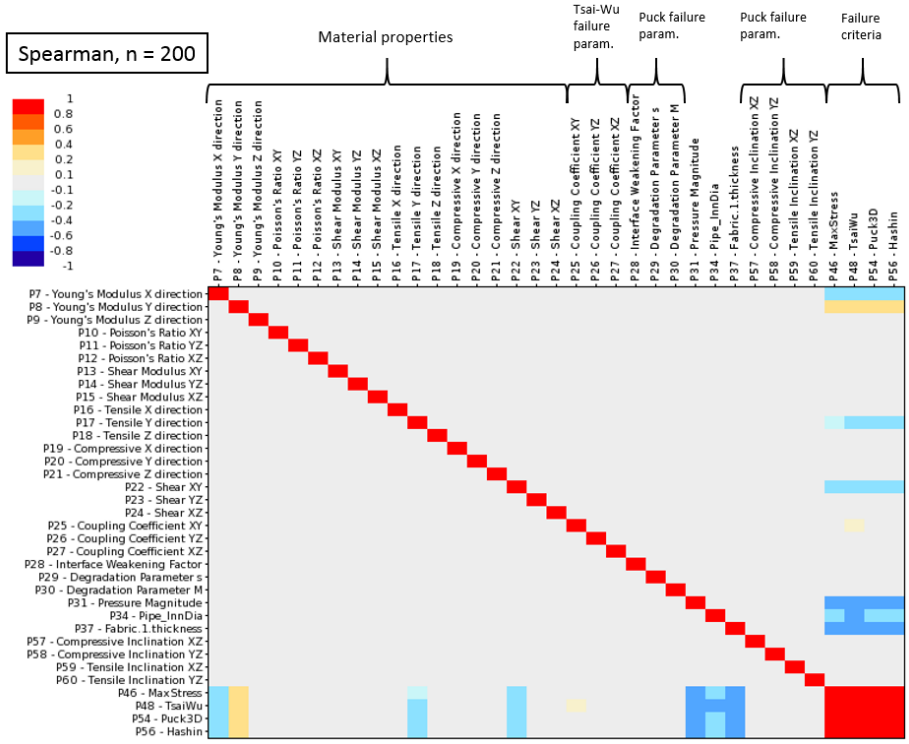

Figure 7. Correlation matrix, Spearman correlation, n = 200

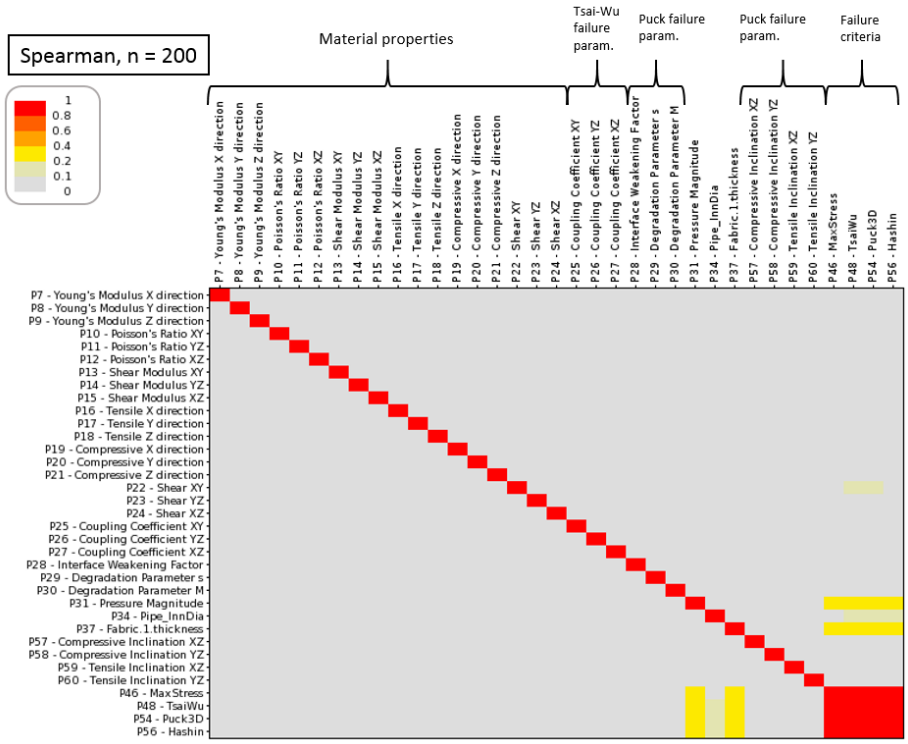

Figure 8. Determination matrix, Spearman correlation, n = 200

5.1.1. Strong correlations between failure criteria. The failure criteria have strong linear and quadratic correlations with one and other. The values of these correlations are all above 0.8. This is intuitive, an increase in the failure value calculated from one failure criterion will imply that the failure values calculated from other failure criteria would also increase. A detailed investigation into the correlation values presented in Table 6 and Table 7 revealed that the correlation is stronger between the Tsai-Wu, Hashin and Puck criteria. The Maximum Stress criterion is not as correlated, particularly for the quadratic correlations. This could be explained that Tsai-Wu, Hashin and Puck criteria are non-linear criteria while the Maximum Stress criterion is a linear criterion. In addition, Tsai-Wu and Hashin have failure functions of a quadratic nature.

Table 6. Spearman linear correlation, n = 200, failure criteria

	Maximum Stress	Tsai-Wu	Hashin	Puck
Maximum Stress	1.00	0.90	0.91	0.91
Tsai-Wu	0.96	1.00	0.96	0.97
Hashin	0.91	0.96	1.00	0.99
Puck	0.91	0.97	0.99	1.00

Table 7. Spearman quadratic correlation, n = 200, failure criteria

	Maximum Stress	Tsai-Wu	Hashin	Puck
Maximum Stress	1.00	0.81	0.83	0.84
Tsai-Wu	0.81	1.00	0.94	0.96
Hashin	0.82	0.94	1.00	0.98
Puck	0.84	0.96	0.98	1.00

5.1.2. Moderate correlations between applied pressure & ply thickness and failure criteria. The applied pressure, $P_{applied}$ and ply thickness, t_{ply} are moderately linearly correlated (0.4 to 0.6 or -0.6 to -0.4) with the failure criteria. These parameters are also slightly quadratically correlated (0.1 to 0.4 or -0.4 to -0.1). It is intuitive to understand that applied pressure and ply thickness would be naturally correlated with the failure criteria. The counter-intuitive thing is that the correlation is not strong. It can be natural to think that since hoop stress is directly proportional to the applied pressure and inversely proportional to wall thickness, therefore the correlation must be very strong. The moderate correlations can be understood by taking a closer examination at the correlation scatter diagram of Puck failure criteria vs. applied pressure and ply thickness as presented in Figure 9. Note the applied pressure (horizontal axis) is plotted in decreasing values, i.e., the right side of the horizontal axis denotes smaller values of applied pressure. From Figure 9, it is clear that the scatter is quite large; this is due to the fact that failure of the flow-line is not just fully dependent on the values of applied pressure and/or ply thickness but a result of many design parameters at play.

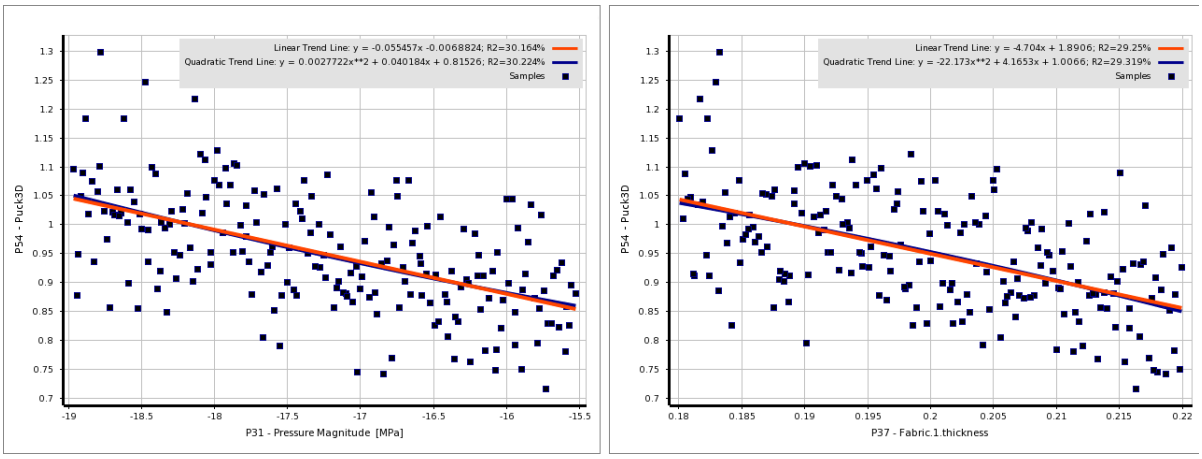

Figure 9. Correlation scatter diagram, Puck failure criterion vs. applied pressure and ply thickness, Spearman correlation, n = 200

5.1.3. Other parameters with slight correlation with failure criteria. The parameters that have slight linear correlations (0.1 to 0.4 or -0.4 to -0.1) with the failure criteria are elastic moduli, E_1, E_2, tensile strength, σ_{ut1}, shear strength, τ_{u12} and outer diameter, OD. In addition, Tsai-Wu constant, $F_{12,}$ has a slight correlation with the Tsai-Wu failure criterion. The other parameters that have slight quadratic correlations (0.1 to 0.4 or -0.4 to -0.1) with the failure criteria are shear strength, τ_{u12} and outer diameter, OD. The slight correlations of tensile strength σ_{ut1} and shear strength τ_{u12} can be surprising to the reader. However, this can be understood by examining their correlation scatter diagrams. Figure 10 presents the correlation scatter diagrams of Maximum Stress criterion vs tensile strength σ_{ut1} and shear strength τ_{u12}. It becomes clear why these two design parameters are only slightly correlated to the Maximum Stress criterion. As previously mentioned in Section 5.1.2. , the failure of the flow-line is not just dependent ontensile strength σ_{ut1} and shear strength τ_{u12} , but it is a result of many design parameters at play.

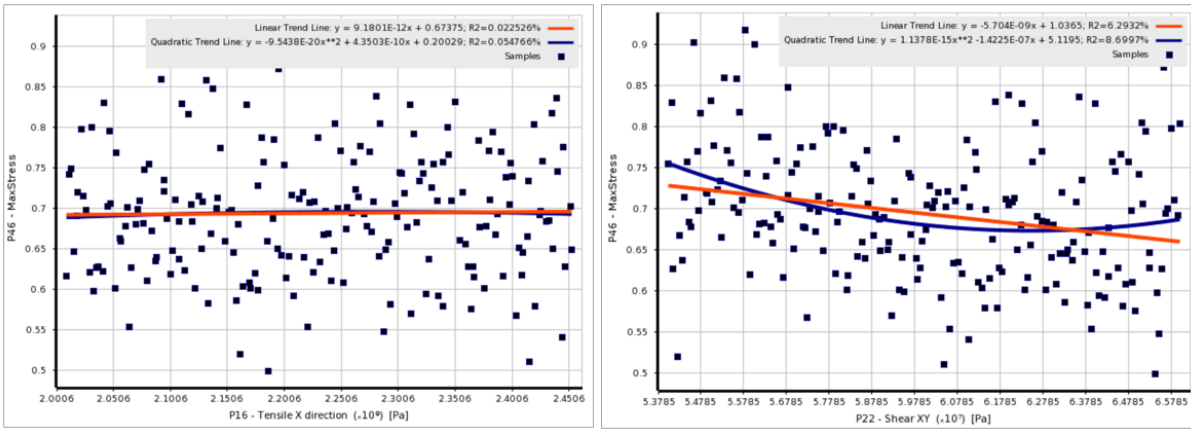

Figure 10. Correlation scatter diagram, maximum stress criterion vs. tensile strength σ_{ut1} and shear strength τ_{u12}, Spearman correlation, n = 200

5.1.4. Most material-related failure parameters insignificantly correlated with failure criteria. Most material-related failure parameters with the exception of Tsai-Wu constant, $F_{12,}$ do not exhibit

correlation (below |0.1|) to the failure criteria. This is due to the nature of the current loading considered which predominantly result in membrane stress along the pipe walls. This causes the load to be predominantly in the fibre direction. The failure parameters in the failure criteria, i.e., Tsai-Wu constants and all Puck constants considered are primarily defined to model transverse, bending and/or inter-laminar loading. It is expected that these failure parameters would play a more important role in the failure criteria when more complex loadings are considered.

5.2. Pearson vs. Spearman

Both Pearson and Spearman correlation methods identified the same set of major design parameters as presented in Figure 11 and Figure 12.

5.3. Effect of sample size

In general, the larger the sample size, the more likely design parameters with lower values of correlation get highlighted in the correlation and determination matrices. However, the governing design parameters, i.e., parameters with higher values of correlation would still be highlighted on the matrices. This is highlighted by the example presented in Figure 13 where the Spearman correlation matrix from n = 50 is compared against n = 200. It is observed that the darker coloured squares, i.e., high correlation values are practically the same for n = 50 and n = 200. The difference is in the lighter coloured squares, i.e., low correlation values. For practical engineering purposes, a sample size of 100 seemed to be sufficient in this paper.

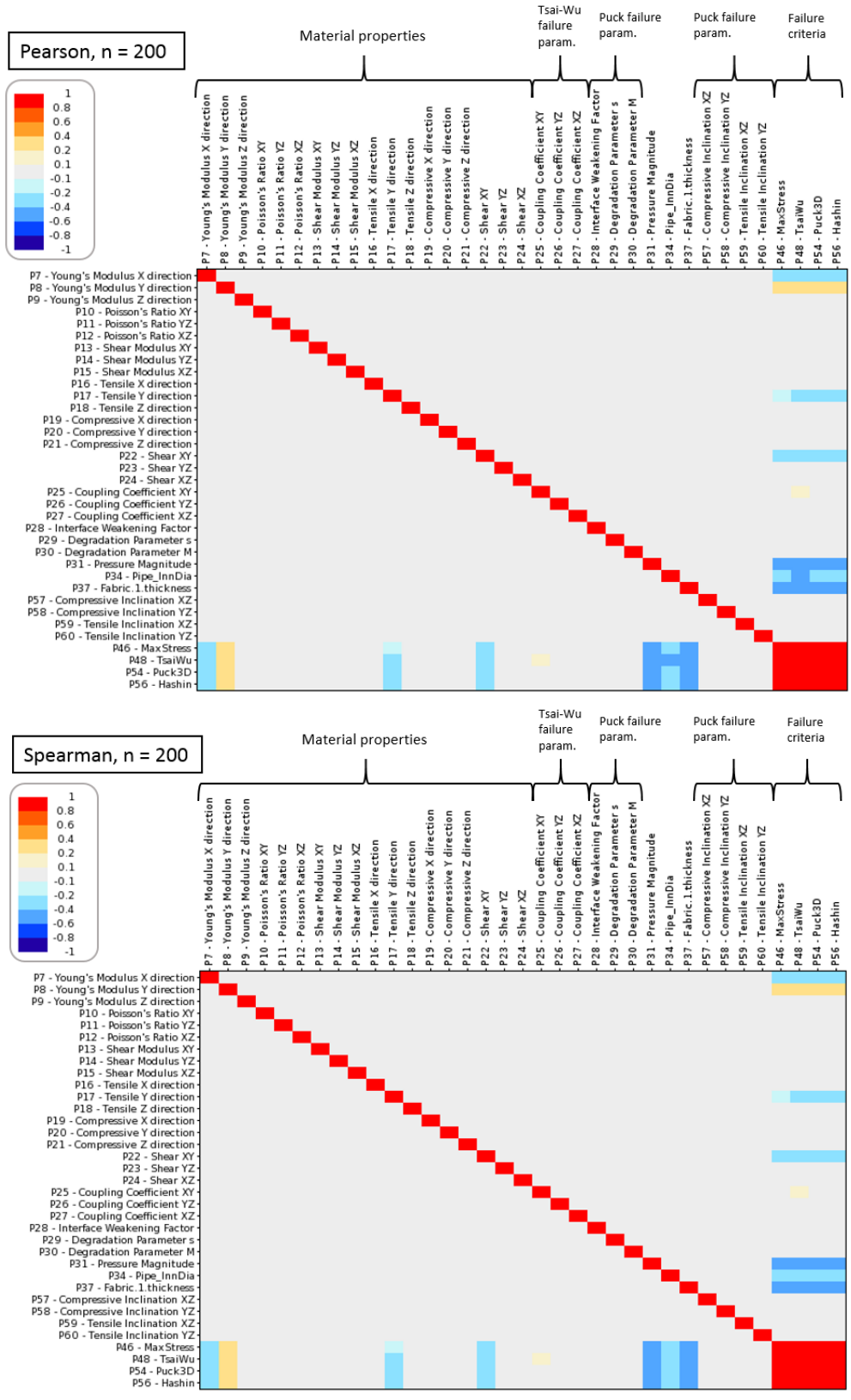

Figure 11. Comparison of linear correlation matrices, Pearson vs. Spearman

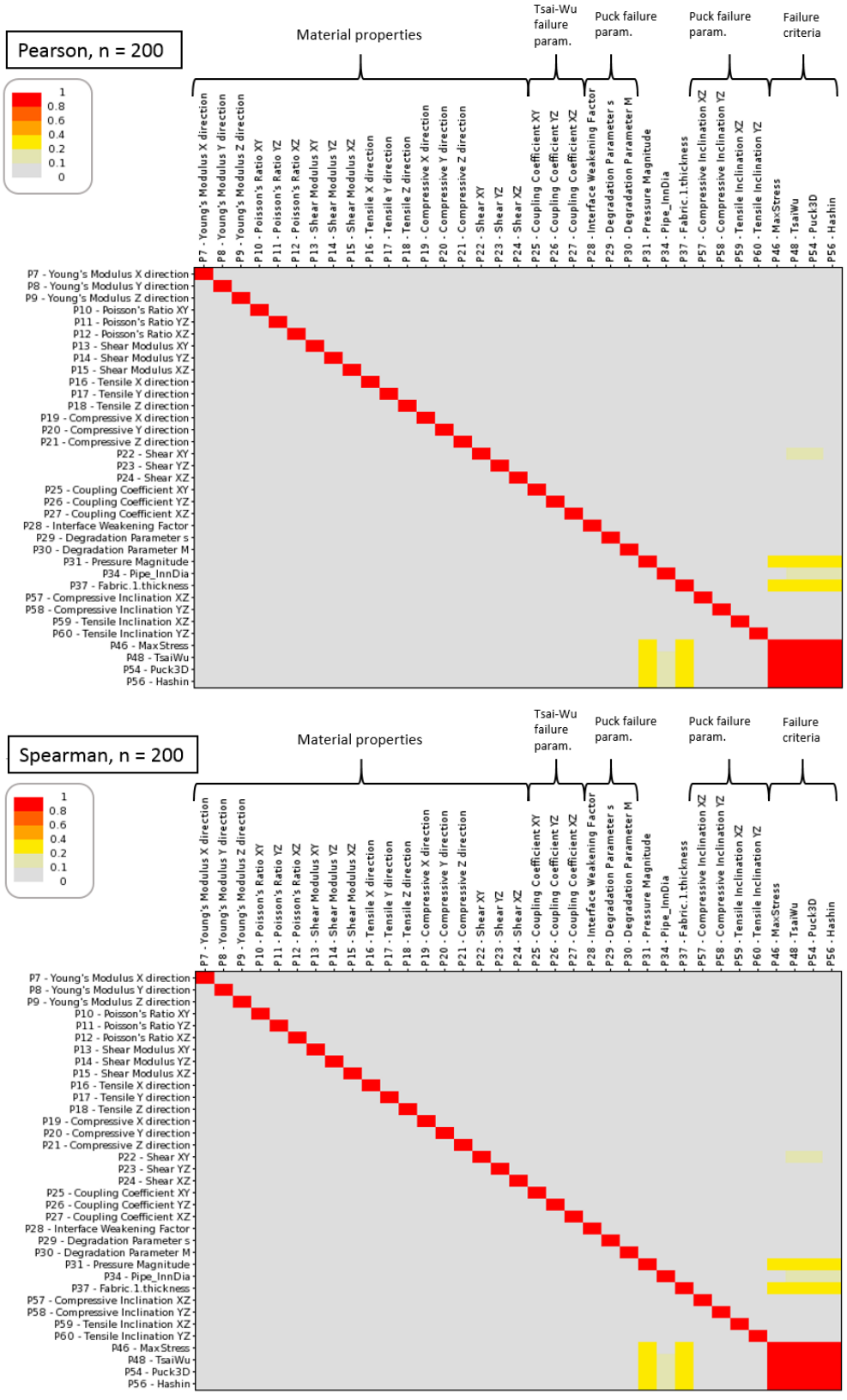

Figure 12. Comparison of quadratic correlation matrices, Pearson vs. Spearman

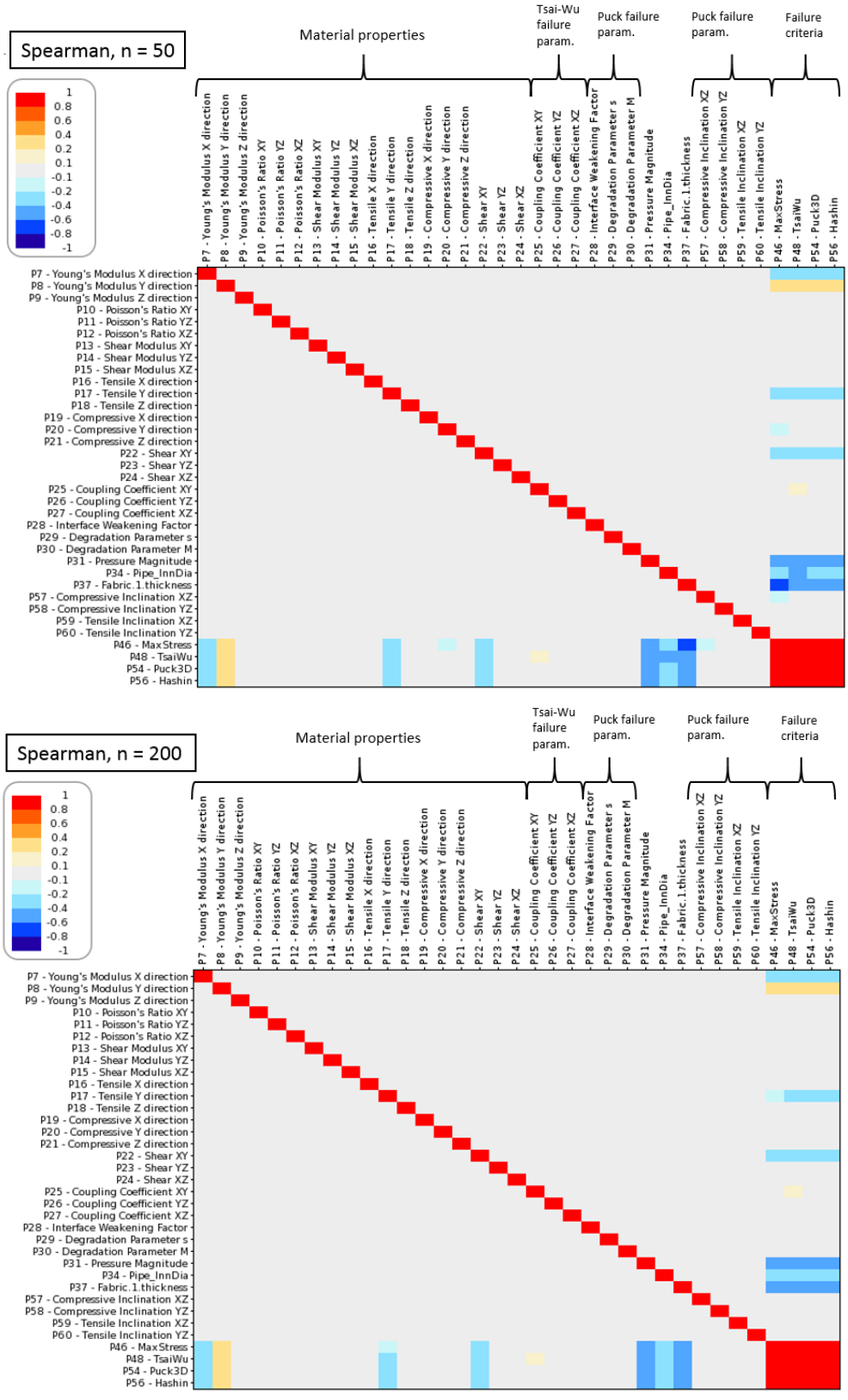

Figure 13. Comparison of correlation matrices, Spearman correlation, n = 50 vs. n = 200

6. Conclusions

The following conclusions are made:

- Strong linear and quadratic correlations are observed between the failure criteria.
- Moderate linear and slight quadratic correlations are observed between applied pressure & ply thickness and the failure criteria.
- Most material failure parameters with the exception of Tsai-Wu constant, $F_{12,}$ are not strongly correlated to the failure criteria. This can be explained by the fact that the loads experienced by the flow-line are pre-dominantly in the fibre direction.
- Both Pearson and Spearman correlation methods identified the same set of major design parameters for the correlation matrix.
- The effect of sample size is not profoundly significant to the results. There were no large differences found in using sample sizes of 50 vs. 100 vs. 200. For practical engineering purpose a sample size of 100 is recommended.

7. Future work

There are plans to extend the study to include (i) external tension/compression forces and bending moments, (ii) response surface development and optimisation and (iii) six-sigma analysis. Furthermore, additional failure modes such as fatigue and collapse can be studied in future work. Other design scenarios such as pipeline global buckling and installation can also be investigated. The objective is to provide a framework for the design optimisation of flow-lines when non-traditional materials such as CFEC are used.

References

[1] Reza Khoshravan Azar M, Emami Satellou A A, Shishesaz M and Salavati B 2013 Calculating the optimum angle of filament-wound pipes in natural gas transmission pipelines using approximation methods, *J. Pressure Vessel Technol.* **135**(2), 021702.

[2] Theotokoglou E E 2006 Behaviour of thick composite tubes considering of delamination, *Theor. Appl. Fract. Mech.* **46**(3), 276-85.

[3] Xia M, Takayanagi H and Kemmochi K 2001 Analysis of multi-layered filament-wound composite pipes under internal pressure, *Compos. Struct.* **53**(4), 483-91.

[4] Chouchaoui C S and Ochoa O O 1999 Similitude study for a laminated cylindrical tube under tensile, torsion, bending, internal and external pressure. Part I: governing equations, *Compos. Struct.* **44**(4), 221-29.

[5] Guz I A, Menshykova M and Paik J K 2017 Thick-walled composite tubes for offshore applications: an example of stress and failure analysis for filament-wound multi-layered pipes, *Ships and Offshore Structures.* **12**(3), 304-22.

[6] Tsai S W and Wu E M 1971 A general theory of strength for anisotropic materials, *J. Compos. Mater.* **5**(1), 58-80.

[7] Hashin Z 1980 Failure criteria for unidirectional fiber composites, *J. Appl. Mech.* **47**(2), 329.

[8] Puck A 1996 Festigkeitsanalyse von faser-matrix-laminaten. (Carl Hanser).

[9] Puck A 1998 Failure analysis of FRP laminates by means of physically based phenomenological models, *Compos. Sci. Technol.* **58**(7), 1045-67.

[10] Puck A 2002 Schürmann H. Failure analysis of FRP laminates by means of physically based phenomenological models, *Compos. Sci. Technol.* **62**(12-13), 1633-62.

[11] Pearson K 1920 Notes on the history of correlation, *Biometrika.* **13**(1), 25-45.

[12] Pearson K 1986 Mathematical contributions to the theory of evolution. III. Regression, Heredity, and Panmixia, *Philos. Trans. R. Soc. London, Ser. A, Containing Papers of a Mathematical or Physical Character.* **187**, 253-318.

[13] Spearman C E 1904 The proof and measurement of association between two things, *Am. J. Psychol.* **15**, 72-101.

[14] Spearman C E 1904 General intelligence, objectively determined and measured, *Am. J. Psychol.* **15**, 201-93.
[15] Spearman C E 1910 Correlation calculated from faculty data, *Br. J. Psychol*, 1904-1920. **3**(3), 271-95.
[16] Vanderplaats G N 2007 Multidiscipline design optimization (Colorado Springs)
[17] Nettles A T 1994 Basic mechanics of laminated composite plates. (Marshall Space Flight Center, NASA).
[18] Palantera M 1998 ESAComp 4.1 - theoretical background of ESAComp analyses.
[19] Jones R M 1975 Mechanics of composite material (Hemisphere).
[20] Kirchhoff G 1850 Über das gleichgewicht und die bewegung einer elastischen scheibe, *J. Reine und Angewante Mathematik* (Crelle). **40**, 51-88.
[21] Love A E H 1906 A treatise on the mathematical theory of elasticity (Cambridge).
[22] Gol'denblat II, Kopnov V A 1966 Strength of glass-reinforced plastics in the complex stress state - english translation, *Polymer Mechanics.* **1**, 54.
[23] ANSYS®. Academic research mechanical, release 17.0, help system, element reference, chapter I, SHELL181, ANSYS, Inc.

Appendix II

Paper 2: Using Kriging Response Surface Method for the Estimation of Failure Values of Carbon-Fibre-Epoxy Composite Flowlines under the Influence of Stochastic Processes

Appendix II contains the paper which has been submitted to Journal of Mechanical Engineering Science

Using Kriging Response Surface Method for the Estimation of Failure Values of Carbon-Fibre-Epoxy Composite Flowlines under the Influence of Stochastic Processes

Yihan Xing*, University of Stavanger

Wenxin Xu, University of Stavanger

Valentina Buratti, Aibel AS

*Corresponding author: yihan.xing@uis.no

Abstract

This paper investigates the use of Kriging response surface method for the estimation of failure values in carbon-fibre-epoxy composite flowlines under the influence of stochastic processes. A case study of a 125 mm flowline is investigated. A comprehensive suite of failure modes that comprises of Maximum Stress, Tsai-Wu and Hashin failure criteria is used to quantify the burst design under combined loading with axial forces, torsion and bending moments. A large set of measured values are generated using Monte Carlo simulation and used as the 'Base Case' population which the results from the response surfaces are compared to. The response surfaces are evaluated in detail in terms of their ability to reproduce the statistical moments, probability and cumulative distributions and failure values at low probabilities of failure. In addition, the optimisation of the response surface calculation would be investigated in terms of reducing the number of input parameters and size of the response surface. Finally, a decision chart which can be used to build a response surface to calculate failures in a CFEC flowline is proposed based on the findings obtained. The results show that the response surface method is suitable to be used and can calculate failure values close to that calculated using a large set of measured values. This paper provides an analysis framework to aid in the identification of the major design parameters, response surface generation and failure prediction for CFEC flowlines.

Keywords

Composite material, Tsai-Wu, Response surface, Optimization, Failure analysis

Nomenclature

σ_h	Hoop stress
σ_l	Longitudinal stress

σ_1	Principle stress in x-direction
σ_2	Principle stress in y-direction
σ_3	Principle stress in z-direction
τ_{12}	Shear stress in xy-plane
τ_{23}	Shear stress in yz-plane
τ_{13}	Shear stress in xz-plane
σ_{uc1}	Compressive strength limit in x-direction
σ_{uc2}	Compressive strength limit in y-direction
σ_{uc3}	Compressive strength limit in z-direction
σ_{ut1}	Tensile strength limit in x-direction
σ_{ut2}	Tensile strength limit in y-direction
σ_{ut3}	Tensile strength limit in z-direction
τ_{u12}	Shear strength limit in xy-plane
τ_{u23}	Shear strength limit in yz-plane
τ_{u13}	Shear strength limit in xz-plane
$\rho_{rgX,rgY}$	Spearman correlation coefficient
$cov(r_{gX}, r_{gY})$	Covariance of the rank variable
σ_{rg_X}	Standard deviation of the rank variable g_X
σ_{rg_Y}	Standard deviation of the rank variable g_Y
D	Flowline Diameter

t	Flowline wall thickness

1 Introduction

Subsea flowlines play an important role in the subsea system. They transport production/injection fluids from the subsea wells to the subsea manifolds and vice versa. A higher number of deep-water oil and gas reservoirs are exploited in recent developments experienced in the oil and gas industry. This increased the average depth of oil wells drilled from 1108 m in 1949 and to 1818 m in 2008 (U.S. Energy Information Administration, 2020). At the same time, the total length of the oil and gas trunk pipeline is expected to increase from 1.9 million km in 2019 to 2.2 million km in 2023 (GlobalData, 2019). This increase in distance and water depth would lead to higher associated capital and operating costs. The average pipeline cost increased from $94000 per inch-mile in 2011 to $155000 per inch-mile in 2002, according to ICF International (ICF International for The INGAA Foundation, 2014). One cost-effective solution which is gaining popularity in the subsea industry is to utilise composite materials instead of the traditionally used steel material for the subsea flowline. Several projects that have utilised composite flowlines are Alder, Åsgard, West Lutong fields. Composite material has long been utilized in industries such as aerospace and automotive industries for a variety of application. Some applications include to use it for components such as the aircraft tail, wings and propellers, boat and scull hulls, storage tanks. They are valued for their high strength-to-weight ratio and the ability to customise the material directional strength properties by adjusting the laminate layout according to the application it is designed for. Composite materials are not new in the subsea industry. They have been utilised to make subsea protection covers and ROV buckets. Their corrosion resistance properties in addition to their strength properties make them particularly attractive in the offshore and subsea oil and gas industry. These properties make composite material an attractive choice in high performance subsea flowline applications where long reaches, deep waters, high loads and temperatures are encountered.

The carbon-fibre epoxy composite (CFEC) which consists of an epoxy matrix with carbon fibres is a commonly used type of composite material when a high strength to weight ratio is desired. The epoxy matrix protects the fibres from external environment and transfer the loads between the fibres, while the fibres provide the strength and stiffness to the component. As presented in Table 1, CFEC is nearly five times lighter and two times stronger than steel. This allows CFEC structures to carry larger loads compared to metal structures of the same weight. Moreover, as with all composite materials, the good corrosion properties also make CFEC suitable for the use in harsh environments such as for subsea oil and gas applications.

Table 1: Comparison of Epoxy Carbon UD (230Gpa) and Steel AISI 4130

	Yield Strength (GPa)	**Ultimate Tensile Strength (GPa)**	**Density (g/cm3)**	**Strength to Weight Ratio**
Epoxy Carbon UD	3.53	2.231	1.49	1.497
Steel, AISI 4130	0.95	1.11	7.85	0.141

The anisotropic nature of CFEC materials demands for very comprehensive and robust stress analyses. Several previous studies were published by various authors within pipeline stress analysis. Some examples include Yang (2000) whom analysed the stresses at composite pipe joints under tensile loading and Jha et al. (2014) whom analysed the stresses in composite flexibles for deep-water applications. Due to the complex subsea terrain, current and other factors, the subsea CEFC flowline experiences a complex form of combined loading. In addition, the joint action of random parameters from loads, materials and geometry means that it may be necessary to apply stochastic models in the engineering design. Some authors have previously presented stochastic process applied in pipeline engineering problems. These include Bazan et al. (2013) whom studied the stochastic process to predict the corrosion growth for pipeline and Oliveira et al. (2016) whom performed probabilistic analysis of the collapse pressure of corroded pipelines. However, applying stochastic considerations in engineering design problems is typically not widely adopted. This is mainly due to the reason that it requires a large sample size, i.e., a large set of realisation values. This requires time resources which can be valuable in engineering projects.

The response surface methodology is an approach that calculate an approximate result based on a response surface. The response surface is modelled by sample results calculated from simulation or measured in real life. This method requires fewer samples compared to the traditional approach when applied in the stochastic analysis of a structure. Some examples of response surface methods applied in engineering problems are presented here. Jia et al. (2016) studied the Kriging-base response surface application in structure reliability. Simpson et al. (1998) compared the response surface and kriging models for multidisciplinary design optimization. Gupta et al. (2004) suggested an improved response surface method of failure probability determination. These studies showed that the response surface is a convenient tool in engineering analysis and optimization. However, the utilization of response surface does require careful consideration since the response results are approximate results. There are a lot of factors that affect the accuracy. These includes the response surface type, chosen of parameters, refinement method, etc.

To the authors' knowledge, there has been no prior studies on using response surfaces as a tool to calculate failure values for CEFC flowlines in a more efficient manner. This paper studies in detail the influence of stochastic processes on the use of Kriging response surface method to predict failure rates in a CFEC flowline subjected to combined loading. Tsai-Wu (Tsai et al., 1971), Maximum Stress and Hashin (Hashin, 1980) failure criteria are used to quantify failure of the composite material. A large set of measured values are generated using Monte Carlo simulation and used as the 'Base Case' population which the results from the response surfaces are compared to. The response surfaces are evaluated in detail in terms of their ability to reproduce the statistical moments, probability and cumulative distributions and failure values at low probabilities of failure. In addition, the optimisation of the response surface calculation would be investigated in terms of reducing the number of input parameters and size of the response surface. Finally, a decision chart which can be used to build a response surface to calculate failures in a CFEC flowline is proposed based on the findings obtained. The modelling and the design optimization are performed using ANSYS Composite Pre/Post, Mechanical and DesignXplorer,

2 Preliminaries

2.1 Failure Criteria

Failure criteria are used in engineering to evaluate the structural integrity of a component. Generally, failure criteria compare the stresses experienced by the structure to the allowable stress values. When the ratio between the two stresses is larger than 1, the component is usually considered "to fail". Failure criteria for composites materials can be grouped into two categories, non-interactive failure criteria and interactive failure criteria, respectively. Non-Interactive failure criteria as the name suggests assumes no interaction between stress or strain tensor components, i.e., the tensor components are evaluated individually. An example is the maximum stress criterion. In contrast, Tsai-Wu (Wu et al., 1971) failure criterion and Hashin (Hashin, 1980) failure criterion are two examples of interactive failure criteria. Interactive failure criteria describe the failure value as a combined function of the stress or strain tensor components. The three failure criteria mentioned above are chosen to study the burst design of CFEC flowline in this paper. It is noted that since classical laminate theory is used, the stresses component in z-direction are neglected, i.e., $\sigma_3 = \tau_{23} = \tau_{13} = 0$ in the following sections.

2.1.1 Maximum Stress Failure Criterion

Maximum Stress failure criterion is a conservative and commonly used criterion for composite materials (Feng et al., 2019). The failure occurs when the stresses in any principle direction exceed the material strength in that direction. The failure value is calculated using Equation (1).

$$f = max\left(\left|\frac{\sigma_1}{X}\right|, \left|\frac{\sigma_2}{Y}\right|, \left|\frac{\sigma_3}{Z}\right|, \left|\frac{\tau_{12}}{S}\right|, \left|\frac{\tau_{13}}{R}\right|, \left|\frac{\tau_{23}}{Q}\right|\right) \quad (1)$$

Where:

$$X = \begin{cases} \sigma_{uc1}, \sigma_1 < 0 \\ \sigma_{ut1}, \sigma_1 \geq 0 \end{cases}, \qquad S = \tau_{u12} \quad (2)$$

$$Y = \begin{cases} \sigma_{uc2}, \sigma_2 < 0 \\ \sigma_{ut2}, \sigma_2 \geq 0 \end{cases}, \qquad R = \tau_{u13}$$

$$Z = \begin{cases} \sigma_{uc3}, \sigma_3 < 0 \\ \sigma_{ut3}, \sigma_3 \geq 0 \end{cases}, \qquad Q = \tau_{u23}$$

2.1.2 Tsai-Wu Failure Criterion

The Tsai-Wu failure criterion (Wu et al., 1971) is based on the work of Gol'denblat and Koponov (Gol'denblat et al., 1965). The criterion assumes the existence of a failure surface and distinguishes between the compressive and tensile strength in the ply failure prediction. The failure criterion uses the following quadratic formulation presented in Equation (3).

$$f = \frac{\sigma_1^2}{\sigma_{ut1}\sigma_{uc1}} + \frac{\sigma_2^2}{\sigma_{ut2}\sigma_{uc2}} + \frac{\tau_{12}^2}{{\tau_{u12}}^2} + \sigma_1\left(\frac{1}{\sigma_{ut1}} - \frac{1}{\sigma_{uc1}}\right) + \sigma_2\left(\frac{1}{\sigma_{ut2}} - \frac{1}{\sigma_{uc2}}\right) + 2F_{12}\sigma_1\sigma_2 \quad (3)$$

F_{12} is a user-specified parameter and is only associated with principle stresses σ_1 and σ_2. One commonly used form of F_{12} is presented in Equation (4).

$$F_{12} = -\frac{1}{2}\sqrt{\left(\frac{1}{\sigma_{ut1}} - \frac{1}{\sigma_{uc1}}\right)\left(\frac{1}{\sigma_{ut2}} - \frac{1}{\sigma_{uc2}}\right)} \quad (4)$$

F_{12} is also commonly obtained using bi-axial tests. Some examples can be found in (Clouston et al., 1998) and (Li et al., 2017).

2.1.3 Hashin Failure Criterion

Hashin failure criterion (Hashin, 1980) was originally developed for unidirectional polymeric composites. The failure criterion distinguishes between three different types of failure modes, namely fibre failure, matrix failure and interlaminate failure, respectively. These failure modes are illustrated in Figure 1.

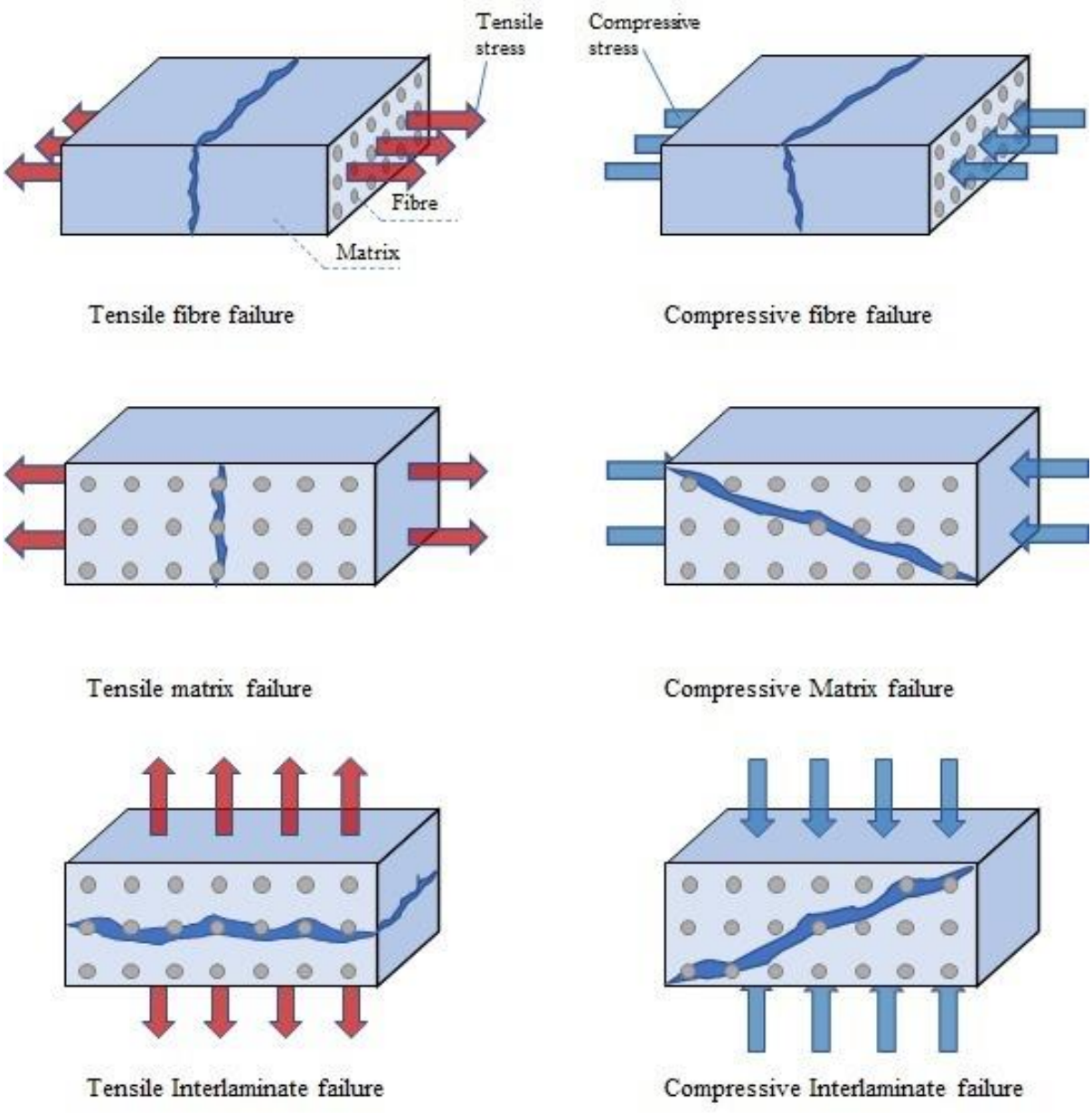

Figure 1: Illustration of the Various Failure Modes in Hashin Failure Criterion

The criterion for tensile fibre failure is presented in Equation (5).

$$f = \left(\frac{\sigma_1}{\sigma_{ut1}}\right)^2 + \left(\frac{\tau_{12}}{\tau_{u12}}\right)^2, \sigma_1 \geq 0 \quad (5)$$

The criterion for compressive fibre failure is presented in Equation (6).

$$f = -\frac{\sigma_1}{\sigma_{ut1}}, \sigma_1 < 0 \quad \textbf{(6)}$$

The criterion for tensile matrix failure is presented in Equation (7).

$$f = \left(\frac{\sigma_2}{\sigma_{ut2}}\right)^2 + \left(\frac{\tau_{23}}{\tau_{u23}}\right)^2 + \left(\frac{\tau_{12}}{\tau_{u12}}\right)^2 + \left(\frac{\tau_{13}}{\tau_{u13}}\right)^2 \quad \textbf{(7)}$$

The criterion for compressive matrix failure is presented in Equation (8).

$$f = \left(\frac{\sigma_2}{2\tau_{u23}}\right)^2 + \left(\frac{\tau_{23}}{\tau_{u23}}\right)^2 + \left(\frac{\tau_{12}}{\tau_{u12}}\right)^2 + \left[\left(\frac{\sigma_{uc2}}{2\tau_{u23}}\right)^2 - 1\right]\frac{\sigma_2}{\sigma_{uc2}} \quad \textbf{(8)}$$

The criterion for tensile interlaminate failure is presented in Equation (9).

$$f = \left(\frac{\sigma_3}{\sigma_{uc3}}\right)^2 + \left(\frac{\tau_{13}}{\tau_{u13}}\right)^2 + \left(\frac{\tau_{23}}{\tau_{u23}}\right)^2, \sigma_3 < 0 \quad \textbf{(9)}$$

The criterion for compressive interlaminate failure is presented in Equation (10).

$$f = \left(\frac{\sigma_3}{\sigma_{ut3}}\right)^2 + \left(\frac{\tau_{13}}{\tau_{u13}}\right)^2 + \left(\frac{\tau_{23}}{\tau_{u23}}\right)^2, \sigma_3 \geq 0 \quad \textbf{(10)}$$

2.1.4 Calculation of Failure Values

The failure values are calculated using ANSYS Composite Pre/Post. The failure results as well as the failure modes will be shown in the ACP solution. As presented in 2.1.1, 2.1.2 and 2.1.3, three failure criteria have different failure modes. For the Maximum stress, the failure modes are associated with σ_1, σ_2 and σ_3, while the Tsai-Wu failure criteria do not distinguish between the failure modes. Hashin failure criteria has matrix failure, fibre failure and interlaminate failure. An example of Hashin failure criterion plot is shown in Figure 2. These are calculated at the middle of the flowline as illustrated in the example plot presented in Figure 3. Details of the flowline model is presented in Section 3.

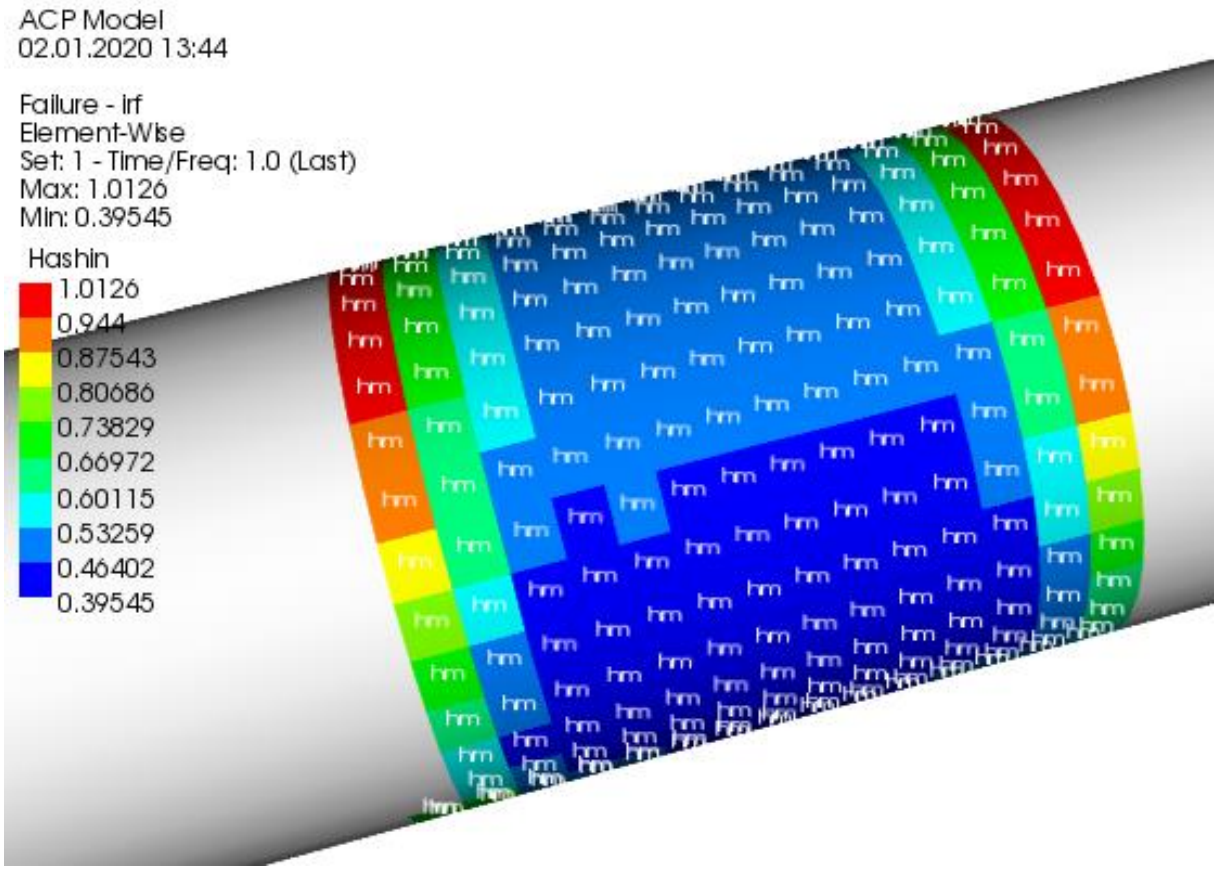

Figure 2: Example of Failure Criterion Plot – Hashin Failure Criterion

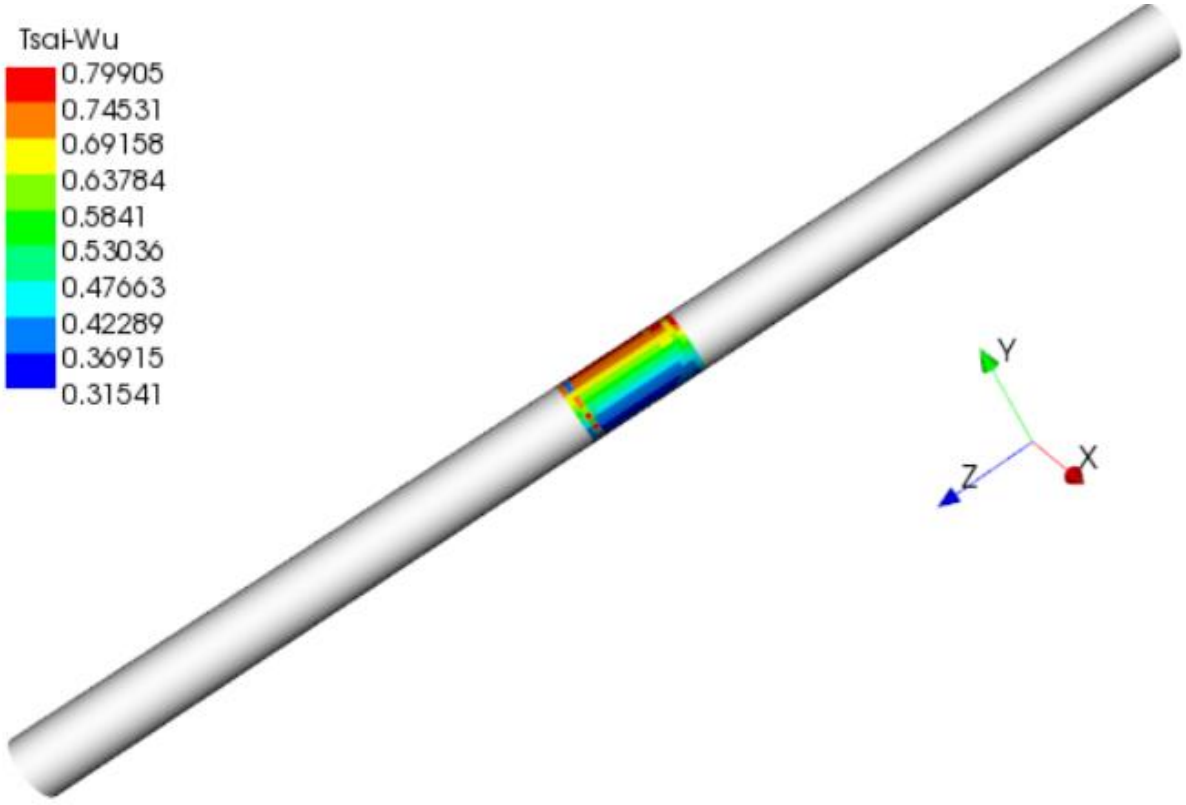

Figure 3: Example of Tsai-Wu Failure Values calculated at the Middle of the Flowline

2.2 Parameter Correlation

In this paper, Spearman (Spearman, 1910) correlation method is applied to identify the most important parameters to be included in the response surfaces; the response surface methodology is presented in Section 2.3. The Spearman correlation method is a rank-order method which calculates the monotonic relationship between two ranked variables as presented in Equation (11).

$$\rho_{rgX,rgY} = \frac{cov(rg_X, rg_Y)}{\sigma_{rg_X}\sigma_{rg_Y}} \quad (11)$$

The calculated correlation coefficient varies from -1.0 to 1.0 and measures the statistical coupling between two parameters, x and y. The values of the calculated coefficient can be interpreted as follows:

- 0.0 to 0.2 – Slightly correlated, the relationship is almost negligible.
- 0.2 to 0.4 – Lowly correlated, but the relationship is definite.
- 0.4 to 0.6 – Moderately correlated, the relationship is substantial.
- 0.6 to 0.8 – Highly correlated, the relationship is marked
- 0.8 to 1.0 – Very highly correlated, the relationship is very dependable

A positive coefficient means that the output parameter increases when the input parameter increases and vice versa. The correlation matrix is a n×n matrix which consists of n^2 correlation coefficients describing the correlation between n design parameters. The matrix provides an overview of which parameters influence the output variables more. The top 20 parameters with the highest values of coefficient are included in the set of parameters used in the generation of the response surface model.

2.3 Response Surface Methodology

The response surface methodology was first introduced by Box and Wilson in 1951 (Box et al., 1951) and uses mathematical modelling to approximate the relationship between one or more input parameters and one or more output variables. This means (Output1, Output 2, …) = F (Input1, Input2, …) where F is the response surface. The response surface methodology is especially useful to describe the model responses in the case when the detailed function describing the input parameters to the output variables is complex and usually unknown. This is because the response surface methodology approximates the function without the need for knowing the details about the function.

The applied response surface method in this paper is Kriging response surface method (Krige, 1950). It is an interpolation method which interpolate the values generated by gaussian process governed by prior covariances.

It is similar to inverse distance weighting method, i.e., it weighs the surrounding measured values to calculate a predicted result at an unknown location. The general formula for Kriging response surface method is presented in Equation (12).

$$\hat{Z}(s_0) = \sum_{i=1}^{n} \lambda_i \hat{Z}(s_i) \quad (12)$$

$Z(s_i)$ is the measure value at the ith location, λ_i is an unknown weight for the measured value at the ith location, s_0 is the predicted location and *n* is the number of measured values.

The response surface tool in ANSYS uses the most correlated parameters identified from the correlation matrix to generate a required size of measured values. This process is called design of experiment. The central composite design method (Box et al., 1951) is used. A larger response surface requires a larger design of experiment exercise, i.e., a larger number of measured values. Verification points are calculated after the response surface is generated. The values from the verification points are checked against the measured values using predicted relative error values as defined in Equation (13).

$$Predicted\ relative\ error = \frac{Predicted\ error}{Maximum\ known\ value - Minimum\ known\ value} \times 100\% \quad (13)$$

Where:

$$Predicted\ error = \frac{Measured\ value}{Predicted\ value - Measured\ value} \quad (14)$$

As observed in Equation (13), the predicted relative error is a value that is normalised by the known maximum variation of the output parameter. This allows for easy comparison across all output parameters in the design space. A predicted relative error of 5 % is used in this paper. The response surface will be refined iteratively with more measured values from the design of experiment until the predicted relative error of all output parameters fall below the threshold. Figure 4 presents an example plot of the refinement of the Kriging response surface. It is observed in Figure 4 that the Tsai-Wu, Maximum Stress and Hashin failure criteria had predicted relative error below 5 % after two iterations.

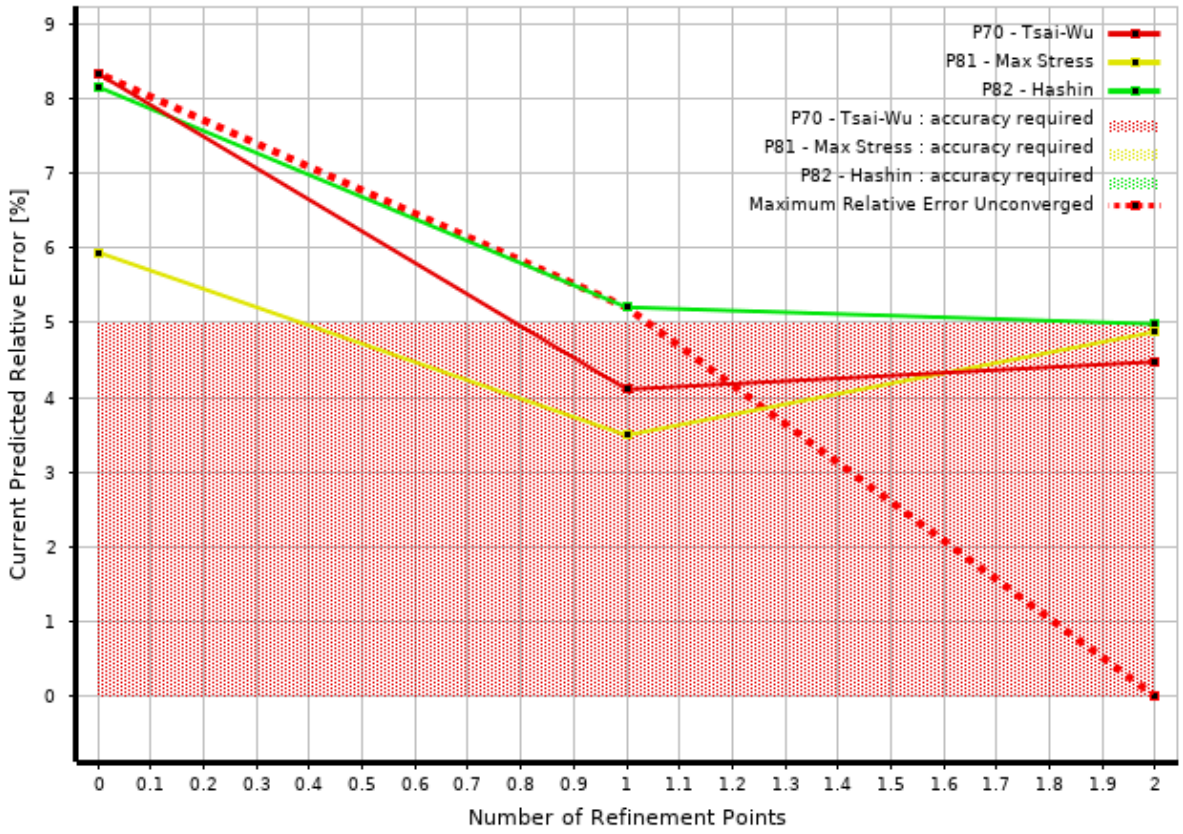

Figure 4: Example Plot of the Refinement of the Kriging Response Surface

3 Case Study of the Burst Design of a Subsea CFEC Flowline

3.1 General Properties

The flowline studied in this paper has the following general properties as listed in Table 2. The material properties of the ply are presented in Table 3. The stacking sequence is presented in Figure 5.

Table 2: General Properties of Subsea CFEC Flowline

Property	**Symbol**	**Value**	**Unit**
Outer Diameter	OD	125	mm
Wall Thickness	t	6	mm
Total Number of Ply	-	30	-
Ply Thickness	t_{ply}	0.2	mm
Fibre Orientation	-	+/- 45	°

Table 3: Material Data – Ply (Prepreg Epoxy Carbon UD 230 GPa)

Material Property	Symbol	Value	Unit
Elastic Modulus	E_1, E_2, E_3	121 000, 8 600, 8600	MPa
Shear Modulus	G_{12}, G_{23}, G_{13}	4 700, 3 100, 4 700	MPa
Poisson's Ratio	ν_{12}, ν_{23}, ν_{13}	0.27, 0.4, 0.27	-
Tensile Strength	σ_{ut1}, σ_{ut2}, σ_{ut3}	2 231, 29, 29	MPa
Compressive Strength	σ_{uc1}, σ_{uc2}, σ_{uc3}	-1 082, -100, -100	MPa
Shear Strength	τ_{u12}, τ_{u23}, τ_{u13}	60, 32, 60	MPa
Tsai-Wu Constants	F_{12}, F_{23}, F_{13}	-1, -1, -1	-

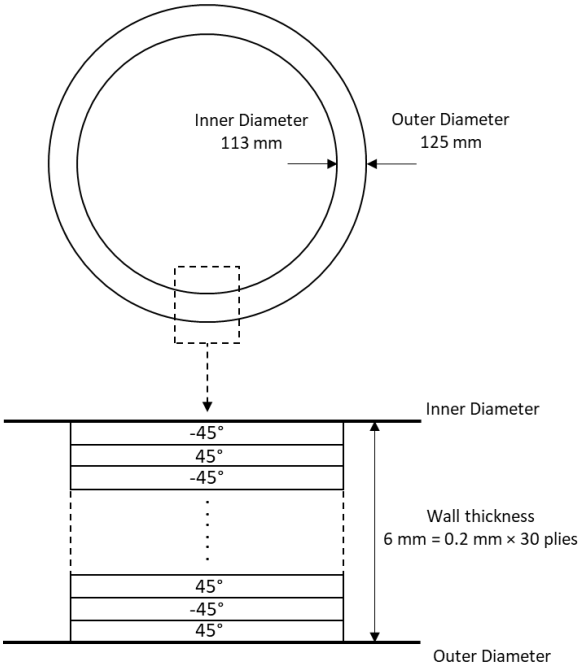

Figure 5: Stacking Sequence

3.2 Nominal Load Values

The nominal load values used in this paper are presented in Table 4.

Table 4: Nominal Load Values

Load	Value	Unit
Internal Pressure	6.9	MPa
Axial Force	20	kN
Torsion	2	kN·m
Bending	2	kN·m

The failure criteria values, corresponding to the nominal loads presented in Table 4 are presented in Table 5. These are calculated using the finite element model presented in Section 3.3.

Table 5: Failure Values Corresponding to Nominal Loads

	Maximum Stress	Tsai-Wu	Hashin
Failure Criterion Value	0.516	0.613	0.563
Failure Mode	σ_2 exceeded	-	Matrix failure

3.3 Finite Element Model

A 2000 mm section of the flowline is modelled. This is sufficiently long by engineering judgement in order to avoid end effects due to loads and boundary conditions in the finite element model. The results are obtained at the middle part of the section, i.e., at the 1000 mm point as illustrated previously in Figure 3 . ANSYS R17.0 is used for the finite element modelling.

3.3.1 Loads and Boundary Conditions

The loads and boundary conditions applied on the model are illustrated in Figure 6. Pressure (Load A) is applied in the interior of the flowline. Fixed support (Load B) is applied on the right edge of the flowline. An end cap force (Load E) due to the internal pressure is applied on the left edge of the flowline. Axial force (Load C), torsion (Load D) and bending (Load F) are also applied at the left edge.

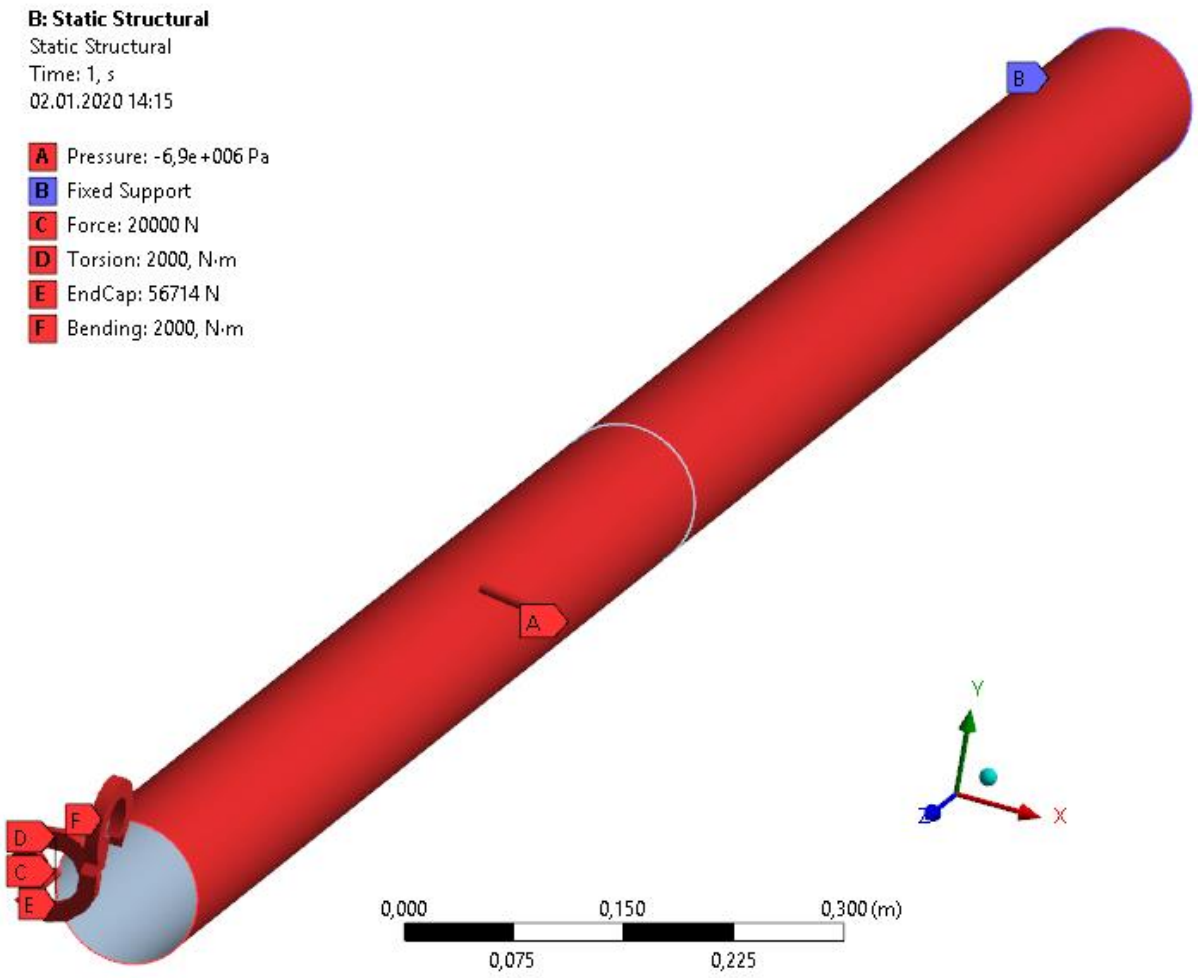

Figure 6: Loads and Boundary Conditions

3.3.2 Mesh Refinement Study

The cases studied and the corresponding results obtained for the mesh refinement study are presented in Table 6 and Figure 7, respectively. The nominal load values as presented in Section 3.2 are used in the mesh refinement study. The element used is the 4-node SHELL181 element (Ansys, 2017). The results show that a 30 mm element size is enough to produce converged solutions for the three failure criteria investigated in this paper. An element size of 10 mm is used in the paper and the mesh details used in this paper are presented in Figure 8.

Table 6: Cases Studied for Mesh Refinement Study

Element Size (mm)	No. of Elements	No. of Nodes
30	900	912
25	1040	1053
20	1536	1552
15	2803	2821
10	6430	6432
5	25344	25408

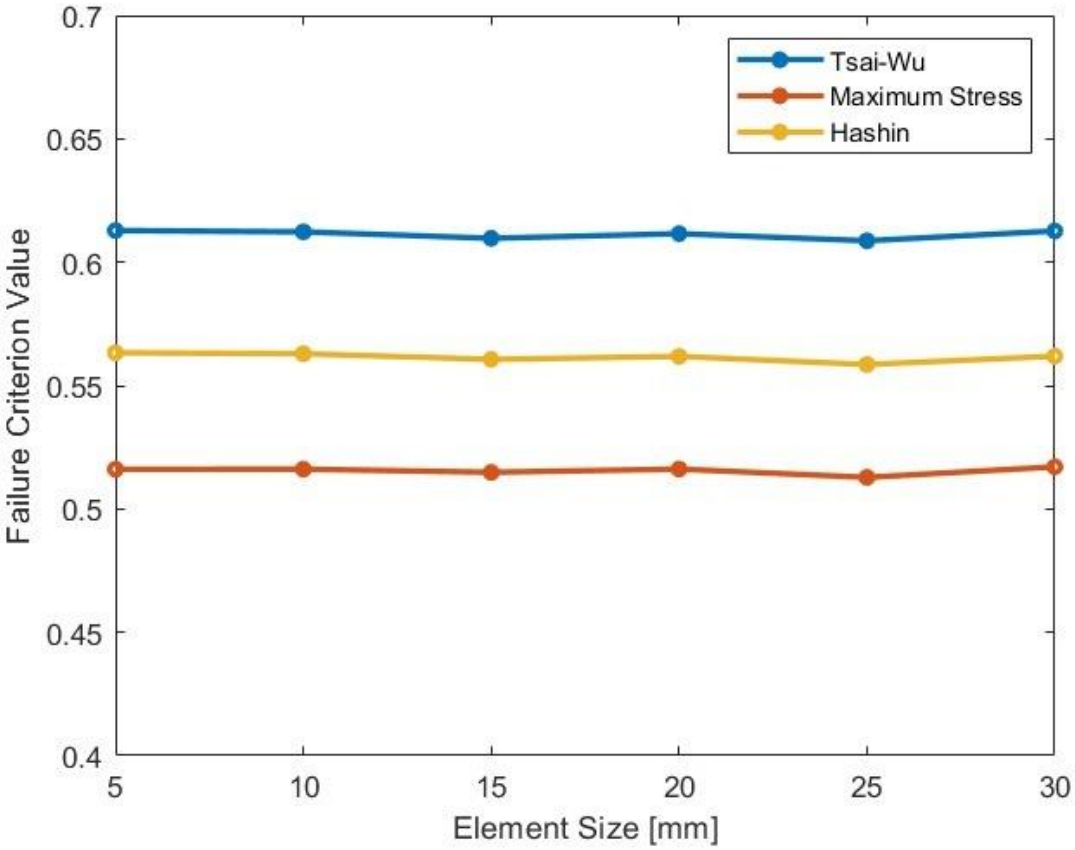

Figure 7: Results of Mesh Refinement Study

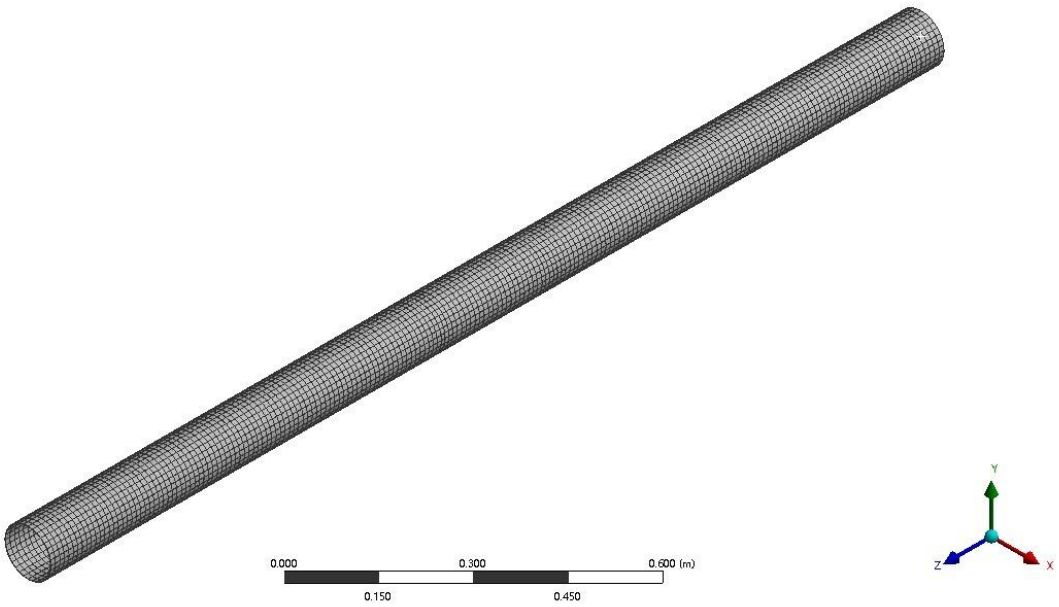

Figure 8: Mesh Details, 10 mm Element Size, 6430 SHELL181 Elements with 6432 Nodes

3.4 Generation of Measured Values

A set of measured values is generated to be used as the reference population in this paper. This is named the 'Base Case' in this paper. The mean and standard deviation of the input parameters used in Base Case are presented in Table 7. The input parameters are normally distributed.

Table 7: Mean and Standard Deviation of Input Parameters used in Base Case

Parameter	Symbol	Unit	Mean	Standard Deviation
Elastic Modulus	E_1	MPa	121000	3630
	E_2, E_3	MPa	8600	258
Poisson's Ratio	ν_{12}, ν_{13}	-	0.27	0.0081
	ν_{23}	-	0.4	0.012
Shear Modulus	G_{13}	MPa	4700	141
	G_{23}	MPa	3100	93
Tensile Strength	σ_{ut1}	MPa	2231	66.93
	σ_{ut2}, σ_{ut3}	MPa	29	0.87
Compressive Strength	σ_{uc1}	MPa	-1082	-32.46
	σ_{uc2}, σ_{uc3}	MPa	-100	-3
Shear Strength	τ_{u12}, τ_{u13}	MPa	60	1.8
	τ_{u23}	MPa	32	0.96
Internal pressure	P	MPa	-6.9	-0.207
Axial Force	A	N	20000	600
Bending	B	N·m	2000	60
Torsion	T	N·m	2000	60
Tsai-Wu Constants	F_{12}, F_{23}, F_{13}		0	0.3
Diameter	D	mm	125	8.75
Thickness	t	mm	0.2	0.01

Using the values in Table 7, the Base Case population of measured values is generated using Monte Carlo simulation. Examples of the cumulative probability distributions are plotted in Figure 9, Figure 10 and Figure 11

for the elastic modulus E_1, diameter D and internal pressure P, respectively. The population size is 500 which is chosen based on a convergence study presented in Section 3.4.1. The population size is chosen to be sufficiently large such that converged statistical moments are achieved.

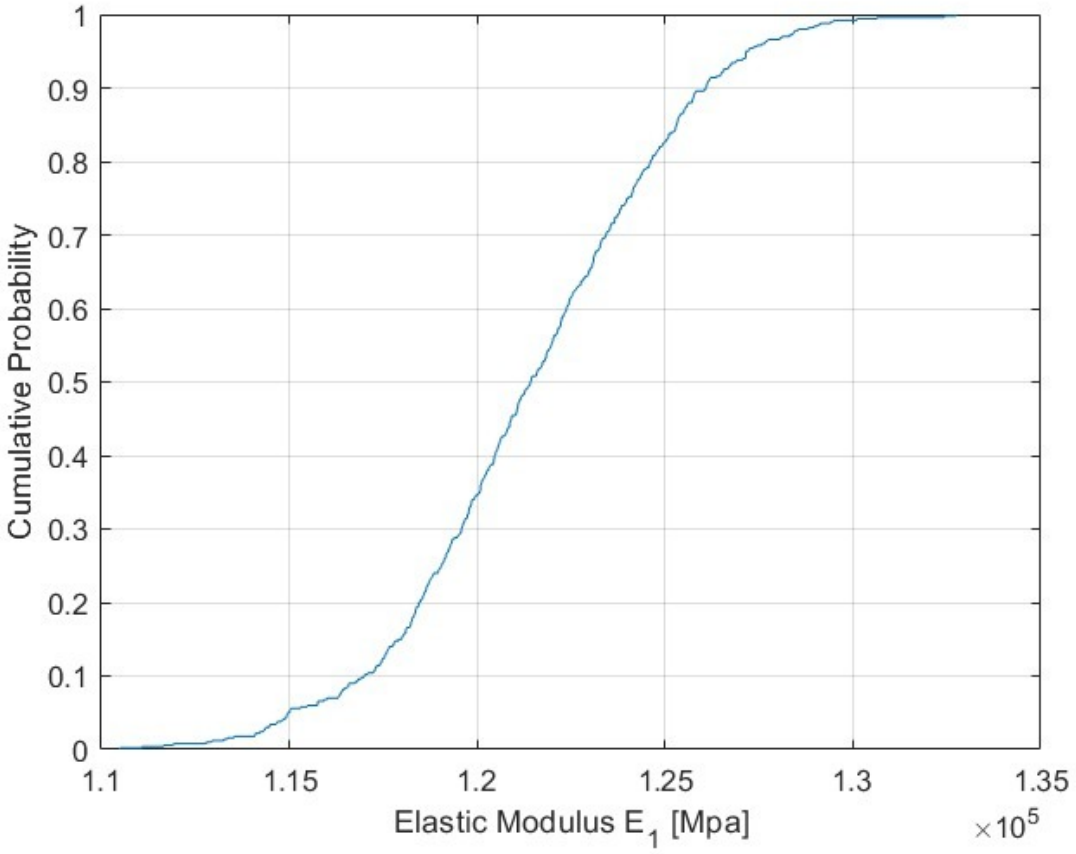

Figure 9: Cumulative Probability Distribution of Elastic Modulus E_1

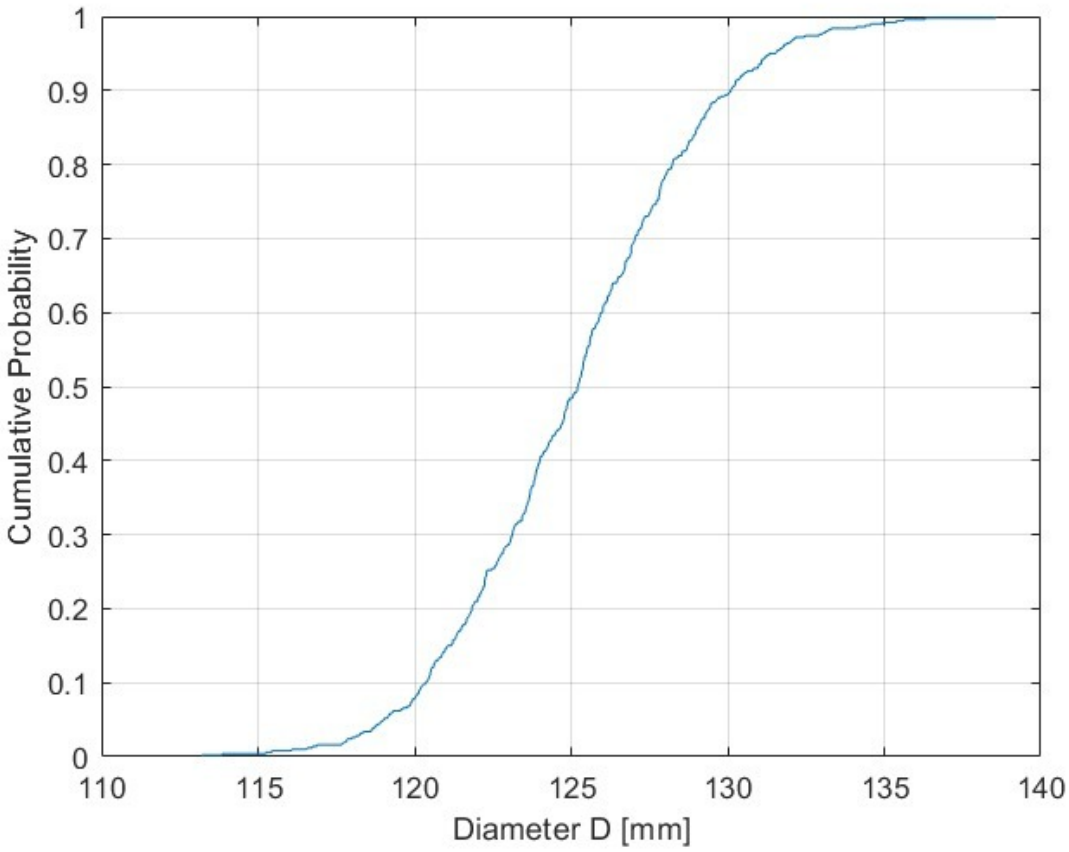

Figure 10: Cumulative Probability Distribution of Diameter D

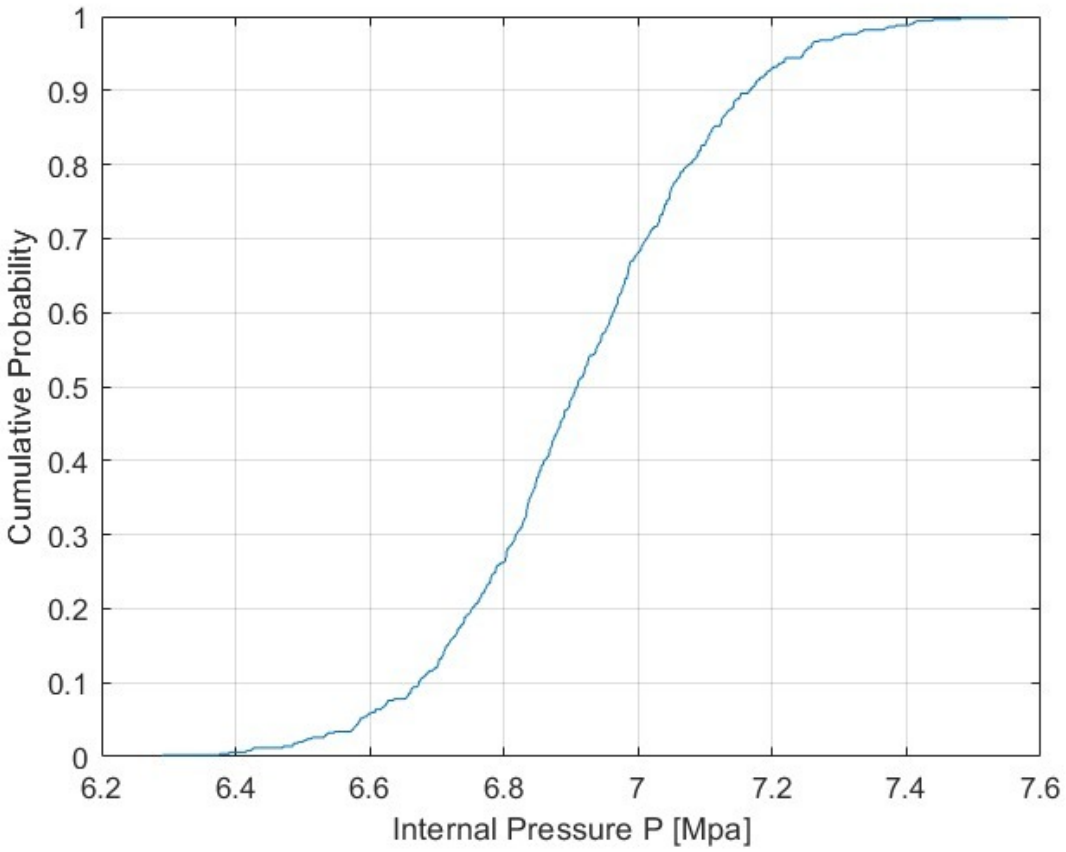

Figure 11: Cumulative Probability Distribution of Internal Pressure P

3.4.1 Convergence Study on Population Size

A convergence study was performed to select a large enough population size such that converged statistical moments are obtained. Figure 12 presents values of mean, standard deviation, skewness and kurtosis versus the sample size. Figure 13 presents the percentage difference for the same statistical moments compared to the values when the population size is 500. The percentage difference is calculated using the formula presented in Equation (15).

$$\% \text{ Difference} = \frac{Current\ value - Value\ @\ N = 500}{Value\ @\ N = 500} \times 100\% \quad \textbf{(15)}$$

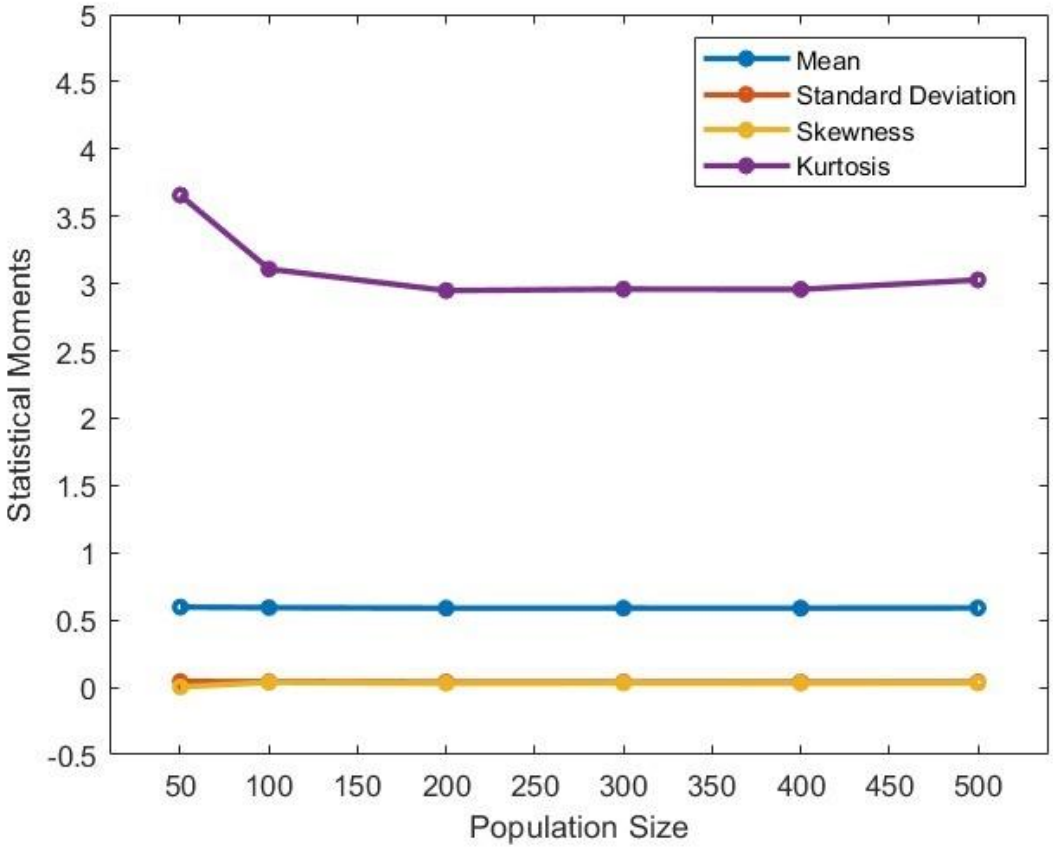

Figure 12: Values of Statistical Moments vs Population Size

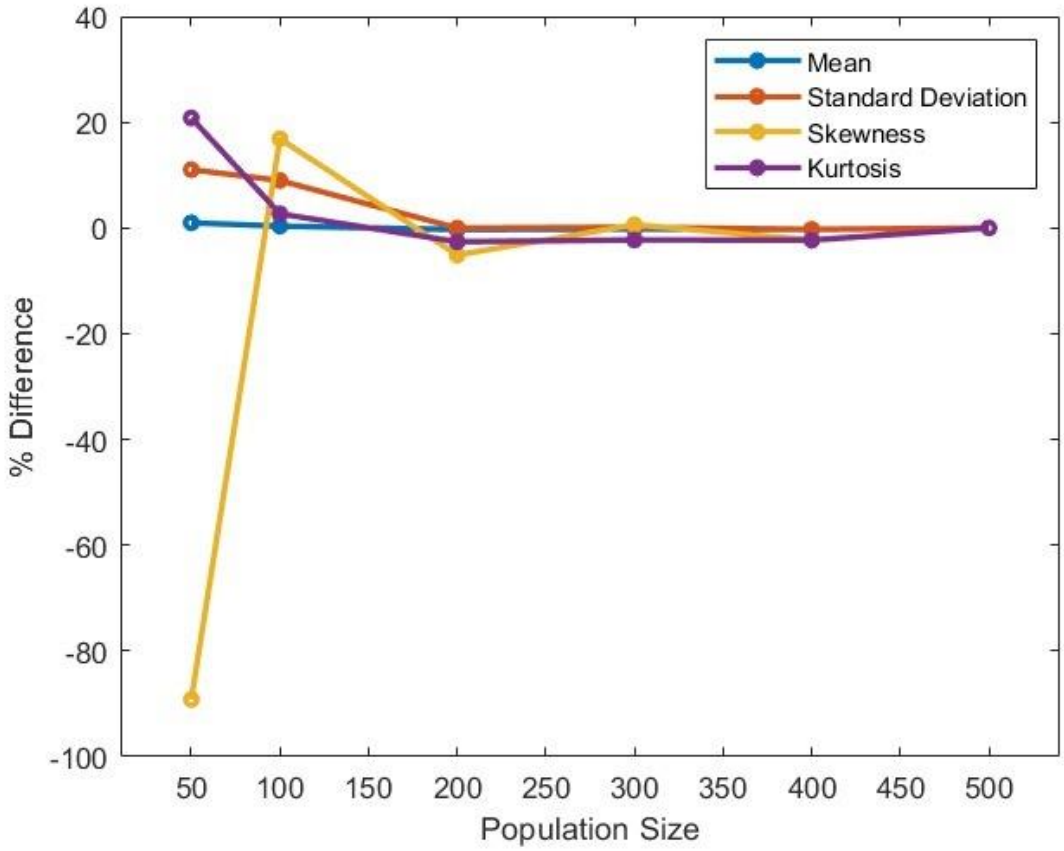

Figure 13: % Difference of Values of Statistical Moments vs Population Size Compared to N = 500

The results presented in Figure 12 and Figure 13 show that converged statistical moments are obtained for a population size larger than 200. A population size of 500 is used in this paper.

3.4.2 Fitting Statistical Models to Measured Values

Statistical models are fitted to the results and used to calculate the exceedance probabilities, i.e., failure rates. In this section, the various statistical models used in the fitting are presented. The Matlab distribution fitting tool is used. Four types of distributions, namely Exponential, Weibull, Normal and Lognormal are fitted and compared with the measured values as shown in Figure 14 and Figure 15. The corresponding R^2 values are presented in Table 8. As previously mentioned, the population size, i.e., the size of the set of measured values is 500.

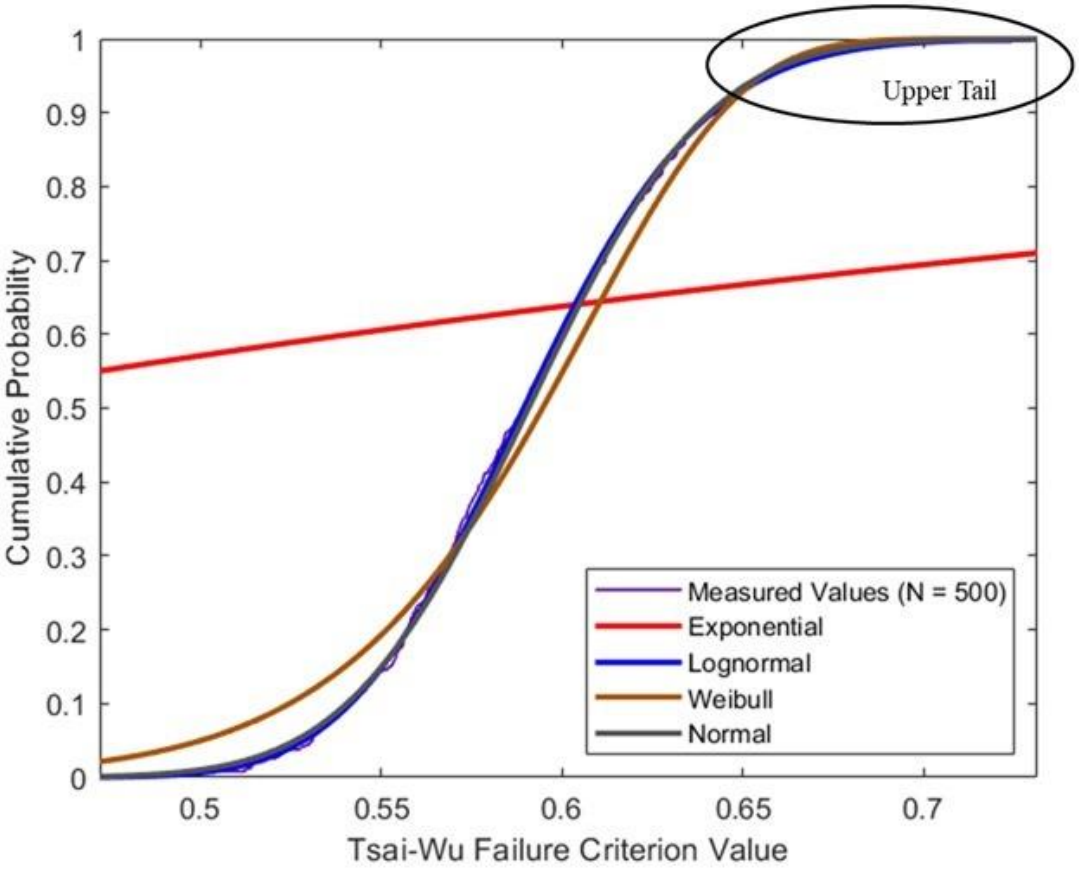

Figure 14: Statistical Models Fitted to Measured Values

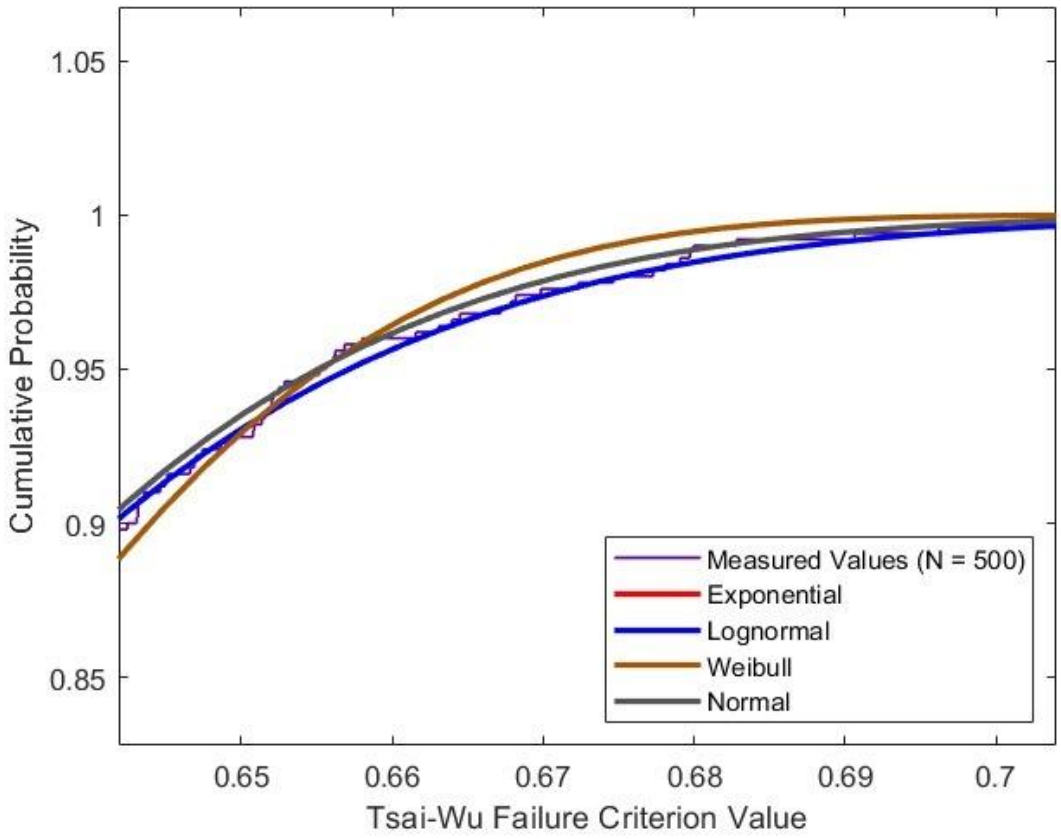

Figure 15: Statistical Models Fitted to Measured Values, Zoom-In @ Upper Tail Region

Table 8: R^2 Values

Statistical Model	Exponential	Lognormal	Normal	Weibull
R^2 Value	0.960	0.999	0.998	0.987

The results show that the Lognormal and Normal distributions are better fits to the measured values. In contrast, the Weibull and Exponential distributions do not fit well. Upon closer inspection into the upper tail region as presented in Figure 15 and the R^2 value considering the tail region presented in Table 8, it is observed that the Lognormal distribution is a better fit than the Normal distribution at the upper tail region. The upper tail region is crucial for the calculation of failure rates. The Lognormal distribution is therefore chosen as the statistical model to be fitted to the measured values.

3.5 Calculating the Response Surface

3.5.1 Parametric Correlation to Identify Most Influential Input Parameters

The parametric correlation matrix is calculated using Spearman correlation method as described in Section 2.2 to identify the most influential input parameters. A sample size of 100 is used in the calculation. The sample size is large enough based on previous studies by the authors on parametric correlation matrices associated with CFEC flowlines (Xing et al., 2019). The parametric correlation matrix is presented in Figure 16. The 20 most influential input parameters identified from the parametric correlation matrix are presented in Table 9. These input parameters are used in the generation of the response surface.

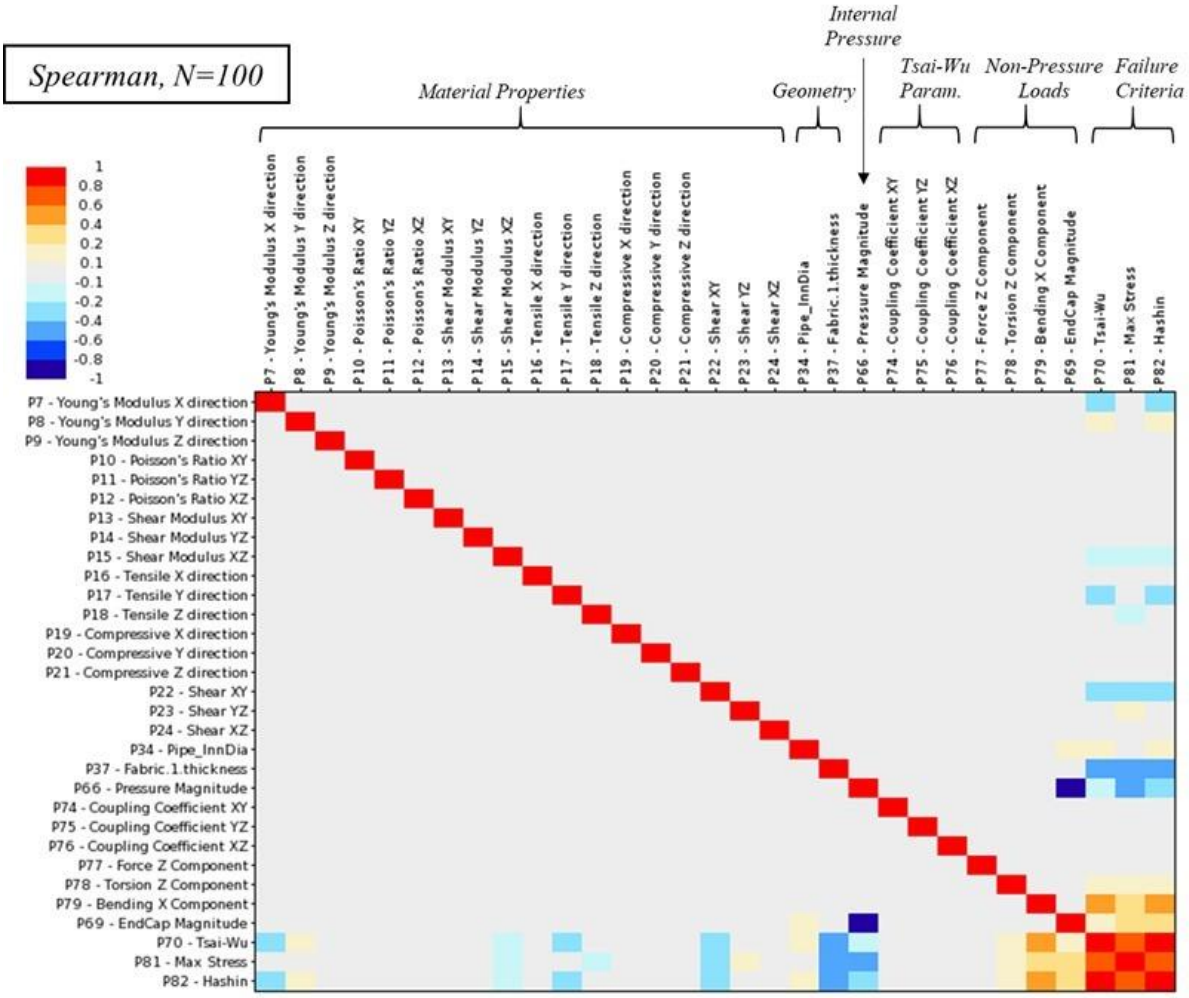

Figure 16: Parametric Correlation Matrix

Table 9: Most Influential Input Parameters

Parameter Group	Parameters	Level of Correlation
Loads	P, T	Moderate
Geometry	t	Moderate
Material properties	E_2, ν_{12}, ν_{23}, ν_{13}, G_{23}, G_{13}, σ_{ut1}, σ_{ut3}, τ_{u23}, D, F_{12}, F_{13}, A, B	Slight
	E_1, σ_{ut2}, τ_{u12}	Low

3.5.2 Range of Input Parameters

The range of input parameters used in the generation of the response surface is presented in Table 10. As previously discussed, the input parameters used in the response surface are the top 20 most influential input parameters found from a parametric correlation study presented in Section 3.5.1.

Table 10: Range of Input Parameters used in Response Surface

Parameters	Symbol	Unit	Lower limit	Upper limit
Elastic Modulus	E_1	MPa	108900	133100
	E_2	MPa	7740	9460
Poisson's Ratio	ν_{12}, ν_{13}		0.243	0.297
	ν_{23}		0.36	0.44
Shear Modulus	G_{13}	MPa	4230	5170
	G_{23}	MPa	2790	3410
Tensile Strength	σ_{ut1}	MPa	2007.9	2454.1
	σ_{ut2}, σ_{ut3}	MPa	26.1	31.9
Shear Strength	τ_{u12}	MPa	54	66
	τ_{u23}	MPa	28.8	35.2
Internal pressure	P	MPa	6.21	7.59
Axial Force	A	N	18000	22000
Bending	B	Nm	1800	2200
Torsion	T	Nm	1800	2200
Tsai-Wu Constants	F_{12}, F_{13}		-1	1
Diameter	D	mm	100	150
Thickness	t	mm	0.18	0.22

4 Using Response Surfaces for Prediction of Failure Rates

In this section, the use of response surfaces for the prediction of failure rates is discussed. The benefit of using response surfaces is that new sampling points are calculated almost instantly after the response surface is generated. This provides time savings in the engineering evaluation of the design and in the case in this paper, the calculation of failure rates. The investigation is carried out as follows in this section. First, the statistical moments are

compared between the samples generated from the measured values, response surface and their corresponding fitted Lognormal distributions. Second, the probability and cumulative distribution plots are compared. Last, the failure rates calculated from the response surface are compared against the 'Base Case'. The workflow process used is presented in Figure 17.

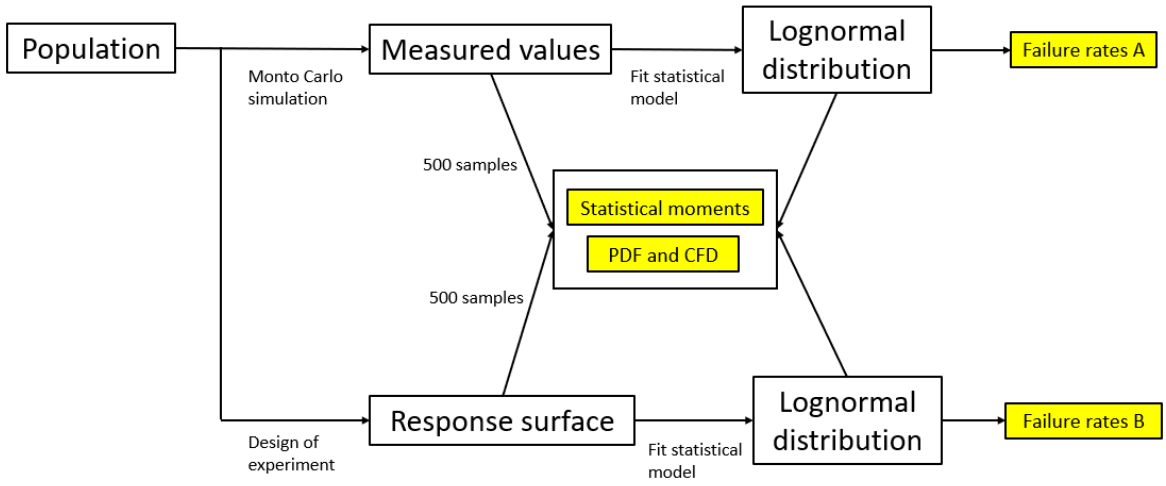

Figure 17: Workflow Process

4.1 Comparison of Statistical Moments

The comparison of the statistical moments is presented in Table 11. An explanation of 'Source' in Table 11 is presented in the following:

- Measured values, 500 samples: These are 500 sample points calculated directly from the finite element model. These 500 samples are considered the 'Base Case' population.
- Lognormal distribution fitted to measured values: This is a Lognormal distribution fitted to 'Measured values, 500 samples'.
- Response surface, 500 samples: These are 500 sample points calculated directly from response surface.
- Lognormal distribution fitted to response surface values: This is a Lognormal distribution fitted to 'Response surface, 500 samples'.
- The % differences are calculated with respected to 'Measured values, 500 samples' using Equation (16)

$$\% \text{ Difference} = \frac{Current\ value - alue\ @\ 'Measured\ values, 500\ samples'}{Value\ @\ 'Measured\ values, 500\ samples'} \times 100\% \quad (16)$$

Table 11: Comparison of Statistical Moments

Source	**Mean**	**Standard Deviation**	**Skewness**	**Kurtosis**
Measured values, 500 samples	0.591	0.039	0.232	3.027
Lognormal distribution fitted to measured values	0.591 (0.0%)	0.039 (0.1%)	0.199 (-14.1%)	3.071 (1.4%)
Response surface, 500 samples	0.592 (0.3%)	0.036 (-8.5%)	0.209 (-9.8%)	2.980 (-1.6%)
Lognormal distribution fitted to response surface values	0.592 (0.3%)	0.036 (-8.6%)	0.182 (-21.7%)	3.059 (1.0%)

The following observations are made from the results presented in Table 11:

- There are negligible differences in the mean values.
- The values obtained from the response surface (also when fitted to the Lognormal distribution) have smaller standard deviation values which are about 9% smaller than the measured values.
- There are large differences in the skewness values. The response surface skewness values are about 10% smaller than the measured values. Fitting the response surface values to a Lognormal distribution makes the skewness values even smaller, i.e., about 22% smaller compared to the measured values. In addition, fitting the measured values to a Lognormal distribution give rise to smaller skewness values of about 14% smaller compared to the measured values.
- There are only small differences of below 2% in the kurtosis values.

4.2 Comparison of Probability and Cumulative Distribution Plots

The comparisons of the probability density and cumulative distribution plots are presented in Figure 18 and Figure 19, respectively.

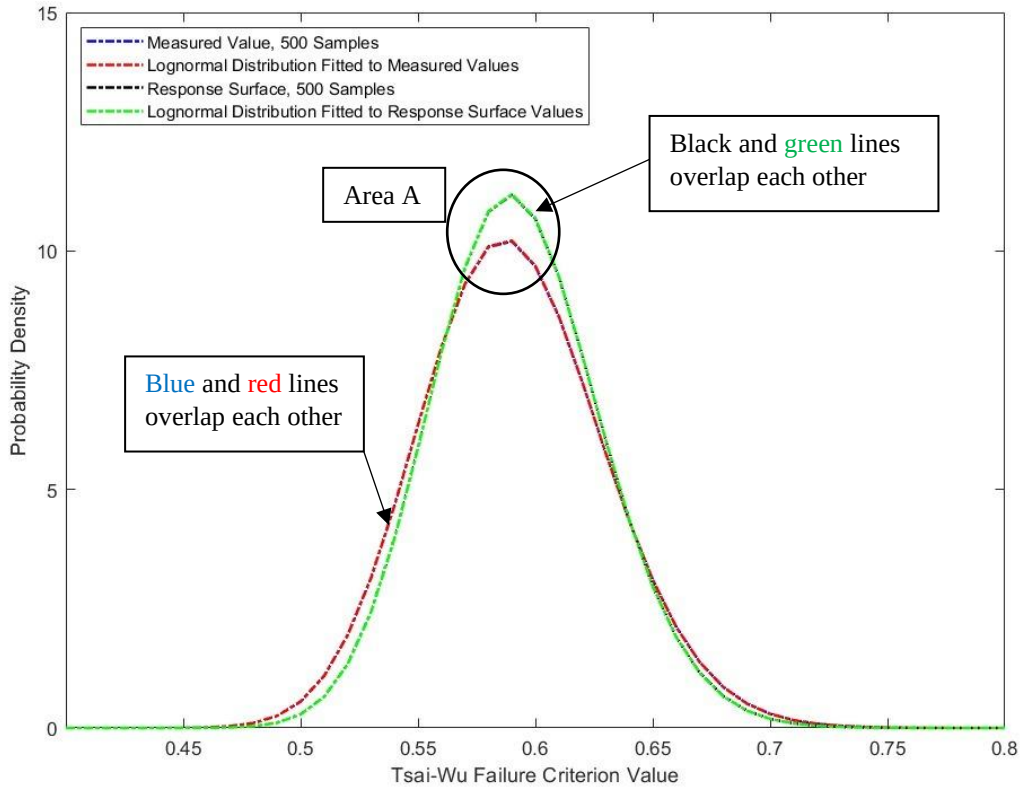

Figure 18: Comparison of Probability Density Functions

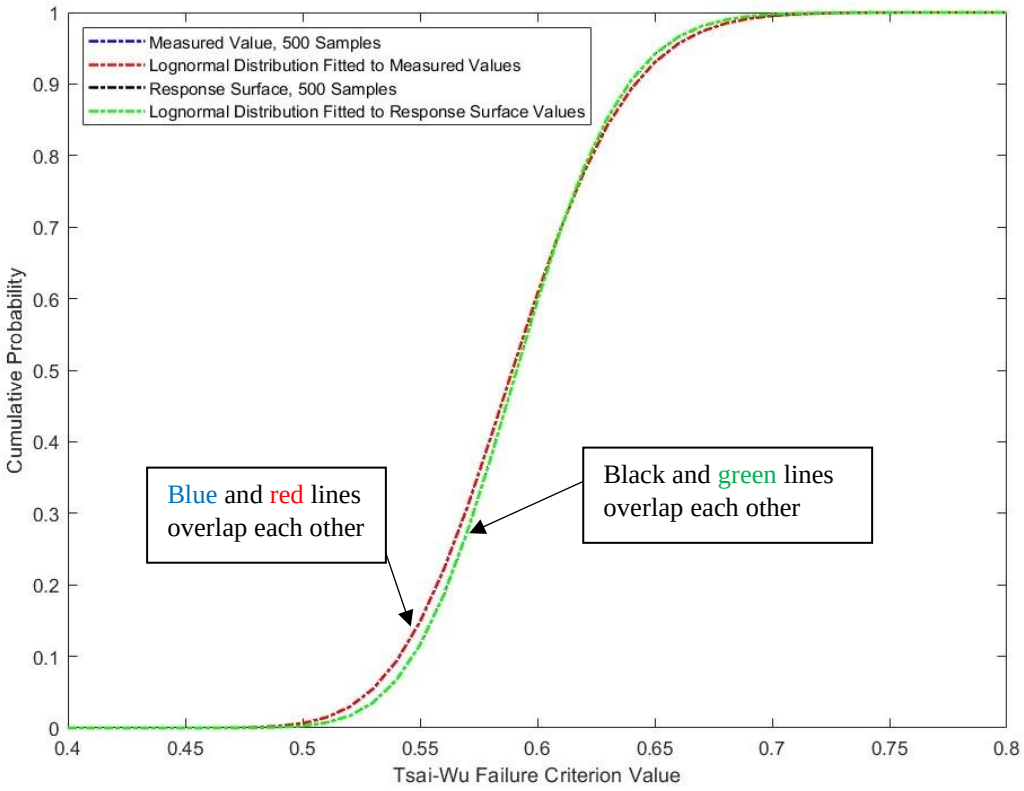

Figure 19: Comparison of Cumulative Probability Distribution Functions

The following observations are made:

- The fitted distribution curves overlap the raw data, i.e., measured values and response surface sampled values.
- The response surface has a higher probability density at the most probable value; refer to area A in Figure 18.
- There are some differences in the tail regions in the cumulative probability distribution functions, refer to Figure 19. However, these difference are not significant and lead to only negligible differences in the failure values which are calculated based on the upper tail region as presented in Section 4.3.

4.3 Comparison of Failure Values

The comparison of failure values at three different failure rates are presented in Table 12.

Table 12: Comparison of Failure Values

Source	**Failure Criterion**	**Failure Rate = 1 in 10^4**	**Failure Rate = 1 in 10^5**	**Failure Rate = 1 in 10^6**
Lognormal distribution fitted to measured values	Maximum Stress	0.64	0.67	0.69
	Tsai-Wu	0.75	0.78	0.81
	Hashin	0.76	0.79	0.81
Lognormal distribution fitted to response surface values	Maximum Stress	0.64	0.66	0.68
	Tsai-Wu	0.74	0.77	0.79
	Hashin	0.75	0.78	0.80

The results presented in Table 12 show that the response surface model produce failure values that are very close to those resulting from the measured values. Therefore, it is a reliable tool that can be used to failure prediction of CEFC flowlines under combined loading.

5 Optimising Response Surface Generation

5.1 Number of Input Parameters

In this section, the number of input parameters used to generate the response surfaces is investigated. Using a smaller number of input parameters requires a smaller design of experiment as presented in Table 13. Choosing 10 input parameters instead of 20 input parameters results in a design of experiment that is less than one-third the size, leading to significant computational savings in the generation of the response surface. It is mentioned that 20 input parameters are used in the response surface presented in results in Section 4.

Table 13: Size of Design of Experiment for Different Number of Input Parameters

Number of Input Parameters	5	10	15	20
Size of Design of Experiment, Number of Samples	27	149	287	551
Minimum Parametric Correlation Value	0.271	0.131	0.079	0.046

The effect on statistical moments, probability distributions and predicted failure values are presented and discussed in Sections 5.1.1, 5.1.2 and 5.1.3, respectively. The results show that using input parameters of 10 do not lead to any observable reduction in accuracy in the results calculated. This is obvious in the case where 5 input parameters are used, parameters that are somewhat correlated (having correlation coefficients between 0.131 to 0.271) to the failure value are excluded to be used in the generation of the response surfaces.

5.1.1 Number of Parameters - Effect on Statistical Moments

The statistical moments are presented in Figure 20 for the response surfaces generated with different number of input parameters together with the measured values (fitted and raw values). The corresponding percentage differences versus the measured values are presented in Figure 21. The following observations are made:

- The mean values are not significantly affected when more than 10 input parameters are used where the differences are within 1%.
- The standard deviations are fairly affected by the number of input parameters used. However, it is mentioned that using the response surface would already result in a difference in the standard deviation of about 9 % as presented in 4.1. Using a smaller number of input parameters will increase this difference to as much as about 20%.
- The skewness values are very affected by the number of input parameters used. However, it is mentioned that using the response surface would already result in a difference in the standard deviation of about 14 % as presented in 4.1. Using a smaller number of input parameters will increase this difference to as much as about 250%.
- The kurtosis values are not significantly affected when enough input parameters are is used. The difference however become as large as 60% when not enough input parameters are used.

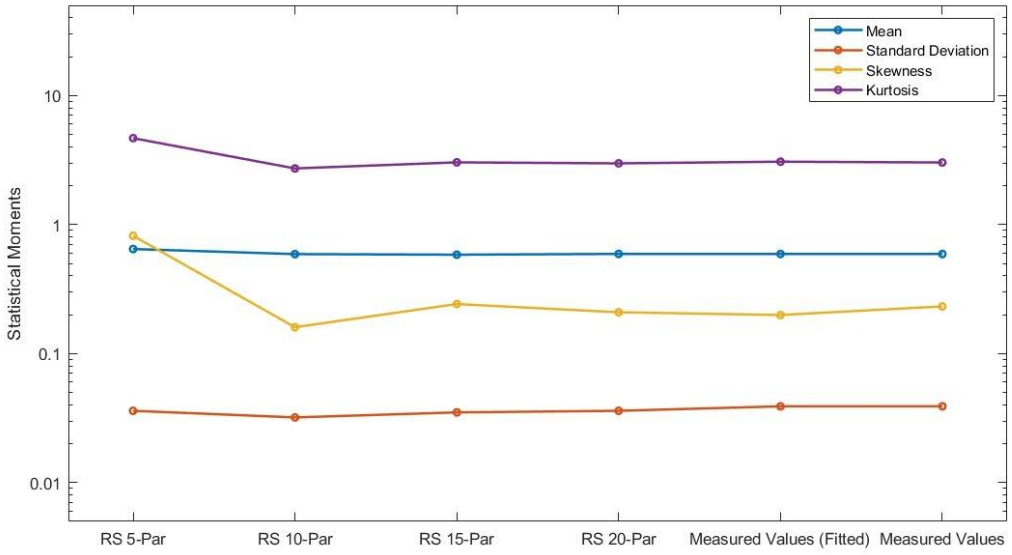

Figure 20: Number of Parameters – Effect on Statistical Moments

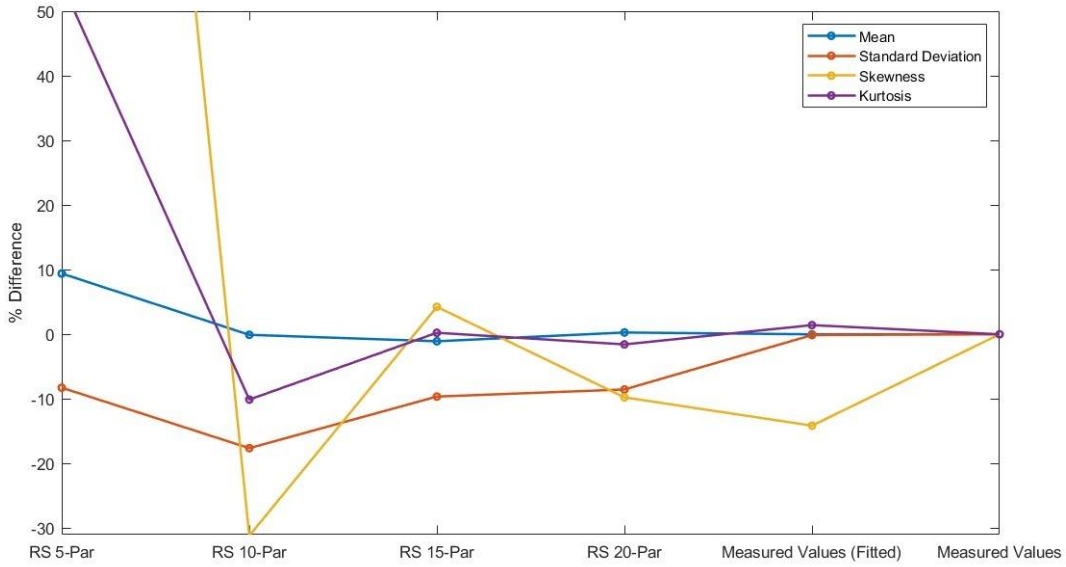

Figure 21: Number of Parameters – Effect on Statistical Moments (% Difference)

5.1.2 Number of Parameters – Effect on Fitted Probability Distributions

The probability distributions (probability density and cumulative probability) fitted to response surface values with different number of input parameters are plotted together with the measured values and presented in Figure 22, Figure 23 and Figure 24.

The following observations are made:

- In general, the probability distribution functions are extremely inaccurate when a small number of input parameters, i.e., 5 is used.
- As presented in Figure 22, the probability density functions fitted from the response surfaces do not in general fit well with the measured values. A similar observation was also previously reported in Figure 18 and Section 4.2.
- As presented in Figure 23 and Figure 24, there are some differences in the cumulative probability distribution functions. These differences increase with decreasing number of input parameters. However, these do not significantly affect the upper tail regions and lead to not too large differences in the failure values calculated as presented in Section 5.1.3. Similar observations were also previously reported in Section 4.2.

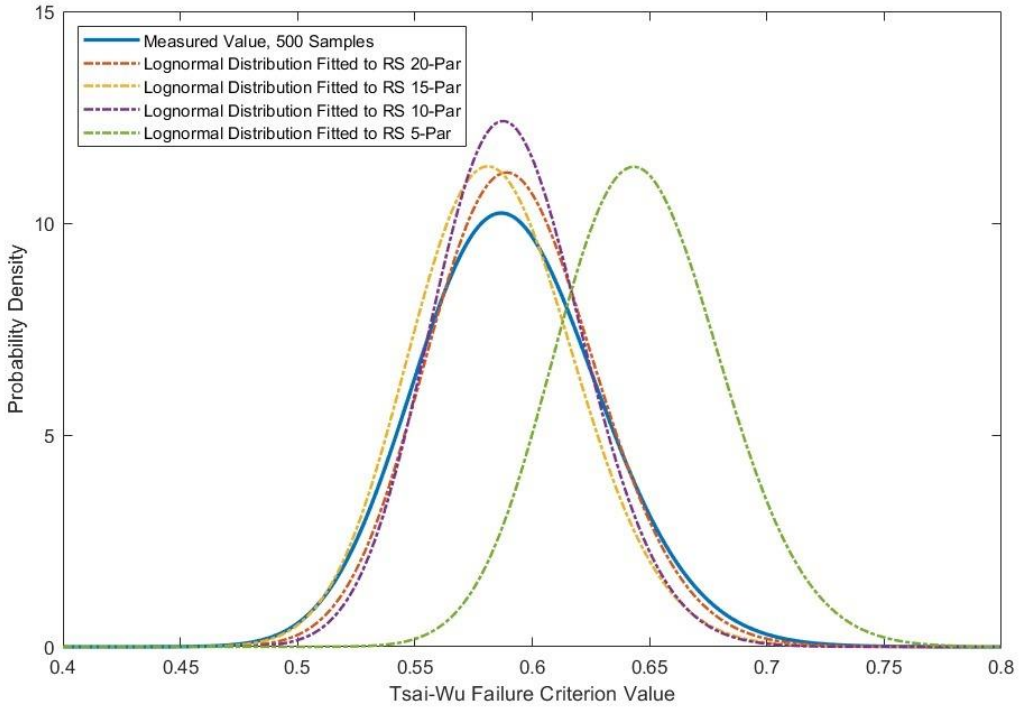

Figure 22: Number of Parameters – Effect on Probability Density Functions

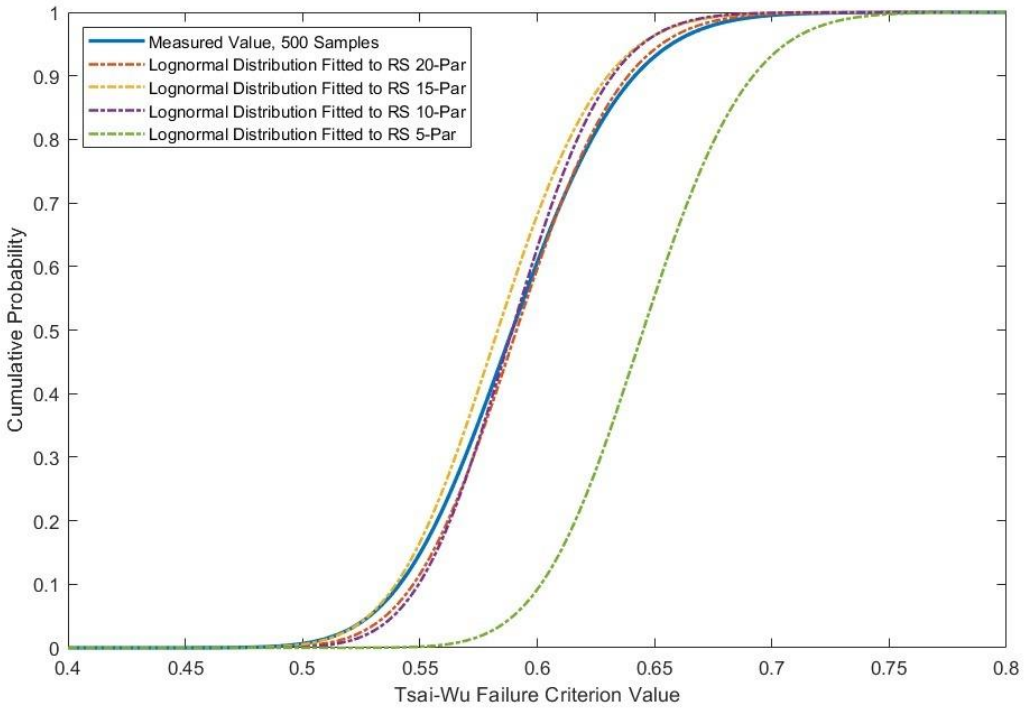

Figure 23: Number of Parameters – Effect on Cumulative Probability Functions

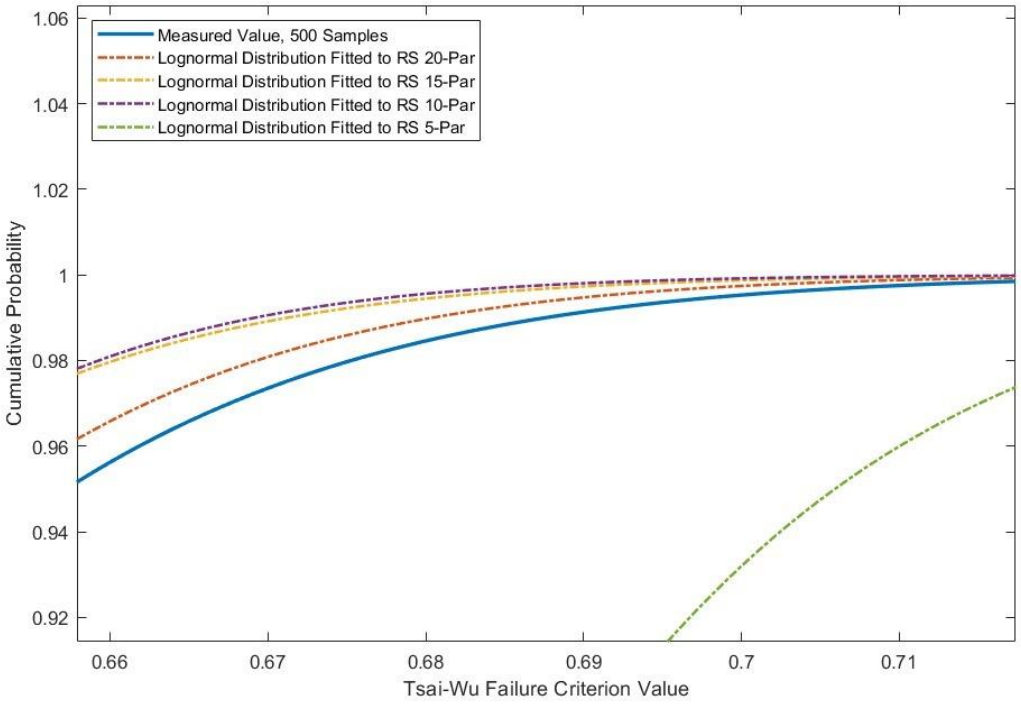

Figure 24: Number of Parameters – Effect on Cumulative Probability Functions (Zoom-In at Upper Tail Region)

5.1.3 Number of Parameters – Effect on Predicted Failure Values

Table 14 presents comparisons of the predicted failure rates calculated from the Lognormal distributions fitted to response surfaces when the different number of input parameters are used. It is observed from the results that reducing the number of input parameters to 10 in general do not lead to poor accuracy in the failure values predicted. The accuracy of the failure values predicted suffer when the number of input parameters are small. This can be expected because the failure values are calculated from distributions fitted to sampled values. As previously discussed in Section 5.1.2, the number of input parameters do not affect the fitted probability distributions unless the number of input parameters is small, i.e., 5.

Table 14: Number of Parameters – Effect on Predicted Failure Values

Source	Failure Criterion	Failure Rate = 1 in 10^4	Failure Rate = 1 in 10^5	Failure Rate = 1 in 10^6	% Diff, Failure Rate = 1 in 10^4	% Diff, Failure Rate = 1 in 10^5	% Diff, Failure Rate = 1 in 10^6
Lognormal distribution fitted to measured values	Maximum Stress	0.64	0.67	0.69	-	-	-
	Tsai-Wu	0.75	0.78	0.81	-	-	-
	Hashin	0.76	0.79	0.81	-	-	-
Lognormal distribution fitted to response surface values (20 input parameters)	Maximum Stress	0.64	0.66	0.68	0.0	-1.5	-1.4
	Tsai-Wu	0.74	0.77	0.79	-1.3	-1.3	-2.5
	Hashin	0.75	0.78	0.80	-1.3	-1.3	-1.2
Lognormal distribution fitted to response surface values (15 input parameters)	Maximum Stress	0.64	0.67	0.69	-1.6	-3.0	-1.4
	Tsai-Wu	0.75	0.78	0.81	-2.7	-2.6	-3.7
	Hashin	0.76	0.79	0.81	-2.6	-2.5	-2.5
Lognormal distribution fitted to response surface values (10 input parameters)	Maximum Stress	0.64	0.66	0.68	0.0	-1.5	-1.4
	Tsai-Wu	0.74	0.77	0.79	-4.0	**-5.1**	**-6.2**
	Hashin	0.75	0.78	0.8	-1.3	-1.3	-1.2
Lognormal distribution fitted to response surface values (5 input parameters)	Maximum Stress	0.63	0.65	0.68	**15.6**	**14.9**	**15.9**
	Tsai-Wu	0.73	0.76	0.78	**5.3**	**5.1**	3.7
	Hashin	0.74	0.77	0.79	2.6	2.5	2.5

5.2 Size of Response Surface

In this section, the effects of response surfaces sizes are studied. Two larger response surfaces are compared against the original surface size used in Sections 3, 4 and 5.1. These larger response surfaces are named 'Larger Size' and 'Extremely Large Size'. The number of input parameters used to generate the response surfaces is the same, i.e., 20, while the range of diameter and ply thickness is varied. An overview of the response surfaces studied is presented in Figure 25 and their corresponding range of diameters and ply thicknesses are presented in Table 15.

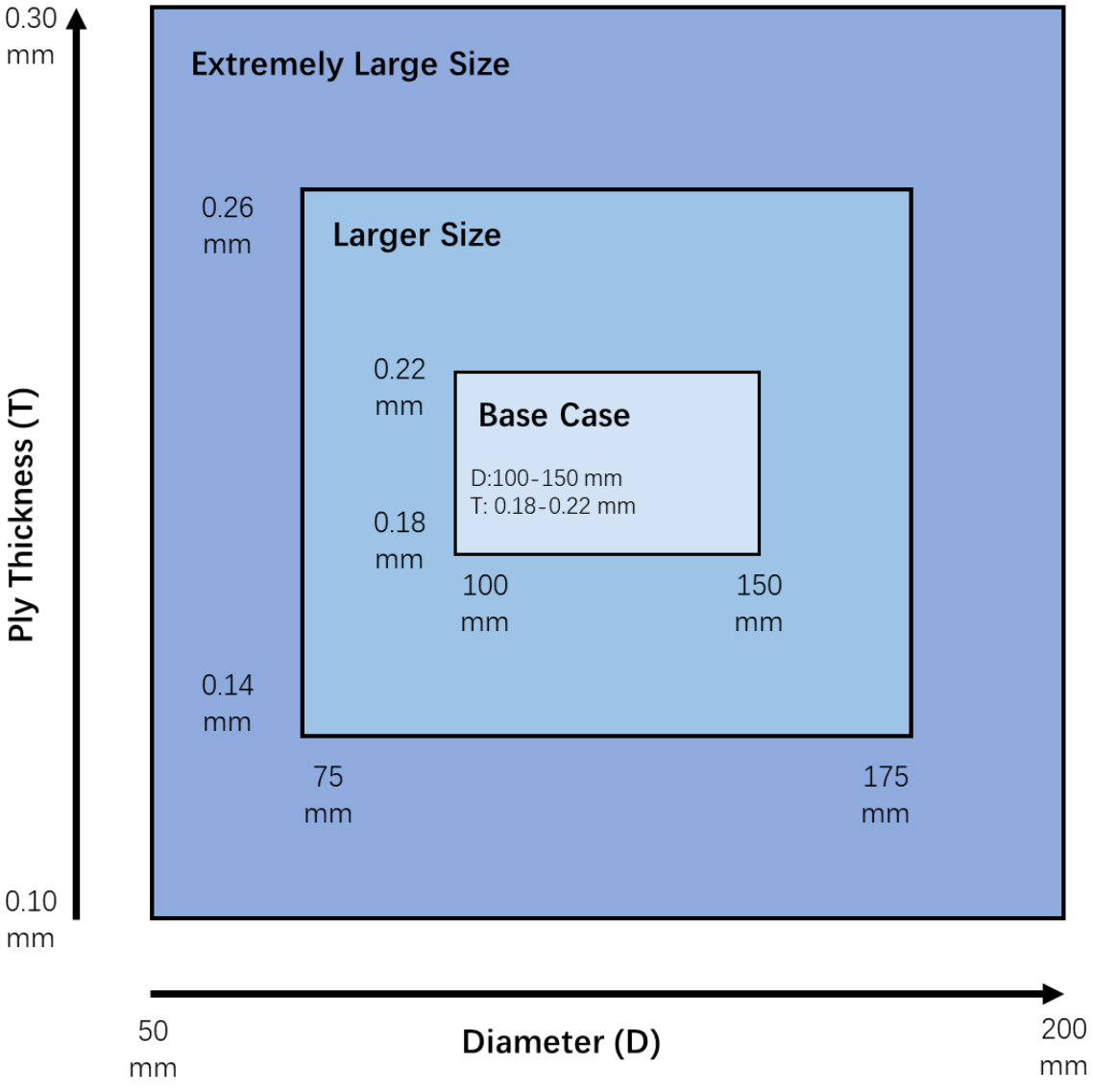

Figure 25: Sizes of Response Surfaces Considered

Table 15: Range of Diameters and Ply Thicknesses Studied

	Diameter [mm]	Thickness [mm]
Base Case	100-150	0.18-0.22
Larger Size	75-175	0.14-0.26
Extremely Larger Size	50-200	0.10-0.30

The effect on statistical moments, probability distributions and predicted failure values are presented and discussed in Sections 5.2.1, 5.2.2 and 5.2.3, respectively. The results show that the extremely large response surface leads to inaccurate skewness values and probability distributions functions. However, the size of the response surface does not have large effect on the upper tail regions of the probability distributions and consequently lead to small differences in predicted failure rates if it is not too large as demonstrated in the 'Larger Size' response surface.

5.2.1 Size of Response Surface - Effect on Statistical Moments

The statistical moments are presented in Figure 26 for the response surfaces generated with different range of diameter and ply thickness together with the measured values (fitted and raw values). The corresponding percentage differences versus the measured values are presented in Figure 27. The following observations are made:

- In general, the differences in statistical moments calculated increase with the size of the response surface used.
- The differences in the mean values increase with the size of the response surface used but are within 10% for 'Extremely Large Size'.
- The response surface size has limited, if not no influence on the standard deviation values. The differences in the standard deviation are within approximately 10% which were like that of the 'Base Case' which had 8.5%.
- The skewness is strongly affected by the response surface size. For the 'Larger Size' and 'Extremely Large Size', the differences are as much as 40%.
- The differences in the kurtosis values increase with the size of the response surface used but are within 10% for 'Extremely Large Size'

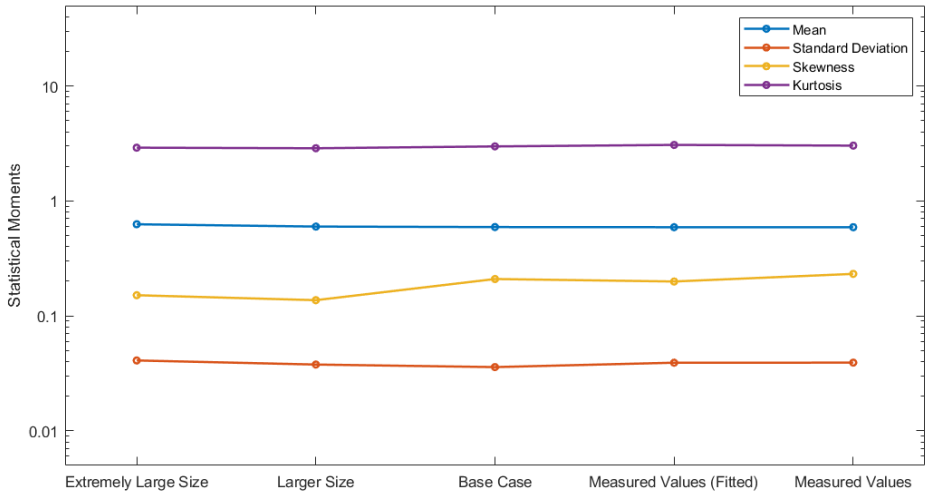

Figure 26: Size of Response Surface – Effect on Statistical Moments

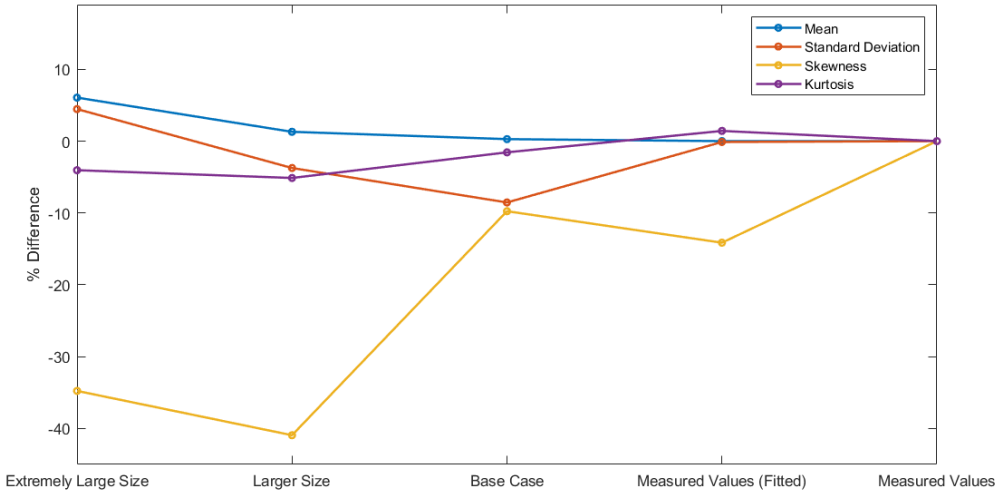

Figure 27: Size of Response Surface – Effect on Statistical Moments (% Difference)

5.2.2 Size of Response Surface – Effect on Fitted Probability Distributions

The probability distributions (probability density and cumulative probability) fitted to response surface values with different response surface sizes are plotted together with the measured values (fitted and raw values) and presented in Figure 28, Figure 29 and Figure 30.

The following observations are made:

- In general, using ‘Extremely Large Size’ results in large differences in the probability distributions.

- As presented in Figure 28, the probability density functions fitted from the response surfaces do not in general fit well with the measured values. The ‘Extremely Large Size’ probability distribution function is especially far away from the ‘Measured Values’.
- As shown in Figure 29, the cumulative probability distributions of ‘Base Case’ and ‘Larger Size’ are quite close to ‘Measured Values’. Furthermore, as presented in Figure 30, these differences become smaller at the upper tail regions. As observed in the probability density functions, the ‘Extremely Large Size’ cumulative probability function is especially far away from the ‘Measured Values’.

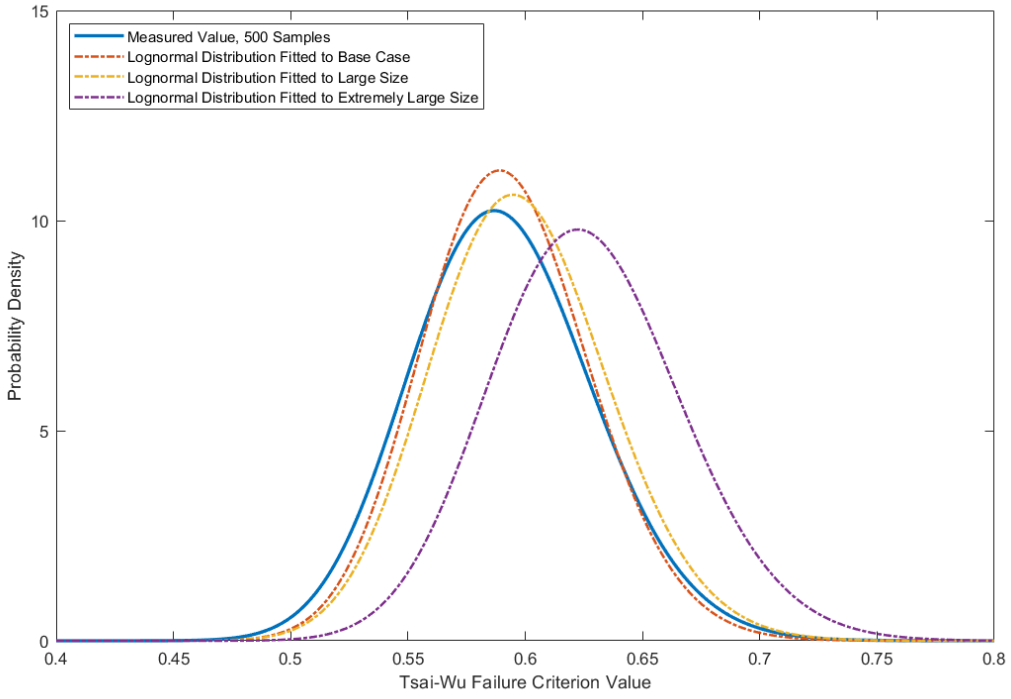

Figure 28: Size of Response Surface – Effect on Probability Density Functions

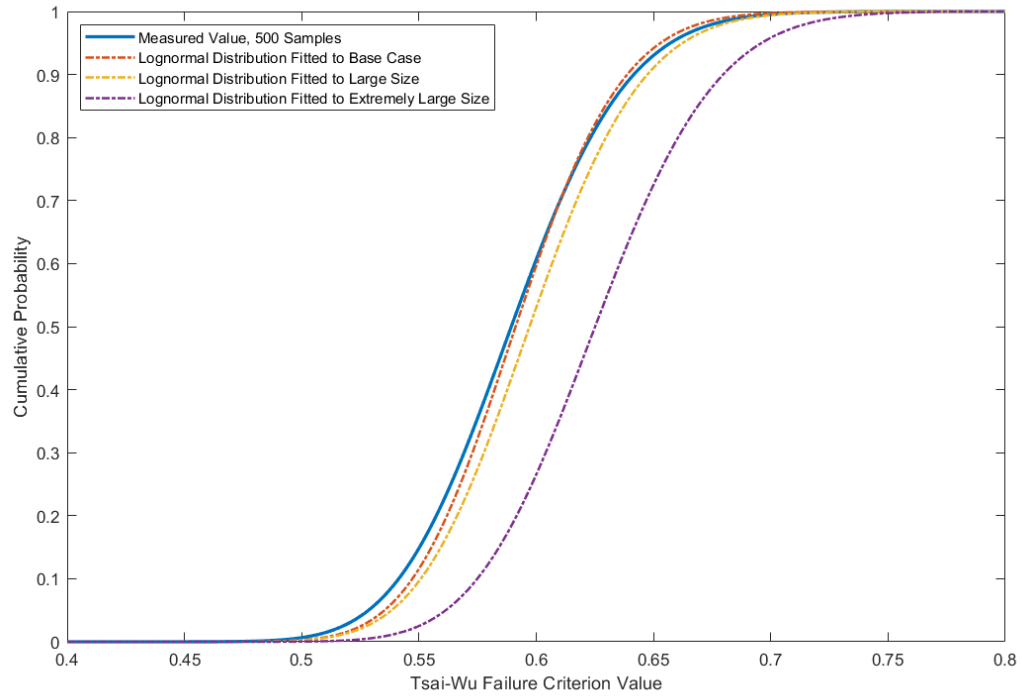

Figure 29: Size of Response Surface – Effect on Cumulative Probability Functions

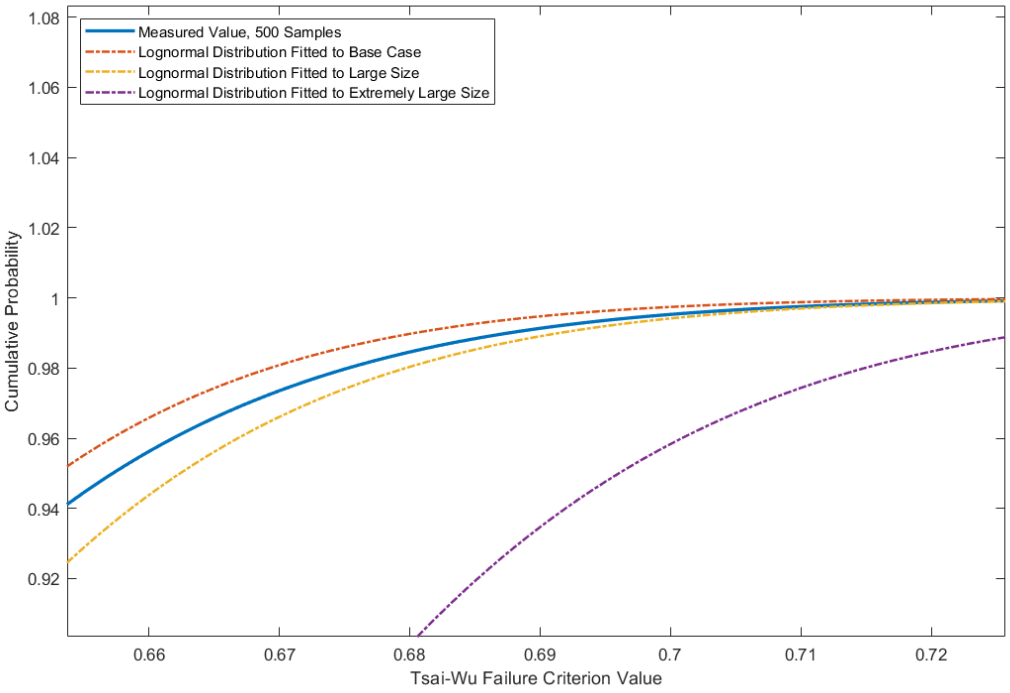

Figure 30: Size of Response Surface – Effect on Cumulative Probability Functions (Zoom-In at Upper Tail Region)

5.2.3 Size of Response Surface – Effect on Predicted Failure Values

Table 16 presents comparisons of the predicted failure rates calculated from the Lognormal distributions fitted to response surfaces with different ranges of diameter and ply thickness. It is observed that the size of the response surfaces does not have significantly effect on the predicted failure values. A larger response surface in general would lead to larger differences in the predicted failure values. Most of the differences are below 5% except for the Tsai-Wu failure value for the 'Extremely Large Sie' response surface.

Table 16: Number of Parameters – Effect on Predicted Failure Values

Source	Failure Criterion	Failure Rate = 1 in 10^4	Failure Rate = 1 in 10^5	Failure Rate = 1 in 10^6	% Diff, Failure Rate = 1 in 10^4	% Diff, Failure Rate = 1 in 10^5	% Diff, Failure Rate = 1 in 10^6
Lognormal distribution fitted to measured values	Maximum Stress	0.64	0.67	0.69	-	-	-
	Tsai-Wu	0.75	0.78	0.81	-	-	-
	Hashin	0.76	0.79	0.81	-	-	-
Lognormal distribution fitted to base case response surface values	Maximum Stress	0.64	0.66	0.68	0.0	-1.5	-1.4
	Tsai-Wu	0.74	0.77	0.79	-1.3	-1.3	-2.5
	Hashin	0.75	0.78	0.80	-1.3	-1.3	-1.2
Lognormal distribution fitted to larger size response surface values	Maximum Stress	0.63	0.65	0.67	-1.8	-1.9	-2.1
	Tsai-Wu	0.75	0.78	0.81	-0.1	-0.1	-0.3
	Hashin	0.75	0.77	0.80	-1.2	-1.4	-1.5
Lognormal distribution fitted to extremely large response surface values	Maximum Stress	0.63	0.66	0.67	-1.4	-1.8	-2.1
	Tsai-Wu	0.80	0.83	0.85	**5.7**	**5.6**	**5.6**
	Hashin	0.76	0.79	0.81	0.6	0.4	0.2

5.3 Recommendations for Optimisation of Response Surface

Based on the findings obtained in Sections 5.1 and 5.2, the following recommendations are made for the optimisation of the response surface:

- Reduce the input parameters selected to generate the response surface by only selecting the parameters with parametric correlation coefficients greater than +/- 0.15.

- Consider using a larger response surface to maximise flexibility if the accuracy in the predicted failure values are not extremely important. A larger response surface would lead to some decreased accuracy in the results.

6 Conclusions

In this paper, the use of Kriging response surface method for the estimation of failure values in carbon-fibre-epoxy composite flowlines under the influence of stochastic processes is investigated. The following conclusions are made:

- In general, the response surface method produced predicted failure results that are closed to that of the measured values. Most errors are small unless too few input parameters are selected to generate the response surface and/or the size of the response surface is too large.
- The skewness values in general are not accurately represented by the response surfaces; there is at least a 9% difference in the results. However, this is not of practical significance as this does not affect the prediction of failure values.
- In general, using more input parameters increases the accuracy of the response surface. However, this also increases the time required to generate the response surface as the design of experiment will increase in size.
- It is recommended to select input parameters that have correlation coefficients greater than +/- 0.15, i.e., input parameters that are at least slightly correlated. In this present study, this results about 10 input parameters.
- In general, a larger response surface leads to reduced accuracy in the results. However, this enables greater flexibility in its utilisation as a larger range of input parameters is covered.

7 References

ANSYS®. (2017). Academic Research Mechanical, Release 17.0, Help System, Element Reference, Chapter I, SHELL181, ANSYS, Inc.

Bazán F, Beck A. (2013) Stochastic process corrosion growth models for pipeline reliability. Corrosion Science 8, 74:50.

Box, G. E. P. and Wilson, K.B. (1951). On the Experimental Attainment of Optimum Conditions (with discussion). Journal of the Royal Statistical Society Series B 13(1):1–45.

Clouston P., Lam F., Barrett D. (1998). Interaction Term of Tsai-Wu Theory for Laminated Veneer. Journal of Materials in Civil Engineering 10 (2), pp.112-116.

Feng N.L., Malingam S.D., Irulappasamy S. (2019) Bolted Joint Behaviour of Hybrid Composites. In: Jawaid M, Thariq M, Saba N, editors. Failure Analysis in Biocomposites, Fibre-Reinforced Composites and Hybrid Composites: Woodhead Publishing. p. 79-95.

GlobalData (2019) H1 2019 Global Length and Capital Expenditure Outlook for Oil and Gas Pipelines – Natural Gas Pipelines Take Lead in New-Build Projects'

Gol'denblat I.I., Kopnov V.A. (1965). Strength of Glass-Reinforced Plastics in the Complex Stress State. Polymer Mechanics. 1(2):54-9.

Gupta S, Manohar C. (2004). An improved response surface method for the determination of failure probability and importance measures. Structural Safety 26:123-39.

Jha, V., Dodds, N., Finch, D., Latto, J., Karabelas, G., Anderson, T.A., Baehmann, P., Vermilyea, M.E. (2014). Flexible Fiber-reinforced Pipe for 10,000-foot Water Depths: Performance Assessments and Future Challenges, OTC-25393-MS, Offshore Technology Conference, Texas, USA, 5-8 May 2014

Jia B, Yu X, Yan Q. (2016). A new sampling strategy for Kriging-based response surface method and its application in structural reliability. Advances in Structural Engineering 20(4):564-81.

Krige, D.G. (1951). A Statistical Approach to Some Mine Valuations and Allied Problems at the Witwatersrand, Master's thesis of the University of Witwatersrand

Hashin Z. (1980). Failure Criteria for Unidirectional Fiber Composites. Journal of Applied Mechanics 47(2):329.

ICF International for The INGAA Foundation. (2014) North America Midstream Infrastructure through 2035: Capitalizing on Our Energy Abundance. INGAA Foundation, assessed on 12 April 2020, https://www.ingaa.org/File.aspx?id=21527&v=6be6e34a>

Li S., Sitnikova E., Liang Y., Kaddour A.S. (2017). The Tsai-Wu Failure Criterion Rationalised in the Context of UD Composites. Composites Part A: Applied Science and Manufacturing 102, pp.207-217.

Oliveira, N., Bisaggio, H., Netto, T. (2016). Probabilistic Analysis of the Collapse Pressure of Corroded Pipelines. In Proceedings of International Conference on Offshore Mechanics and Artic Engineering, OMAE2016-54299, Busan, South Korea, June 19-24, 2016

Simpson T, Mauery T, Korte J, Mistree F. (1998) Comparison of Response Surface and Kriging Models For Multidisciplinary Design Optimization. American Institute of Aeronautics and Astronautics, AIAA-98-4755.

Spearman C. (1910). Correlation Calculated from Faculty Data. British Journal of Psychology, 1904-1920. 3(3):271-95.

Tsai S.W., Wu E.M. (1971) A General Theory of Strength for Anisotropic Materials. Journal of Composite Materials. 5(1):58-80.

U.S. Energy Information Administration (2020). U.S. Average Depth of Crude Oil and Natural Gas wells, U.S. Energy Information Administration, assessed on 12 April 2020, https://www.eia.gov/dnav/ng/hist/e_ertw0_xwd0_nus_fwa.htm

Xing, Y.H., Wu. X., Buratti, V. (2019). The Correlation and Determination Matrices associated with the Burst Design of a Subsea Carbon-Fibre-Epoxy Composite Flow-Line, IOP Conference Series: Materials Science and Engineering 700 012021

Yang C. (2000). Design and Analysis of Composite Pipe Joints under Tensile Loading. Journal of Composite Materials 34:332-49.